SYNAPTIC AND INTRINSIC PLASTICITY IN LATERAL HYPOTHALAMIC SLEEP/WAKE REGULATORY NEURONS FOLLOWING ACUTE SLEEP DEPRIVATION: IMPLICATIONS FOR SLEEP HOMEOSTASIS

by

Chantalle L. Briggs

Submitted in partial fulfillment of the requirements
for the degree of Doctor of Philosophy

at

Dalhousie University
Halifax, Nova Scotia
March 2017

TABLE OF CONTENTS

LIST OF TABLES

LIST OF FIGURES

ABSTRACT

Sleep/wake behaviour is regulated by a network of sleep- and wake-promoting neurons that exhibit reciprocal activity patterns. This circuit is under the influence of the circadian clock, which maintains stable diurnal sleep/wake rhythms, and homeostatic control, which regulates sleep based on prior time spent awake. Astrocytes can modulate synaptic plasticity through high-affinity transporters like glutamate transporter 1 (GLT1). It was previously unknown whether GLT1 plays a role in the coordinated activation and silencing of sleep/wake neurons during challenges to sleep homeostasis.

With quantitative immunoconfocal analysis, I examined the spatial relationship between GLT1 and sleep/wake neurons from two brain regions involved in the homeostatic regulation of sleep. These include orexin (ORX) and melanin concentrating hormone (MCH) neurons in the lateral hypothalamus (LH), and cholinergic and parvalbumin-expressing neurons in the basal forebrain (BF) of the rat. Following acute sleep deprivation (SD; 6 h) there was no change in GLT1 juxtaposition with BF neurons compared to a time-matched undisturbed group (Rest). In the LH, SD decreased GLT1 juxtaposition with wake-promoting ORX neurons and increased GLT1 juxtaposition with sleep-promoting MCH neurons compared to Rest. These changes were reversed by a short subsequent period of sleep opportunity (3 h).

Using whole-cell patch-clamp electrophysiology, I demonstrated that SD-induced changes in GLT1 juxtaposition modulated excitatory synaptic transmission to LH neurons. Following SD, but not Rest, there was tonic presynaptic inhibition of excitatory transmission to ORX neurons through group III metabotropic glutamate receptors. This may represent a homeostatic mechanism promoting transition to sleep. In contrast, no presynaptic change was detected in MCH neurons, yet a large, slow kainate receptor-mediated EPSC induced by train-stimulation was significantly reduced following SD. This synaptic plasticity in the LH is consistent with decreased glutamate clearance at times when GLT1 juxtaposition is reduced.

Finally, SD increased the intrinsic excitability of both ORX and MCH neurons. ORX neurons exhibited a reduced afterhyperpolarizing potential and spike frequency adaptation, while MCH neurons exhibited reduced A-current, following SD.

These synaptic and intrinsic changes may have novel and important implications for homeostatic and non-homeostatic sleep regulation.

LIST OF ABBREVIATIONS USED

5-HT	Serotonin
ACh	Acetylcholine
ACSF	Artificial Cerebrospinal Fluid
AHP	Afterhyperpolarizing Potential
AMPA	α-amino-3-hydroxy-5-methyl-4-isoxazolepropionic acid
ANOVA	Analysis of Variance
AP	Action Potential
ATP	Adenosine Triphosphate
BF	Basal Forebrain
ChAT	Choline Acetyltransferase
CPPG	(RS)-α-Cyclopropyl-4-phosphonophenylglycine
DHK	Dihydrokainate
DNQX	6,7-Dinitroquinoxaline-2,3-dione
EPSC	Excitatory Post Synaptic Current
ER	Extended Rest
GABA	γ-Aminobutyric Acid
GFAP	Glial Fibrillary Acidic Protein
GLT1	Glutamate Transporter 1
GYKI52466 (GYKI)	4-(8-Methyl-9H-1,3-dioxolo[4,5-h][2,3]benzodiazepin-5-yl)-benzenamine dihydrochloride
HA	Histamine
iGluR	Ionotropic Glutamate Receptor
IPSC	Inhibitory Post Synaptic Current
KA	Kainic Acid (also Kainate)
KOR	κ-Opioid Receptor
L-AP4	L-(+)-2-Amino-4-phosphonobutyric acid
LH	Lateral Hypothalamus
LY367385 (LY)	(S)-(+)-α-Amino-4-carboxy-2-methylbenzeneacetic acid
MCH	Melanin Concentrating Hormone
mGluR	Metabotropic Glutamate Receptor

LIST OF ABBREVIATIONS USED (Cont.)

MPEP	2-Methyl-6-(phenylethynyl) pyridine hydrochloride
NA	Noradrenaline
NMDA	N-methyl-D-aspartate
NREM	Non Rapid Eye Movement
ORX	Orexin
PDC	L-trans-Pyrrolidine-2,4-dicarboxylic acid
PKC	Protein Kinase C
PPR	Paired Pulse Ratio
PV	Parvalbumin
R	Rest
Rec	Recovery
REM	Rapid Eye Movement
RMP	Resting Membrane Potential
SCN	Suprachiasmatic Nucleus
SD	Sleep Deprivation
SEM	Standard Error of the Mean
SON	Supraoptic Nucleus
TTX	Tetrodotoxin

ACKNOWLEDGEMENTS

I will forever be grateful to the network of inspiring people who have helped me succeed in this endeavour.

Thesis Panel:

Dr. Kazue Semba (supervisor): Thank you for being everything I could have hoped for in a mentor; kind, motivating, supportive, and intellectually nurturing. I really appreciate how you have supported my development both inside and outside of the lab, and how you have been supportive of my alternative career ambitions. I remember fondly the day I first stepped into your office years ago, around this time of the year, for an interview in the middle of a snow storm. Thank you for taking a chance on me as a graduate student, even though I came with no external funding. These past years have been a bit of a rollercoaster, and I will look back on this time with great affection.

Dr. Michiru Hirasawa (supervisor): I have been infinitely lucky to have won the mentor lottery not once, but twice, during my graduate training. You not only opened your lab to me, providing me with invaluable technical and intellectual training, but you also opened your home to me, spoiling me with home cooking while I joined you at Memorial University for collaborative work. I would also like to thank the rest of the Hirasawa Clan: **Haruki** and **Rikuo Hirasawa** for enduring my presence at meal time, and especially **Dr. Ken Hirasawa**, for many useful discussions about science and future career paths.

Dr. Robert Greene: Thank you for making the trek to the Great White North in the middle of winter! Kazue and I had hoped your trip would land during a more welcoming time of the year. Sorry about that!

Dr. Stefan Krueger: Thank you for participating as a committee member for over half a decade. I really appreciate all the input and suggestions you have given me along the way.

Dr. William (Bill) Baldridge: Thank you for being the Chair of my advisory committee over the years, and for agreeing to be a Reader at my final committee meeting. I hope I didn't make the reading too tedious!

Colleagues, Family, and Friends:

Current/Past Members of the Semba Lab: To Dr. Sam Deurveilher, thanks for putting up with me as an office mate for the first few years of my degree. Thanks especially for all the delightful conversations about science and movies! To Joan Burns, thanks for all the technical assistance. You are a well of knowledge! To Shannon Hall, your turn is coming next! Thanks for helping with the immunochemistry analysis at the beginning of your time in the lab. It was a big help. Thanks especially for all the fun beyond the science! To Dr. Elizabeth Seary, you made my first two years in the lab (and out of the lab) a blast! It wasn't quite the same after you left! And to the former members of the Semba lab, thanks for everything! Andrew Baldin, Kirsten Ko, Tareq Yousef, Maxine Profitt, Dr. Erik Wibowo, Alex Madore.

Current/Past Members of the Hirasawa Lab: Thanks to all the members of the Hirasawa Lab for making my time at Memorial memorable: Victoria Linehan, Todd Rowe, Dr. Maria Licursi, Christian Alberto, Josue Lilly. A special thanks to Christie Costello, Lisa Fang, Jared Crane for the help with sleep dep!

Stephen Whitefield: Thank you for the technical assistance with the microsocopy.

Michael Lovell: Thank you so much for putting up with me these past few years. I know it hasn't been easy with me jetting around the country and the continent! Thanks especially for your unending patience during the final 6 weeks of thesis-writing. We can go skiing now!

Family and Friends: Thanks Mom (Isabelle Briggs) for supporting me throughout this degree. I was so surprised when you got me my first ever journal subscription (Nature Neuroscience) the year I started my degree. I later learned that this was after secretly tracking down Kazue online, and asking her which journal was prominent in my field! Thanks Dad (Dale Briggs) for always encouraging education, and teaching me the power of perseverance. You were right! I can do it! Thanks Sis (Dominique Briggs) for letting me live vicariously through you! Yes, I'll go find a "real job" now… And thanks to the supportive network of friends that have stuck by me for years and years (Catherine Nadeau, Deny Hamel, Ginette Gautreau, Pierre Richard, Sylvie Poirier, etc. You know who you are!)

CHAPTER 1

INTRODUCTION

1.1 Introduction to Sleep

1.1.1 Basics of Sleep Behaviour

Sleep is a conserved behaviour present in virtually every animal species investigated to date, from the nematode to the human (Joiner, 2016). Mammalian sleep, best studied in humans and rodents, is a state of behavioural inactivity characterised by reduced arousal (Joiner, 2016), reduced reactivity to sensory stimuli (Livingstone and Hubel, 1981; Portas et al., 2000; Czisch et al., 2002), and reduced muscle tone (Mignot, 2008). *Why* we sleep is still a contentious issue, and sleep has been proposed to serve a variety of functions including memory consolidation (Girardeau et al., 2009; Rothschild et al., 2016), synaptic pruning/homeostasis (Vyazovskiy et al., 2008; Li et al., 2017), metabolic clearance (Xie et al., 2013), and energy conservation (Nofzinger et al., 2002; Wisor et al., 2012).

1.1.2 Societal Impact of Sleep Loss

Insufficient sleep is endemic in our society. Recent data from the National Sleep Foundation on self-reported sleep durations indicated that 30 percent of Canadians between 25 and 55 years of age are regularly getting less than the recommended 7-9 hours of sleep per night (National Sleep Foundation, 2013; Watson et al., 2015). Although why we sleep is unclear, there is little doubt that sleep is imperative; insufficient sleep leads to a variety of negative consequences. A recent report from the RAND Corporation, a non-profit global policy think tank, estimated that the annual loss to the Canadian economy resulting from insufficient sleep is equivalent to 0.85 to 1.56 percent of the gross domestic product (up to 24.7 billion USD; Hafner et al., 2016). While the RAND model accounted for loss in workforce productivity, it did not assess the additional economic burden of associated health care costs. For example, chronic sleep loss is associated with increased all-cause mortality (Kronholm et al., 2011; Yeo et al., 2013; Shen et al., 2016) and increased risk for cardiometabolic diseases such as obesity, cardiovascular disease, and type II diabetes (Lyytikäinen et al., 2011; Rangaraj and Knutson, 2016; Xiao et al., 2016).

Short periods of sleep deprivation impair cognition, particularly through reductions in sustained attention (Basner and Dinges, 2011; Goel et al., 2013). A single night of prior sleep loss impairs new learning on the subsequent day (Yoo et al., 2007), slows reaction times (Basner and Dinges, 2011; Cain et al., 2011) and results in impairment equivalent to a blood alcohol content of 0.1 % on a variety of cognitive tasks (Williamson and Feyer, 2000). Chronic sleep loss exacerbates these effects. One study demonstrated dose-dependent increases in impairment on a variety of cognitive tasks through 14 consecutive days of sleep restriction (sleep was limited to 4 h or 6 h/day; Van Dongen et al., 2003). Interestingly, participants in this study were largely unaware of their increasing cognitive deficits (Van Dongen et al., 2003). It is therefore unsurprising that sleep loss has been identified as a contributing factor to accidents both on the road (Martiniuk et al., 2013; Herman et al., 2014; Howard et al., 2014) and in the workplace (Uehli et al., 2014; Kling et al., 2010).

Insufficient sleep clearly results in large economic, safety, and health burdens. It is therefore vital that we understand the fundamentals of sleep/wake biology to inform better policy, and develop more effective interventions and treatments for sleep loss. Due to the significant homology in sleep regulation within mammalian species, the rodent model has provided troves of relevant information regarding mammalian sleep regulation (Mistlberger, 2005; Abel et al., 2013; Joiner, 2016). Most of the following research was conducted in the rodent model.

1.2 SLEEP NEUROBIOLOGY

1.2.1 THE TWO-PROCESS MODEL

Sleep is regulated by two biological processes that are continuously interacting: the circadian process and the homeostatic process (Borbély, 1982; Daan et al., 1984; Borbély et al., 2016). The circadian process is primarily regulated by a hypothalamic area called the suprachiasmatic nucleus (SCN; Mistlberger, 2005; Colwell, 2011). The SCN houses a genetic transcription/translation "clock" oscillating with a roughly 24-hour period that serves as the principal clock in mammals (Büttner and Wollnik, 1984; Czeisler et al., 1999; Welsh et al., 2010). The circadian signal from this genetic clock

promotes wake during the subjective day and sleep during the subjective night (Mistlberger, 2005). The endogenous circadian clock is normally entrained by light (Sharma, 2009; LeGates et al., 2014) as the principal Zeitgeber, and can also be entrained by other stimuli such as exercise (Tahara et al., 2017). Acute misalignment between the circadian clock and the external environment results in a series of symptoms commonly referred to as jet lag (Thorpy, 2012). Luckily for globetrotters, the circadian clock can shift over time to accommodate a new environment. Chronic misalignment between the endogenous circadian clock and the external clock, which frequently occurs among shift workers, can lead to a high incidence of developing cancer and cardiometabolic diseases (Potter et al., 2016).

While the circadian process maintains stable diurnal rhythms of sleep and wake, the homeostatic process regulates sleep and wake according to recent sleep/wake behaviour (Borbély et al., 2016). As such, homeostatic sleep pressure increases as a function of prior time spent awake. As sleep debt builds, the homeostatic process promotes adequate amounts of subsequent sleep to offset the debt accrued during previous wake. Both the circadian and homeostatic processes can be overridden to an extent by environmental challenges, which is clearly advantageous. It would permit one to seek food during subjective night in situations of food scarcity, and prioritize the immediate necessity of danger avoidance over the less immediate need for sleep. In principle, however, it is a combination of both the circadian process and the homeostatic process that determines the timing of sleep and wakefulness (Borbély, 1982; Daan et al., 1984; Borbély et al., 2016).

1.2.2 Investigating the Homeostatic Process: Acute Sleep Deprivation

One straightforward way to experimentally examine the homeostatic process of sleep regulation is with acute sleep deprivation (SD). By comparing the behaviour, physiology, and anatomy of an organism that has received an acute period of SD to those of a time-matched organism that was permitted to sleep during the same period, one effectively removes the confounding circadian component of sleep regulation, permitting assessment of the homeostatic process. This principle has been demonstrated in the

human (Goel et al., 2013), the rodent (Elliott et al., 2014), the zebrafish (Chiu and Prober, 2013), and the fruit fly (Donlea et al., 2014). While this technique is effective at examining the homeostatic process, it is important to note that the isolation from circadian effects is incomplete, as the circadian and homeostatic process continuously interact (Borbély et al., 2016).

In rodent research, SD by gentle handling is a commonly employed technique for acute total SD. It is designed to prevent the spurious effects of stress on sleep studies (Fenzl et al., 2007). During SD by gentle handling, the animal is permitted to freely behave. When it assumes a sleeping posture or appears drowsy, the experimenter intervenes to prevent sleep onset. These interventions can take several forms such as presenting the animal with a new toy, rustling its bedding, and lightly tapping its cage (Deurveilher et al., 2011). It is rarely necessary, in my experience, to physically interfere with the animal (e.g. petting) when using gentle handling for acute SD periods of up to 6 h. Acute SD studies in rodents are also conveniently timed; unlike humans, many rodents are nocturnal, and the common lab rat spends up to 80 % of the day sleeping (Shiromani et al., 2000). Acute SD for 3-6 h has been shown to induce similar patterns of immediate-early gene expression as spontaneous wakefulness (Pompeiano et al., 1994; Cirelli et al., 1995).

1.2.3 The Stages of Sleep

Sleep in mammals can be further divided into two broad categories: rapid eye movement (REM) sleep, and non-REM (NREM) sleep. Wake, NREM, and REM sleep can be observed and distinguished using a combination of electroencephalogram (EEG) recordings, which measure global brain electrical activity, and electromyogram (EMG) recordings, which measure electrical activity in skeletal muscles (Hobson and Pace-Schott, 2002; Cui et al., 2008; Brown et al., 2012). Wake is characterized by a strong EMG signal, and high-frequency low-amplitude EEG activity that reflects neuronal desynchrony during wakefulness. NREM sleep is characterized by a reduction in the EMG signal, as well as an increase in low-frequency, high-amplitude EEG activity that results from neuronal synchrony. REM sleep, like wake, is characterized by high-frequency, low-amplitude EEG activity. However, except for phasic muscle activities

such as rapid eye movements, muscle atonia predominates during REM sleep (Brown et al., 2012).

NREM and REM sleep are both important for mammalian physiology and behaviour, yet they serve different functions (Siegel, 2005; Abel et al., 2013). Likewise, many of the neuronal populations involved in sleep/wake regulation show distinctions in their activity patterns between these two sleep states and compared to wake, indicating that these neurons have different roles in sleep/wake behaviour (see below).

1.2.4 Select Anatomy of the Sleep/Wake Neurocircuit

The regulation of sleep/wake behavior involves many different neuronal populations from regions such as the brainstem, the hypothalamus, and the basal forebrain (BF; Richter et al., 2014; Weber and Dan, 2016). They include both wake-promoting and sleep-promoting neuronal populations that are often mutually inhibitory (Richter et al., 2014; Weber and Dan, 2016). This circuitry is under the influence of the circadian process regulated by the principal clock in the SCN. The homeostatic process is thought to be associated with this neurocircuit via cellular mechanisms involving both neurons and glia (Frank, 2013). Multiple neuronal populations underlie the emerging behavioural states under the influence of both processes. Here, I will highlight several important neuronal populations that will reappear in later chapters of this thesis. The sleep/wake activity profiles of these regulatory neurons are summarized in Table A.1

A number of sleep/wake-regulatory neuronal populations are monoaminergic. In the brainstem, noradrenaline (NA) neurons from the locus coeruleus and serotonergic (5-HT) neurons from the raphe nuclei are primarily wake-active (Takahashi et al., 2010; Sakai, 2011). NA neurons are particularly important for arousal. They send extensive projections throughout the brain, including many to other sleep/wake regulatory areas (Samuels and Szabadi, 2008). Optogenetic activation of neurons in the locus coeruleus promotes transitions from sleep to wake (Carter et al., 2010), and chemogenetic activation of NA neurons speeds recovery from anaesthesia (Vazey and Aston-Jones, 2014). Histaminergic (HA) neurons from the tuberomammillary nucleus of the posterior hypothalamus are also wake-active (Takahashi et al., 2006). HA neurons project widely throughout the brain (Panula et al., 1989), and hypothalamic HA levels increase with

wake in a circadian manner (Mochizuki et al., 1992). Mice lacking the HA synthesizing enzyme histidine decarboxylase show increased sleep fragmentation and difficulty maintaining wake (Parmentier et al., 2002; Anaclet et al., 2009). Additionally, HA has a direct excitatory effect on NA neurons (Korotkova et al., 2005). These wake-promoting centers have reciprocal, often mutually inhibitory connections with sleep-promoting GABAergic neurons in the ventrolateral preoptic nucleus (Weber and Dan, 2016).

In the lateral hypothalamus (LH), there are two mutually inhibiting peptidergic neuronal populations regulating sleep/wake behaviour: the orexin (ORX; also known as hypocretin) neurons and the melanin concentrating hormone (MCH) neurons. ORX neurons are wake-active, wake-promoting neurons (Lee et al., 2005; Modirrousta et al., 2005; Adamantidis et al., 2007) that project throughout the brain (Peyron et al., 1998; Horvath et al., 1999), including to the BF and NA, 5-HT, and HA wake-promoting cell groups (Horvath et al., 1999; Liu et al., 2002; Schöne et al., 2012). NA and 5-HT neurons send reciprocal projections to ORX neurons, although NA projections are sparse (Sakurai et al., 2005; Yoshida et al., 2006). ORX peptides have an excitatory effect on these three monoaminergic neuronal populations (Hagan et al., 1999; Horvath et al., 1999; Brown et al., 2002; Liu et al., 2002; Yamanaka et al., 2002), yet the effects of these neuromodulators on ORX neurons are more complex. For example, histamine has little effect on ORX neurons (Li et al., 2002; Yamanaka et al., 2003), and the effect of NA on ORX neurons in rat changes from excitatory to inhibitory following short (2 h) periods of prolonged wake (Grivel et al., 2005; Uschakov et al., 2011). However, this SD-dependent change from excitation to inhibition may not be common among all rodents. ORX neurons in mice are inhibited by NA regardless of time-of-day or sleep pressure (Yamanaka et al., 2006).

In contrast to ORX neurons, MCH neurons are inactive during wake and primarily active during REM sleep (Modirrousta et al., 2005; Hassani et al., 2009b), although a recent study has identified that MCH neurons can become active during wake under certain conditions (González et al., 2016). Stimulation of MCH neurons promotes sleep (Konadhode et al., 2013; Blanco-Centurion et al., 2016), particularly REM sleep (Jego et al., 2013; Vetrivelan et al., 2016), with some diurnal differences. The MCH peptide inhibits ORX neurons (Rao et al., 2008). While orexin peptides are excitatory to MCH

neurons (van den Pol et al., 2004; Li and van den Pol, 2006), ORX neurons can inhibit MCH neurons either through a local inhibitory pathway (Apergis-Schoute et al., 2015) or through release of the inhibitory cotransmitter dynorphin (Li and van den Pol, 2006). MCH neurons also receive input from monoaminergic sleep/wake centers (González et al., 2016), and the effects of monoamines on MCH neurons are inhibitory (van den Pol et al., 2004; Bayer et al., 2005; Parks et al., 2014a). MCH, in turn, inhibits these monoaminergic neuronal populations (Jego et al., 2013; Monti et al., 2013; Devera et al., 2015).

Finally, there are two populations of sleep/wake neurons in the BF that are relevant to this thesis. Both cholinergic neurons and parvalbumin-expressing GABAergic neurons are active during wake and REM sleep, but silent during NREM sleep (Duque et al., 2000; Manns et al., 2000; Hassani et al., 2009a; Kim et al., 2015). Both have been implicated in sleep/wake regulation and cortical arousal (Kaur et al., 2008; Kim et al., 2015). These BF neurons project heavily to the cortex, while providing transmitter-specific innervation of many additional forebrain and midbrain regions (Do et al., 2016). GABAergic and glutamatergic, but not cholinergic BF neurons form synapses on LH neurons (Henny and Jones, 2006a, 2006b; Agostinelli et al., 2016), where they have inhibitory effects on MCH neurons and excitatory effects on ORX neurons (Bayer et al., 2005; Zhou et al., 2015; Agostinelli et al., 2016). In turn, ORX neurons project to the BF (España et al., 2005), and ORX has a direct excitatory effect on cholinergic and possibly parvalbumin expressing BF neurons (Arrigoni et al., 2010). Locally within the BF, cholinergic neurons have an excitatory effect on BF parvalbumin neurons (Yang et al., 2014; Xu et al., 2015), yet these parvalbumin neurons do not innervate cholinergic BF neurons (Xu et al., 2015).

Many of these sleep/wake regulatory neurons drive sleep/wake behaviour under both circadian influence and homeostatic pressure (Richter et al., 2014; Weber and Dan, 2016), and their activities are therefore under the regulation of the homeostatic process.

1.2.5 Molecular Determinants of the Homeostatic Process

As stated in Section 1.2.1, homeostatic sleep pressure accumulates throughout periods of wake and dissipates during subsequent sleep. One of the first molecules

demonstrated to mediate the homeostatic response is adenosine. Adenosine is a metabolic by-product of neuronal activity that results from the breakdown of ATP and can be released into the extracellular space via equilibrative nucleoside transporters (Bjorness and Greene, 2009). ATP released by glia also contributes to adenosine via extracellular enzymatic breakdown (Bjorness and Greene, 2009). Extracellular adenosine accumulates in the BF during prolonged periods of both spontaneous wake and SD (Porkka-Heiskanen et al., 1997, 2000; Basheer et al., 1999). Adenosine acts to inhibit both cholinergic and parvalbumin expressing neurons through activation of A1 receptors (Arrigoni et al., 2006; Yang et al., 2013a). Administering exogenous adenosine or an adenosine transport inhibitor by microdialysis has confirmed the sleep-promoting effects of adenosine, increasing NREM sleep and concurrent EEG delta power (a well-established measure of sleep propensity or pressure), as well as REM sleep, at the expense of wake (Porkka-Heiskanen et al., 1997; Basheer et al., 1999). Additionally, in the LH, neuronal activity-derived adenosine inhibits excitatory transmission to ORX neurons through A1 receptors (Xia et al., 2009), essentially providing negative feedback to these wake-active neurons.

Other substances, such as nitric oxide (NO), also mediate the homeostatic process and may precede and initiate the accumulation of adenosine during wake and SD (Kalinchuk et al., 2006b). NO production increases in the BF during prolonged wake and promotes NREM sleep rebound (Kalinchuk et al., 2006a, 2006b). It is therefore unsurprising that NO reduces the activity of wake-active BF neurons (Kostin et al., 2008, 2009). The expression of inducible NO synthase, a synthesizing enzyme for NO, increases in BF cholinergic neurons during SD (Kalinchuk et al., 2015); therefore, NO can inhibit the very neurons that produce it. NO production also increases in the LH with SD, and NO has an inhibitory effect on wake-active (and therefore potentially ORX) LH neurons (Kostin et al., 2011).

In addition to these extrinsic factors, synaptic plasticity within the sleep/wake neuronal network could mediate the homeostatic process of sleep regulation. This has previously been demonstrated for ORX neurons, where SD (4 h) increases both the frequency and amplitude of quantal excitatory events (Rao et al., 2007). Likewise, intrinsic plasticity of membrane properties of sleep/wake neurons could be altering their excitability based on sleep-need, thus impacting synaptic integration and neuronal output

in a behaviourally relevant manner (Sehgal et al., 2013). This has also been demonstrated in ORX neurons, where SD (4 h) results in a mild depolarization of their resting membrane potential (Liu et al., 2011).

While much is known regarding the anatomy of the sleep/wake network underlying the homeostatic process, surprisingly little is known about whether synaptic or intrinsic plasticity of sleep/wake regulatory neurons are involved in this process.

1.3 Astrocytes and Sleep

As briefly reviewed in Section 1.2.4, detailed knowledge exists for the neuronal systems regulating sleep and wake states under circadian and homeostatic influences (Richter et al., 2014; Weber and Dan, 2016). Yet neurons are not the only brain cells that regulate behaviour. Increasing evidence has implicated a class of glial cells called astrocytes in sleep regulation (Jackson, 2011; Frank, 2013; Petit and Magistretti, 2016).

1.3.1 The Many Roles of Astrocytes

Astrocytes are a multifunctional population of brain cells. Their name, a combination of *astro-* meaning "star" and *-cyte* meaning "cell", derives from their stellate morphology when visualized using conventional staining methods such as Golgi staining and glial fibrillary acidic protein (GFAP) immunostaining (Oberheim et al., 2012). Astrocyte morphology, however, is much more extensive and complex than first appreciated, with the extent of GFAP only representing roughly 15 % of total astrocytic volume (Bushong et al., 2002). Astrocytes in the grey matter of the central nervous system can be intimately associated, via their fine processes, with blood vessels, neuronal cell bodies, dendrites, and synapses (Ventura and Harris, 1999; Leybaert, 2005). They have traditionally been considered the support cells of the brain due to their roles in ion buffering (Wallraff et al., 2006), metabolic support (Bélanger et al., 2011), and clearance of synaptically-released neurotransmitters (Bak et al., 2006). Yet, since the discovery that astrocytes can release neuroactive molecules of their own, called gliotransmitters, it has become widely accepted that astrocytes play an active role in a variety of neuronal

functions and behaviours (Perea et al., 2014). One such gliotransmitter is ATP (Harada et al., 2015).

1.3.2 Astrocytic Roles in Sleep/Wake Regulation

As mentioned in Section 1.2.5, ATP is converted to adenosine which acts on A1 receptors to inhibit wake-active neurons in both the BF (Arrigoni et al., 2006; Yang et al., 2013a) and the LH (Xia et al., 2012). Blocking exocytotic release specifically in astrocytes prevents the accumulation of adenosine in the BF during SD and attenuates the build-up of sleep pressure (EEG delta power) and subsequent rebound sleep through a reduction in A1 receptor activity (Halassa et al., 2009). This suggests that astrocytes are necessary for the normal accumulation of adenosine-mediated homeostatic sleep pressure. One recent paper, however, has placed doubt on this interpretation, based on the demonstration that impaired exocytotic release in this transgenic model may not be as specific to astrocytes as previously claimed (Fujita et al., 2014). However, it has since been demonstrated that reducing astrocytic, but not neuronal, adenosine kinase, the primary metabolizing enzyme for adenosine, results in increased homeostatic sleep pressure and rebound sleep (Bjorness et al., 2016). Astrocytes are therefore key regulators of adenosine-mediated homeostatic pressure.

Another likely astrocytic marker for sleep propensity is lactate. Extracellular lactate concentrations in the BF and cerebral cortex increase during wake and SD, and decrease during subsequent sleep (Shram et al., 2002; Wigren et al., 2009). In the LH, ORX neurons increase their firing rate in response to increasing lactate concentrations, a neuronal metabolic substrate often derived from astrocytes (Parsons and Hirasawa, 2010). Additionally, astrocytes in the locus coeruleus increase the activity of local (potentially NA) neurons through lactate release (Tang et al., 2014). Since lactate increases the activity of wake-promoting neurons rather than inhibiting them, lactate is not likely a molecular determinant of homeostatic sleep pressure, but rather an indicator of prior time spent in wake. Yet, it is indeed an avenue by which astrocytes could impact sleep/wake regulation, particularly according to metabolic status (Petit and Magistretti, 2016).

Finally, optogenetic stimulation of astrocytes in the posterior hypothalamus during the subjective day increases time spent sleeping, suggesting that hypothalamic astrocytes

are involved in sleep/wake regulation (Pelluru et al., 2016). It is unclear through which mechanism astrocytes were promoting sleep, but it is possibly through ATP-derived adenosine or a yet-unidentified pathway.

1.3.3 Astrocytes and Glutamate Reuptake

Astrocytes also impact behaviour through the reuptake of synaptically-released glutamate by high-affinity glutamate transporters like glial glutamate transporter 1 (GLT1) (Danbolt, 2001; Petr et al., 2015). GLT1 is the most abundant protein in the brain (Lehre and Danbolt, 1998), and it is predominantly, though not exclusively, astrocytic (Danbolt et al., 2016). For example, axon terminals in the CA1 region of the hippocampus express GLT1 (Furness et al., 2008). Whether there is also neuronal expression of GLT1 in the brain regions involved in sleep homeostasis (such as the BF and LH) is unknown. Conditionally knocking out GLT1 from astrocytes results in a more pronounced phenotype than knocking out GLT1 specifically from neurons; the astrocyte knockout results in increased susceptibility to seizures and increased mortality (Petr et al., 2015).

GLT1 can shorten glutamate activity at the synapse, limiting the activation of synaptic and extrasynaptic glutamate receptors, and impacting synaptic plasticity (Rusakov and Kullmann, 1998; Oliet et al., 2001; Zheng et al., 2008). This has been demonstrated in several brain regions, including the supraoptic nucleus of the hypothalamus (Oliet et al., 2001), the barrel cortex (Genoud et al., 2006), the cerebellum (Marcaggi et al., 2003), and the hippocampus (Huang et al., 2004; Omrani et al., 2009). In the hippocampus, GLT1 has been shown to impact learning and memory through a variety of mechanisms (Bechtholt-Gompf et al., 2010; Yang et al., 2013b; Matos-Ocasio et al., 2014).

While it is clearly well-established that astrocytes can modulate behaviour through glutamate transport, this possibility had never been investigated in brain regions implicated in the homeostatic regulation of sleep (like BF and LH), where astrocytic glutamate uptake could be modulating the homeostatic process of sleep regulation. BF neurons receive glutamatergic afferents from many brain regions (Carnes et al., 1990; Jolkkonen et al., 2002; Hur et al., 2009), including those involved in sleep/wake regulation, such as the midbrain reticular formation and parabrachial nuclei (Carnes et al.,

1990; Wu et al., 2004; España et al., 2005). LH ORX neurons receive glutamatergic afferents from other wake-promoting brain areas (Henny and Jones, 2006a, 2006b; Yoshida et al., 2006) and local neurons (Li et al., 2002; Acuna-Goycolea et al., 2004; Yamanaka et al., 2010). The source of glutamatergic afferents to MCH neurons is not well-defined, but may include other sleep/wake brain areas (Henny and Jones, 2006b; González et al., 2016), as well as the local neurons known to innervate ORX neurons (Li et al., 2002; Acuna-Goycolea et al., 2004; Yamanaka et al., 2010).

1.4 Rationales and Hypotheses

While much is known about the neuronal networks underlying the regulation of sleep and wake, comparatively little was previously known about whether the coordinated activation and silencing of sleep/wake neuronal populations involves homeostatic changes at the synaptic and cell-intrinsic levels. In many brain regions, astrocytes modulate synaptic plasticity through GLT1, yet whether astrocytes regulate sleep/wake neuronal populations via GLT1 was unknown. The principal hypothesis of this thesis is: Prior sleep history induces synaptic plasticity through GLT1, and intrinsic plasticity, in sleep/wake regulatory neurons. Specific hypotheses for each study in this thesis are stated below.

1.4.1 Changes in GLT1 Juxtaposition with Sleep/Wake Regulatory Neurons: Consequences for Synaptic Transmission (Chapter 2 and Chapter 3)

If GLT1 plays a functional role in sleep/wake regulation, this may be apparent as a change in its spatial relationship with sleep/wake regulatory neurons following acute SD.

Hypothesis 1: GLT1 apposition with sleep/wake regulatory neurons changes following SD.

Hypothesis 2: SD-dependent changes in GLT1 apposition are opposite for sleep-active and wake-active neurons.

Hypothesis 3: SD-dependent changes in GLT1 apposition with sleep/wake regulatory neurons are reversed by a short period of sleep opportunity.

To test these hypotheses, I analyzed brain tissue samples obtained from rats that either received acute SD or were left undisturbed (Rest). To investigate GLT1 apposition with neurons, I performed quantitative immunohistochemical analyses on LH and BF tissue slices. I measured apposition between GLT1 and ORX and MCH neurons in the LH, and apposition between GLT1 and cholinergic and parvalbumin-expressing neurons in the BF (Chapter 2). Note that SD-dependent change was observed in the LH but not the BF. Therefore, all further experiments were conducted only in the LH.

Next, I investigated the physiological consequences of SD-dependent changes in GLT1 apposition with sleep/wake LH neurons using whole-cell patch-clamp electrophysiology. In particular, I examined the impact of SD-dependent changes in GLT1 apposition on excitatory synaptic transmission to LH neurons (Chapters 2 and 3).

Hypothesis 4: SD dependent changes in GLT1 apposition with sleep/wake LH neurons impact excitatory synaptic transmission to sleep/wake LH neurons

Hypothesis 5: SD/GLT1-dependent changes in excitatory synaptic transmission are opposite for sleep- and wake-active LH neurons

Hypothesis 6: SD/GLT1-dependent changes in excitatory synaptic transmission to sleep/wake LH neurons support the homeostatic process

1.4.2 Effects of Acute SD on Intrinsic Membrane Properties of Sleep/Wake Regulatory Neurons (Chapter 4)

It is possible that SD also induces intrinsic plasticity in sleep/wake LH neurons independent of GLT1.

Hypothesis 7: SD induces intrinsic plasticity in sleep/wake LH neurons.

Hypothesis 8: SD-dependent intrinsic plasticity has opposite functional consequences for sleep-active and wake-active neurons, which support the homeostatic process.

To test these hypotheses, I performed whole-cell patch-clamp electrophysiology in acute LH slices obtained from rats that either received acute SD or were left undisturbed (Rest). I assessed several intrinsic membrane properties including the resting membrane potential (RMP), A-current and after hyperpolarizing potential (AHP).

CHAPTER 2

SLEEP DEPRIVATION DIFFERENTIALLY ALTERS GLT1 APPOSITION AND EXCITATORY TRANSMISSION TO OREXIN AND MCH NEURONS

2.2.1 INTRODUCTION

Research on the regulation of sleep/wake behavior historically focused on neurons, resulting in detailed knowledge of the neuronal systems regulating sleep and wake states under homeostatic and circadian influences (Saper et al., 2010; Weber and Dan, 2016). Increasing evidence however has implicated glia, particularly astrocytes, in sleep regulation. Astrocytes can promote sleep by releasing ATP, which is degraded to adenosine (Porkka-Heiskanen et al., 1997; Pascual et al., 2005). Extracellular adenosine levels increase during sleep deprivation (SD) in the basal forebrain (BF) (Porkka-Heiskanen et al., 1997), where adenosine inhibits excitatory transmission in several types of wake-active BF neurons via A1 receptors (Arrigoni et al., 2006; Yang et al., 2013a). Blocking gliotransmission prevents adenosine accumulation and reduces sleep rebound during subsequent sleep (Halassa et al., 2009). A recent study identified astrocytic adenosine kinase as the key regulator of extracellular adenosine levels according to sleep need (Bjorness et al., 2016). Astrocytes also play a causal role in shifting neocortical neuronal activity to synchronized slow-oscillations, a hallmark of slow-wave sleep, by altering extracellular glutamate (Poskanzer and Yuste, 2016). While these forms of astrocytic regulation appear fairly non-selective in terms of neuronal effects, astrocytes can also fine tune single synapses (Oliet et al., 2001; Takata et al., 2011; Pannasch et al., 2014). As sleep/wake cycles are closely coordinated by interactions between discrete groups of neurons (Saper et al., 2010; Weber and Dan, 2016), it is important to determine whether astrocytes regulate synaptic inputs to sleep- and wake-promoting neurons, thereby coordinating their reciprocal activity patterns according to homeostatic and other demands.

One key function of astrocytes is to uptake synaptically-released glutamate via high-affinity glutamate transporters like glial glutamate transporter 1 (GLT1) (Petr et al., 2015), the main glutamate transporter in the forebrain (Danbolt, 2001). GLT1 regulates glutamate diffusion and spillover, thus controlling the activation of extrasynaptic glutamate receptors, heterosynaptic signaling, and synaptic plasticity, as demonstrated in various brain regions (Oliet et al., 2001; Marcaggi et al., 2003; Huang et al., 2004; Genoud et al., 2006; Omrani et al., 2009). However, the possibility that GLT1 is involved

in regulating neuronal activity patterns underlying the sleep/wake cycle or sleep homeostasis was not investigated.

The lateral hypothalamus (LH) houses two populations of peptidergic neurons with opposite roles in sleep/wake regulation. Orexin (ORX) neurons are active during spontaneous or forced wake periods and silent during sleep, and their activation promotes wakefulness (Lee et al., 2005; Modirrousta et al., 2005; Adamantidis et al., 2007). In contrast, melanin-concentrating hormone (MCH) neurons are active during rapid eye movement (REM) sleep, and quiescent during wake or SD (Modirrousta et al., 2005; Hassani et al., 2009b). Their activation has been reported to promote REM sleep (Jego et al., 2013; Vetrivelan et al., 2016) or both non-REM and REM sleep (Konadhode et al., 2013; Blanco-Centurion et al., 2016), with some diurnal differences.

Here we aimed to determine whether and how astrocytic GLT1 modulates the two functionally reciprocal populations of neurons located in a single brain region, the LH, and how acute SD alters this modulation. To the best of our knowledge, this is the first study to address the role of glutamate transport in the synaptic regulation of sleep/wake-regulatory neurons.

2.2 METHODS: IMMUNOCONFOCAL EXPERIMENTS

2.2.1 ANIMALS

All procedures were conducted in accordance with the Canadian Council on Animal Care and were approved by the Dalhousie University Committee on Laboratory Animals. A total of 36 adult male Wistar rats (Charles River Canada, St. Constant, QC, Canada) were used in this study. Animals weighed 225–250 g on arrival and were housed in pairs under a 12 h light/12 h dark cycle (lights on at 07:00) in a colony room. Food and water were available ad libitum.

One week following arrival, animals were transferred in their home cages (2 rats/cage) to individual experimental chambers for 3-4 days of habituation. Each chamber was equipped with a fan and an incandescent light controlled by a timer to maintain the same light/dark cycle as in the colony room. The pairs of rats were randomly assigned to one of 4 behavioral treatment groups on the experimental day at 09:00. One group was

left undisturbed and, thus, received 6 h of sleep opportunity (Rest, R; n = 12); a second group was subjected to 6 h of sleep deprivation (SD; n = 12); a third group received 9 h of sleep opportunity (extended Rest, ER; n = 6); a fourth group was subjected to 6 h of SD followed by 3 h of sleep opportunity (Recovery; n = 6). The first two groups were euthanized immediately at 15:00. The last two groups were euthanized immediately at 18:00. SD was conducted by gentle handling, a commonly used SD method that minimizes stress (Deurveilher et al., 2011).

2.2.2 Perfusion and Sectioning

Animals were injected with an overdose of an anesthetic mixture (208 mg/kg ketamine, 9.6 mg/kg xylazine, and 1.8 mg/kg acepromazine, i.p.), and perfused intracardially with 100 ml of 0.1 M phosphate-buffered saline (PBS; pH = 7.4) followed by 400 ml of 4% paraformaldehyde in 0.1 M phosphate buffer (pH 7.4). The brains were quickly removed, postfixed for 2 h in the same fixative, and then placed in 30% sucrose in 0.01 M phosphate buffer for a minimum of 2 days at 4 °C. Coronal brain sections (30 μm) through the basal forebrain (BF; from bregma to 1.5 mm posterior to it) and the lateral hypothalamus (LH; from 2.5 mm to 3.5 mm posterior to bregma) were cut on a freezing microtome. Sections through these two anatomical regions were collected in 6 serial sets in 0.05 M Tris-buffered saline (TBS, pH 7.4).

2.2.3 Immunohistochemistry

BF section sets were first incubated with a polyclonal guinea pig anti-GLT1 antibody (1:2000; AB1783; Millipore, Temecula, CA) overnight at room temperature or for 2 days at 4°C. The anti-GLT1 antibody was raised against the C-terminal sequence of the GLT1 protein that is conserved among human, mouse, and rat. Sections were subsequently incubated for 1-2 h at room temperature with a Cy3-conjugated donkey anti-guinea pig IgG antibody (1:200). Adjacent BF sets were then incubated overnight at room temperature or for 2 days at 4°C with a polyclonal goat anti-choline acetyltransferase (ChAT) antibody (1:50; AB144P; Millipore), or either a monoclonal mouse anti-parvalbumin (PV) antibody (1:800; P3088; Sigma-Aldrich Canada, Oakville, ON) or a

rabbit anti-PV antibody (1:100; supplied by Dr. K. G. Baimbridge) to identify cortically projecting GABAergic BF neurons (Duque et al., 2000; Gritti et al., 2003; Hassani et al., 2009a). Sections were subsequently incubated for 1-2 h at room temperature with either a Cy2 (1:100) or Dylight 488-conjugated donkey anti-goat IgG antibody (1:200), a Cy2-conjugated donkey anti-mouse IgG antibody (1:100), or a Cy2-conjugated donkey anti-rabbit IgG antibody (1:100), as appropriate.

LH section sets were first processed to visualize GLT1, as described above. Adjacent LH sets were then incubated overnight at room temperature or for 2 days at 4 °C with either a polyclonal goat anti-orexin A antibody (1:300; sc-8070; Santa Cruz Biotechnology, Dallas, TX) or a rabbit anti-MCH antibody (1:1500; H-070-47; Phoenix Pharmaceuticals, Belmont, CA). Sections were subsequently incubated for 1-2 h at room temperature with either a Cy2 (1:100) or Dylight 488-conjugated donkey anti-goat IgG antibody (1:200), or a Cy2 (1:100) or Dylight 488-conjugated donkey anti-rabbit IgG antibody (1:200), as appropriate. All LH sections were incubated for a further 20 min with Neurotrace Deep-Red fluorescent stain (1:75; N-21483; Molecular Probes, Eugene, OR). While ORX and MCH immunostains did not appear to fill the entire cytoplasm, Neurotrace Nissl stain clearly and reliably outlined the somata of the peptide-containing neurons for GLT1 apposition analysis (Figure 2.1A) (Cronk et al., 2012; Derecki et al., 2012).

Sections were mounted on glass slides, air dried, and coverslipped with Cytoseal 60 mounting medium (Richard-Allan Scientific, Kalamazoo, MI).

2.2.4 Confocal Imaging

Immunofluorescent images were acquired with a laser scanning confocal microscope (Zeiss LSM 510 Meta). The Dylight 488 and Cy2 fluorophores were excited with an argon laser (at 488 nm). Cy3 and NeuroTrace deep-red were each excited with HeNe lasers, at 548 nm and 633 nm, respectively. Separate emission channels were captured sequentially to limit non-specific fluorescence. Laser power and emission filters were also adjusted to minimize bleed-through artifacts.

For each section, the brain region of interest (either BF or LH) was identified at a low magnification (25x oil immersion lens; NA = 0.8) with the Dylight 488/Cy2 channel, to locate the neuronal somata of interest. The objective was then switched to one of higher magnification (63x oil immersion; NA = 1.4) for image acquisition. Neurons were selected throughout the rostro-caudal regional distribution of cells of interest, while the experimenter remained blind to the GLT1 fluorescence channel. Neuronal somata were selected randomly using the criteria of the presence of the nucleus and clear immunostaining. Images were acquired using the ZEN software package (Carl Zeiss Meditec, Oberkochen, Germany). Roughly 20 neurons per cell-type were imaged per rat. Briefly, a neuronal soma was centered in the field of view. The confocal pinhole was adjusted to the size of a single airy disk for each emission channel. Gain and offset were also adjusted for each emission channel such that all pixels were set within the dynamic range of the photodetector (one single pixel at 0 % saturation, and one pixel at 100 % saturation). Labelling was sampled through each neuronal soma by taking optical slices with a thickness of 0.4 μm (z-stack). Stacks of 1024 x 1024 pixel images were collected. Each pixel measured 130 nm x 130 nm.

2.2.5 Image Processing and Analysis

Each image was corrected for electrical noise using the mixed Poisson-Gaussian noise filter plugin, PureDenoise (by F. Luisier; Biomedical Imaging Group; http://bigwww.epfl.ch/algorithms/denoise/) (Luisier et al., 2007, 2011) for ImageJ (public domain, developed by the National Institutes of Health). Image stacks were then deconvolved using a theoretical point-spread function using Huygens Professional (Scientific Volume Imaging, Hilversum, Netherlands). The point-spread function was set using parameters from the Zeiss confocal microscope.

Following deconvolution, one image from each z-stack was selected for analysis. The selection criteria were: 1) the location through the middle of the neuronal soma as indicated by a clearly visible nucleus surrounded by visible cytoplasm, and 2) optimal labelling of the relevant transmitter marker, GLT1, and, where applicable, Neurotrace Nissl stain. GLT1 apposition was assessed using methods modified from Doucet et al. (2009), and a combination of steps with Adobe Photoshop CS4 (Adobe Systems Canada,

Ottawa, ON), and ImageJ. Briefly, each image was cropped to 400 x 400 pixels with the neuron soma located at the center of the image to limit possible unevenness in immunofluorescence within each image, due to technical reasons. Greyscale images for cell body markers (the transmitter marker with or without Neurotrace Nissl stain) and for GLT1 immunofluorescence were treated separately (Figure 2.1B, C). Binary images were generated from these two greyscale images (Figure 2.1D, E). The threshold for positive GLT1 immunoreactivity was set using the pixel intensity histogram and the following formula:

$$Threshold = Mode\ Pixel\ Intensity + 0.18(Maximum\ Pixel\ Intensity - Mode\ Pixel\ Intensity)$$

This threshold permitted selection of pixels that appeared clearly and definitively labeled to the eye in a pilot study.

Next, a one pixel (130 nm)-wide cell body outline was generated to delineate the neuronal soma (Figure 2.1F). When either a proximal dendrite or an axon extending from the soma was present in the image, the cell body outline was discontinued immediately prior to this outward protrusion in the outline (e.g., Figure 2.2C2, D2). Consequently, the reported somatic perimeter was, on average, slightly underestimated relative to true somatic perimeter. The somatic outline was then superimposed onto the binary GLT1 image, also in a 130 nm pixel resolution. Neurons were excluded from analysis if more than 15% of the area within the cell body outline was positive for GLT1, which suggested the possibility of an overabundance of non-specific staining. The combined GLT1/cell body outline image produced a visualization of both the somatic perimeter in apposition with GLT1 (red) and the perimeter not in apposition with GLT1 (blue) (Figure 2.1G). GLT1 and the somatic perimeter outline were judged to be in apposition when pixels containing respective markers were directly adjacent to each other without any gap. Several measurements were taken from this perimeter using the Simple Neurite Tracer plugin for ImageJ (Longair et al., 2011): total perimeter length, number of discrete GLT1 appositions, average apposition length, and percent apposition.

2.3 METHODS: ELECTROPHYSIOLOGY EXPERIMENTS

2.3.1 ANIMALS

All procedures were conducted in accordance with the Canadian Council on Animal Care and were approved by the Memorial University Institutional Animal Care Committee. Male Sprague Dawley rats were obtained from the breeding colony at Memorial University or from Charles River Canada (St. Constant, QC, Canada). Animals were housed in pairs under a 12 h light/12 h dark cycle (lights on at 08:00) in a colony room. Food and water were available ad libitum. Experiments were performed on brain slices from rats aged 29 to 58 days old.

Rats were randomly assigned to one of two treatment groups at 08:00, and individually housed during behavioural treatment; one group underwent 6 h of sleep opportunity (Rest), and the other was subjected to 6 h of SD by gentle handling as previously described (Deurveilher et al., 2011). Both groups were euthanized immediately after the respective conditions at 14:00 for generating brain slices (see below). A total of 171 cells from 94 rats were included in the analyses reported in this study.

2.3.2 IN VITRO ELECTROPHYSIOLOGY

Rats were deeply anesthetized with isoflurane and decapitated, and brains were quickly removed. Coronal brain slices (250 µm thick) through the hypothalamus were cut in ice-cold artificial cerebrospinal fluid (ACSF) containing (in mM): 126 NaCl, 2.5 KCl, 1.2 NaH2PO4, 1.2 MgCl2, 18 NaHCO3, 2.5 glucose, 2 CaCl2. Slices were then incubated in ACSF at 33-34 °C for 30-45 mins and then at room temperature until recording. ACSF was continuously bubbled with O2 (95%) and CO2 (5%).

Patch-clamp recordings were performed on hemisected hypothalamic slices superfused with 30-34 °C ACSF at 2-2.5 ml/min. Under a differential interference contrast microscope (DM LFSA; Leica Microsystems), LH neurons that were located dorsomedial to the fornix and had a soma diameter of 10-20 µm were selected for recording. Recordings were performed using a Multiclamp 700B amplifier and pClamp

10.3 software (Molecular Devices, Sunnyvale, CA). The whole-cell internal solution contained (in mM): 123 potassium gluconate, 2 MgCl2, 8 KCl, 10 Hepes, 0.2 EGTA, 5 Na2-ATP, 0.3 Na2-GTP, adjusted to pH 7.29-7.30 with KOH. Biocytin (0.1-0.2%) was added to the internal solution to label recorded cells. Filled recording electrodes had a tip resistance of 3-7 MΩ.

Once whole-cell access was achieved, a series of hyperpolarizing and depolarizing current steps (300 or 600 ms each) was applied to the cell to characterize its electrophysiological properties. ORX and MCH neurons, which have overlapping anatomical distributions, were tentatively identified by their well-established electrophysiological properties. ORX neurons are spontaneously active, have a depolarized resting membrane potential (RMP), display H-current when hyperpolarized, display rebound depolarization when hyperpolarizing current is removed, and have a uniphasic afterhyperpolarizing potential (Eggermann et al., 2003; Parsons et al., 2012b; Linehan et al., 2015). MCH neurons are not spontaneously active in vitro, have a hyperpolarized RMP, lack H-current and rebound depolarization, and display spike-adaptation upon positive current injection (Alberto et al., 2011). A subset of cells was filled with biocytin and the brain slices were processed for post-hoc immunohistochemistry to confirm the neurochemical identity of recorded cells (see below).

For EPSC recording, neurons were held at -70 mV and membrane currents were filtered at 1 kHz, digitized at 5-10 kHz and stored for offline analysis. Picrotoxin (50 μM) was always present in the bath to block GABAA receptors and isolate EPSCs. In order to study evoked EPSCs (eEPSCs), a bipolar tungsten stimulating electrode was placed within the LH lateral to the recorded cell. Paired pulses were applied at 25 Hz every 15 s, and PPR was calculated as the amplitude of eEPSC2/eEPSC1. The rate of decay (τ) was measured by fitting a single exponential curve to the decay slope of eEPSC1. Train stimulation consisted of 20 pulses at 50 Hz every 30 s. The amplitude of the fast eEPSCs with peaks within 10 ms following each pulse was measured, along with the amplitude of the slow EPSC, measured at 25 ms after the final stimulation artifact, and the subsequent area of the slow EPSC for 750 ms. A 20-mV hyperpolarizing pulse (100 ms) was applied every 15-30 s, and the steady-state and capacitive currents were monitored as measures of

input resistance and series/access resistance, respectively. Cells that showed significant change (>20%) in these parameters during electrophysiological recordings were excluded from analysis.

Recordings were performed during the remainder of the light phase, and were discontinued prior to the beginning of the dark phase at 20:00. Neither time-since-dissection (Appendix B), nor age of the rat (Appendix C), were correlated with measures in this study.

2.3.3 Post-hoc Immunohistochemistry

Immediately following recording, brain slices containing biocytin-filled cells were placed in 10% formalin and fixed for >24 h at 4 °C. To confirm the transmitter phenotypes of recorded cells, fixed slices were individually incubated with a cocktail of goat anti-orexin A (1:2000; same as above) and rabbit anti-MCH (1:2000; same as above) antibodies for 3 days at 4 °C. Next, slices were incubated with secondary antibodies (1:500; Alexa 594-conjugated donkey anti-goat IgG, and Alexa 488-conjugated donkey anti-rabbit IgG) as well as Alexa 350-conjugated streptavidin to visualize biocytin in recorded cells. Stained slices were examined with an epifluorescence microscope to examine for co-localization of orexin A or MCH with biocytin. Immunohistochemical phenotype confirmed the electrophysiological phenotype in >90% of neurons examined.

2.3.4 Drugs

All drugs were bath-perfused at final concentrations indicated, by diluting stock solutions in the ACSF immediately before use. Picrotoxin and biocytin were purchased from Sigma Aldrich Canada (Oakville, ON, Canada), and DHK, CPPG and L-AP4 from Tocris Bioscience (Minneapolis, MN).

2.3.5 Data Analysis

eEPSCs were analyzed using Clampfit 10.3 software (Molecular Devices, Sunnyvale, CA). Statistical analyses were conducted with GraphPad Prism 6 (GraphPad Software, La Jolla, CA). Independent t-tests were used to compare means between sleep

state conditions (Rest or SD) within each neuronal population. Linear regressions were performed to examine correlations between variables. eEPSC amplitude and paired pulse ratio (PPR) during baseline and peak drug effect were compared using paired t-tests for single drug conditions, and using one-way repeated measures ANOVA when multiple drugs were applied sequentially to the same cell. For group comparisons of drug effects, the drug effect was normalized to its respective baseline for each cell, and then compared using a one-way ANOVA for comparisons within sleep state conditions, and using independent t-tests when comparing between sleep history conditions. When sleep conditions were compared in the 20 pulses x 50 Hz experiments, a mixed model ANOVA was used; when baseline was compared to the drug effect within a sleep condition, a two-way repeated measures ANOVA was used. The Holm-Sidak post hoc test was used for all multiple comparisons. P values < 0.05 were considered statistically significant. Values are expressed as means ± SEM.

2.4 RESULTS

2.4.1 ACUTE SD BIDIRECTIONALLY ALTERS PERISOMATIC GLT1 APPOSITION WITH ORX AND MCH NEURONS

We used confocal microscopy to examine the immunohistochemical juxtaposition of GLT1 (Figure 2.1) with LH and BF neurons following acute (6 h) SD and in a time-matched undisturbed control group that was mainly asleep as typical of nocturnal rodents in the light phase (Rest). In addition to ORX and MCH neurons in the LH, we analyzed cholinergic (ChAT) and parvalbumin (PV)-containing GABAergic neurons in the BF for comparison. Unlike ORX and MCH neurons, they are both active during wake and rapid eye movement (REM) sleep (Duque et al., 2000; Manns et al., 2000; Hassani et al., 2009a; Kim et al., 2015). GLT1 immunoreactivity was present in juxtaposition with every soma from all four neuronal populations (Figure 2.2A-D).

SD had no effect on the somatic perimeter length of these neurons (n = 59-135/treatment group/neuron type; Figure 2.2E and Table 2.1) or the number of discrete GLT1 appositions with their somata compared to Rest (Figure 2.2F and Table 2.1). In contrast, SD altered the mean length of each GLT1 apposition with ORX and MCH

neurons in an opposite direction (Figure 2.2G and Table 2.1). Consequently, the percentage of the total somatic perimeter in apposition with GLT1 was reduced by 10.1 % in ORX neurons ($P = 0.0281$, unpaired t-test), and increased by 15.9 % in MCH neurons ($P = 0.0210$, unpaired t-test; Figure 2.2H and Table 2.1). Linear regression analyses confirmed that mean length of individual GLT1 appositions was the best predictor of total percent GLT1 apposition regardless of sleep history (Figure 2.3). Unlike LH neurons, there was no change in these measures in ChAT and PV neurons in the BF (Figure 2.2G, H and Table 2.1), indicating that the changes in GLT1 apposition are specific to neuron type and brain region.

Next, we asked whether the changes in GLT1 apposition with ORX and MCH neurons observed after SD were reversible. After an additional 3 h period of sleep opportunity following 6 h of SD (Recovery), no GLT1 apposition measure was significantly different from that obtained from time-matched Rest animals (extended Rest, or ER; n = 62-82/treatment group/neuronal type), indicating that the SD-induced changes in GLT1 apposition are reversible (Figure 2.4 and Table 2.2).

These data indicate that 6 h of SD results in opposite and reversible changes in the extent of GLT1 surrounding the somata of ORX vs. MCH neurons, via shortening or lengthening of individual GLT1 appositions without changing their numbers.

2.4.2 GLT1 Facilitates Excitatory Transmission to ORX Neurons by Preventing Activation of Presynaptic Group III mGluRs

To determine the physiological consequences of SD-dependent GLT1 apposition dynamics in LH neurons, we conducted patch-clamp recordings, initially under the Rest condition. First, to investigate the role of GLT1 in glutamatergic transmission to ORX neurons, we tested the effects of the GLT1-specific inhibitor dihydrokainate (DHK) in hypothalamic slices obtained from undisturbed rats (Rest). DHK (100 μM) reduced the amplitude of evoked excitatory postsynaptic currents (eEPSCs) by 46% ($n = 8$, $P = 0.0009$, paired t-test; Figure 2.5A, F) while increasing paired pulse ratio (PPR; $P < 0.0001$, paired t-test; Figure 2.5A, G), indicating a decrease in presynaptic release probability. It had no effect, however, on the decay rate of eEPSCs (Figure 2.5B). A decrease in glutamate clearance may result in activation of presynaptic receptors such as

inhibitory group III metabotropic glutamate receptors (mGluRs) known to be expressed by glutamatergic afferents to ORX neurons (Acuna-Goycolea et al., 2004). We therefore examined whether these mGluRs mediate the observed presynaptic inhibition. Indeed, pre-treatment with the group III mGluR antagonist CPPG (200 μM) prevented the effects of DHK on both eEPSC amplitude (n = 5, P = 0.0690, paired t-test; Figure 2.5C, F) and PPR (P = 0.1664, paired t-test; Figure 2.5G). Furthermore, the group III mGluR agonist L-AP4 (50 μM) mimicked and occluded the effects of DHK on eEPSC amplitude (n = 7, one-way repeated measures ANOVA, baseline vs. L-AP4, P = 0.0014; L-AP4 vs. L-AP4+DHK, P = 0.3525; Figure 2.5D, F) and PPR (one-way repeated measures ANOVA, baseline vs. L-AP4, P = 0.0247; L-AP4 vs. L-AP4+DHK, P = 0.9366; Figure 2.5G).

Collectively these data show that blocking GLT1 results in the activation of inhibitory presynaptic group III mGluRs, indicating that GLT1 normally prevents the activation of these receptors and consequently facilitates glutamatergic synaptic transmission to ORX neurons. In addition, under Rest conditions glutamate clearance by GLT1 appears to be efficacious at completely preventing the activation of these presynaptic receptors, as CPPG alone had no effect on eEPSC amplitude (n = 8, P = 0.4646, paired t-test; Figure 2.5E, F) or PPR (P = 0.9794, paired t-test; Figure 2.5G).

2.4.3 SD Reduces Release Probability at Glutamatergic Synapses to ORX Neurons

We next investigated the effect of SD on excitatory transmission using hypothalamic slices from rats that underwent 6 h of SD. We found that SD increased PPR relative to the Rest condition (n = 43 cells for Rest, and n = 31 cells for SD; P = 0.0066, unpaired t-test; Figure 2.6A), suggesting that SD decreases the release probability of glutamatergic synapses to ORX neurons. This appears to be due to tonic presynaptic inhibition via the activation of group III mGluRs, as CPPG alone increased eEPSC amplitude (n = 11, P = 0.0456, paired t-test; Figure 2.6B, E) and decreased PPR (P = 0.0094, paired t-test; Figure 2.6C, E). This contrasts with a lack of CPPG effect in Rest (Figure 2.6B, C). The GLT1 blocker DHK reduced eEPSC amplitude under SD (n = 7, P = 0.0185, paired t-test; Figure 2.6B, F) again via group III mGluRs, as it was prevented by pre-treatment with CPPG (n = 6, CPPG alone vs. CPPG+DHK, P = 0.1018, paired t-

test; Figure 2.6E). However, the DHK effect on eEPSC amplitude and PPR was significantly attenuated by SD (n = 8 cells for Rest, and n = 7 cells for SD; Δ eEPSC amplitude, P = 0.0189; Δ PPR, P > 0.0001, unpaired t-tests; Figure 2.6B, C). There was no significant effect of DHK on the decay rate of eEPSCs under SD (Figure 2.6D).

Together, these data indicate that SD reduces the release probability of excitatory synapses to ORX neurons. This is due to reduced efficacy of GLT1 in preventing tonic activation of the inhibitory group III mGluRs, which is consistent with the reduction in GLT1 appostion with ORX neurons under the SD condition.

2.4.4 SD Reduces Synaptic Depression of Fast Glutamatergic Transmission to ORX neurons: GLT1-Dependent Metaplasticity

It is possible that SD-induced changes in the glutamate-clearing efficacy of GLT1 are more pronounced during intense synaptic activation, as a greater amount of glutamate will be released at the synapse. To test this possibility, we employed a train-stimulation protocol (20 pulses at 50 Hz) under both Rest and SD conditions. In the Rest condition train stimulation induced strong short-term synaptic depression in ORX neurons, which was significantly attenuated after SD (n = 12 cells for Rest, and n = 13 cells for SD; P = 0.0006 for sleep state, mixed model ANOVA; Figure 2.7A). This SD effect was reversed by CPPG (n = 5, P = 0.0059 for drug x time interaction; Figure 2.7B) while mimicked by DHK (10 μM) in the Rest condition (n = 5, P = 0.0012 for drug effect, 2-way repeated measures ANOVA; Figure 2.7C).

These data demonstrate that SD results in attenuation, relative to the Rest condition, of activity dependent short-term synaptic depression in ORX neurons. This metaplasticity involves GLT1 and presynaptic group III mGluRs.

2.4.5 SD Reduces a Slow EPSC in MCH Neurons

Our quantitative immunohistochemical study indicated that GLT1 apposition with MCH neurons was reduced by SD, a change in the opposite direction compared to ORX neurons (Figure 2.2G, H). We therefore asked whether SD also had the opposite effect on fast excitatory transmission to MCH neurons. In these neurons, SD had no effect on PPR

(n = 38 for Rest, and n = 13 for SD; P = 0.7391, unpaired t-test; Figure 2.8A). Furthermore, DHK failed to alter the amplitude (n = 10, P = 0.7915, paired t-test; Figure 2.8B, C), PPR (P = 0.2420, paired t-test; Figure 2.8D), or the decay constant of fast eEPSCs (Figure 2.8E).

During a train stimulation (20 pulses at 50 Hz), it was apparent that EPSCs consisted of a fast and a slow component in MCH neurons (Figure 2.8F). Fast EPSCs immediately followed each stimulation with fast decay, while a slow inward current accumulated with repeated stimuli and persisted up to 500 ms beyond the train stimulation (Figure 2.8F), consistent with a previous report (Huang and van den Pol, 2007). The amplitude of fast EPSCs displayed an initial transient synaptic facilitation, which was not affected by SD (n = 5 for Rest, and n = 5 for SD; P = 0.9018 for sleep state, mixed-model ANOVA; Figure 2.8G). In contrast, the slow EPSC was decreased by SD in both amplitude (n = 12 for Rest, and n = 9 for SD; P = 0.0021, unpaired t-test; Figure 2.8H) and area (n = 12 for Rest, and n = 9 for SD; P = 0.0159, unpaired t-test; Figure 2.8I). The slow EPSC component was present but much smaller in ORX neurons under the Rest condition, and there was no change after SD (n = 11 for Rest, and n = 15 for SD; P = 0.9907, unpaired t-test; Figure 2.9).

These results indicate that the altered GLT1 apposition with MCH neurons after SD may directly affect the postsynaptic response without involving presynaptic mechanisms. Thus, the opposite changes in GLT1 apposition with ORX and MCH neurons in SD vs. Rest do not translate to opposite functional consequences via the same mechanisms.

2.5 DISCUSSION

We demonstrate that acute (6 h) SD induces reversible and cell type-specific changes in GLT1 apposition with sleep/wake-regulatory neurons in the LH, resulting in distinct functional plasticity of excitatory synapses to these neurons (Figure 2.10). Immunomicroscopically, perisomatic GLT1 apposition decreased in ORX neurons and increased in MCH neurons following SD. These changes were reversed by a subsequent brief (3 h) period of sleep opportunity, demonstrating that GLT1 remodeling is rapid and dynamic, occurring on the order of hours. The bidirectional changes in GLT1 apposition

in ORX and MCH neurons after SD is somewhat surprising as these neurons have overlapping perikaryal distributions within the LH (Hahn, 2010), and receive monosynaptic inputs from similar neuronal groups within the brain (González et al., 2016). ORX neurons in particular have almost six excitatory synapses for every inhibitory synapse on their somata (Horvath and Gao, 2005), indicating that perisomatic changes in GLT1 could have profound effects on excitatory transmission to these neurons. No SD-dependent changes in GLT1 apposition occurred in wake/REM sleep-active cholinergic and PV-containing GABAergic neurons in the BF (Duque et al., 2000; Gritti et al., 2003; Hassani et al., 2009; Kim et al., 2015), indicating that the SD-induced GLT1 plasticity is cell type and region specific. It is possible that the increased activity of these BF neurons not only during wake but also during REM sleep obscures differences in GLT1 apposition in response to Rest vs. SD.

In light of well-documented state-dependent activity profiles of ORX and MCH neurons (Lee et al., 2005; Modirrousta et al., 2005; Hassani et al., 2009b), we infer that in both neuronal populations a decrease in GLT1 apposition occurs after a period (6 h) of increased neuronal activity (i.e., SD for ORX neurons, and Rest for MCH neurons). Two mechanisms could explain this fairly rapid plasticity. First, GLT1 could redistribute within astrocytic processes to change its spatial relationship with neurons at synaptic sites. This is supported by the findings that GLT1 is primarily located in astrocytic membranes facing synapses (Chaudhry et al., 1995), and can diffuse laterally within the astrocytic membrane away from the site of glutamate release (Murphy-Royal et al., 2015). In addition, GLT1 can undergo substrate transport-induced internalization (Nakagawa et al., 2008). Second, changes in GLT1 localization could be explained by structural withdrawal or protrusion of astrocytic processes relative to the synaptic cleft (Pannasch et al., 2014; Perez-Alvarez et al., 2014). In the hippocampus and somatosensory cortex, the motility of distal astrocytic processes increases following the activation of astrocytic group I mGluRs by neuronally released glutamate, thus altering the positioning of astrocytic processes relative to dendritic spines (Perez-Alvarez et al., 2014). Structural remodeling of astrocytes in response to homeostatic signals has also been reported to occur in the supraoptic nucleus (Theodosis and Poulain, 1993). This possibility is consistent with Santiago Ramón y Cajal's conjecture that the "contraction"

and “relaxation” of astrocytic processes regulate synapses to induce or prevent sleep (García-Marín et al., 2007). These two possible mechanisms are not mutually exclusive.

GLT1 activity can shorten the glutamate transient at the synapse and thereby curtail the activation of synaptic and extrasynaptic glutamate receptors (Rusakov and Kullmann, 1998; Oliet et al., 2001; Zheng et al., 2008). However, we found that blocking GLT1 with DHK had no effect on the decay kinetics or amplitude of fast eEPSCs in ORX or MCH neurons in the absence of presynaptic modulation. This apparent lack of effect on synaptic, as opposed to extrasynaptic, receptor activation is similar to that in the hippocampal CA1 region, where glutamate transporters such as GLT1 act mainly to limit glutamate spillover (Isaacson and Nicoll, 1993; Rusakov and Kullmann, 1998) and maintain low tonic levels of extracellular glutamate (Isaacson and Nicoll, 1993; Tanaka et al., 1997). Indeed, our data show that reduced somatic GLT1 apposition with ORX neurons following SD was accompanied by the activation of presynaptic group III mGluR (depicted in Figure 2.10), an effect mimicked in the Rest condition by the GLT1 blocker. In MCH neurons, we found that SD-induced increase in GLT1 apposition was accompanied by the inhibition of a slow EPSC, a current previously identified as being mediated by postsynaptic group I mGluRs and sensitive to changes in glutamate transport (Huang and van den Pol, 2007). Therefore, we conclude that the role of GLT1 for these LH neurons is to regulate the activity of extrasynaptic glutamate receptors.

One consequence of unmasking presynaptic inhibition in SD for ORX neurons is modulation of short-term synaptic depression. In the Rest condition, glutamatergic transmission to ORX neurons was most effective at low frequency, essentially acting as a low-pass filter. This type of synapse could potentially activate ORX neurons through relatively low activity levels thereby facilitating transitions from sleep to wakefulness should even sparse arousal-promoting signals arrive from other brain regions (Sakurai et al., 2005; Yoshida et al., 2006) or local neurons (Li et al., 2002; Acuna-Goycolea et al., 2004) including ORX neurons, which are known to co-release glutamate (Yamanaka et al., 2010). However, following SD, release probability at this synapse decreases due to unmasking of group III mGluR-mediated presynaptic inhibition, making it less prone to synaptic fatigue while sparse signals are selectively suppressed. This may be a synaptic correlate of sleepiness, or an increase in homeostatic drive for transition to sleep, where

stronger (high-frequency) wake-promoting signals to ORX neurons are necessary for these neurons to maintain and stabilize the wake state via reinforcement of other wake-promoting systems (Hagan et al., 1999; Saper et al., 2010).

Unlike ORX neurons, the sleep history-dependent synaptic modulation in MCH neurons does not appear to involve presynaptic mechanisms. The magnitude of slow EPSCs induced by train stimulation decreased following SD, likely a direct result of reduced glutamate spillover onto postsynaptic group I mGluRs, since GLT1 apposition with MCH neurons increased in this condition. Intriguingly, these changes are in keeping with maintenance of the wake state during SD, as less excitatory signal to MCH neurons would hinder sleep. We speculate that in MCH neurons, the astrocytic correlate of homeostatic drive for sleep might be found in their inhibitory, rather than excitatory, inputs such as those from ORX neurons (Apergis-Schoute et al., 2015) and from stress-related GABAergic limbic neurons (González et al., 2016).

2.6 CONCLUSIONS

In conclusion, our study demonstrates that via GLT1, astrocytes can regulate the activity of wake- and sleep-promoting LH neurons in a cell-type specific and reversible manner in response to acute sleep loss. In ORX neurons, SD reduced GLT1 apposition and the efficacy of glutamate clearance via GLT1, resulting in presynaptic inhibition and metaplasticity at glutamatergic synapses via activation group III mGluRs. These changes are consistent with a role for GLT1 and group III mGluRs in the homeostatic regulation of sleep/wake states. In contrast, in MCH neurons, SD increased GLT1 apposition and inhibited a slow EPSC. Thus, MCH neurons receive strong excitatory signals during sleep and less during wake, which may permit wake maintenance despite increasing sleep drive during SD. These consequences of SD are consistent with a role for GLT1 in both homeostatic and non-homeostatic regulation of sleep and wake states. This GLT1-mediated plasticity in LH neurons revealed by forced wakefulness is expected to be similarly involved in the regulation of spontaneous sleep/wake cycles.

Figure 2.1. Image analysis procedures for GLT1 apposition. (A) A triple-fluorescence image of an ORX neuron (green) surrounded by GLT1 immunoreactivity (red). The ORX neuron is fluorescent Nissl-stained (blue). Scale bar: 10 μm. (B) Grayscale image of the somatic markers (combined orexin A and fluorescent Nissl). (C) Grayscale image of GLT1 immunoreactivity. Both grayscale images are then converted to binary images, where black pixels represent areas positive for fluorescence, using a threshold formula (See Section 2.2.5). (D) The binary image for somatic markers. (E) The binary image for GLT1. A one pixel-wide outline is generated to delineate the neuronal soma (F). This outline is superimposed onto the binary image representing GLT1 immunoreactivity (G), revealing the portions of the somatic perimeter in direct apposition (i.e., without any pixel gap) with GLT1 (red) and those that are not (blue).

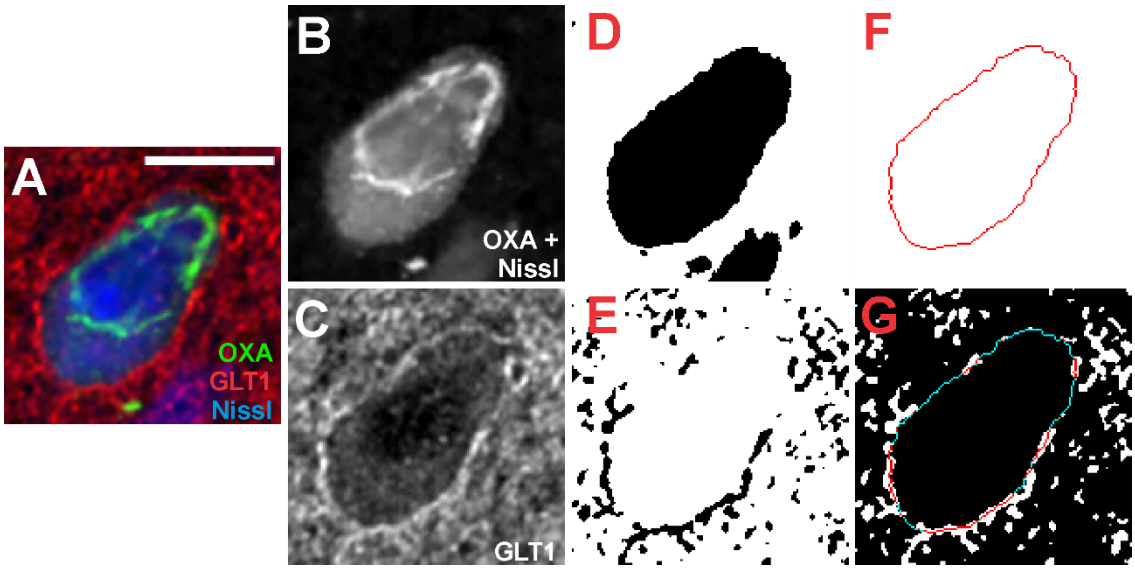
A
OXA
GLT1
Nissl
B
OXA +
Nissl
C
GLT1
D
E
F
G

Figure 2.2. Sleep deprivation (6 h) alters somatic GLT1 apposition with ORX and MCH neurons, but not ChAT or PV neurons. (A-D) Fluorescence images showing an ORX neuron (A1), an MCH neuron (B1), a ChAT neuron (C1), or a PV neuron (D1) with somatic apposition with GLT1. Binary images (A2 - D2) display pixels positive for GLT1 immunoreactivity (white) with overlaid somatic perimeters. Perimeter segments in red are directly juxtaposed with GLT1 immunoreactivity and perimeter segments in blue are negative for GLT1 apposition. Scale bar: 10 μm. (E) Total somatic perimeter length is unaffected by sleep state. (F) Number of GLT1 appositions is unaffected by sleep state. (G) Mean length of GLT1 apposition by sleep state. There are opposite changes following SD in ORX vs. MCH neurons. No change is seen in ChAT and PV neurons. (H) Percent somatic apposition with GLT1 by sleep state. There are opposite changes following SD in ORX vs. MCH neurons, consistent with the opposite changes in mean apposition length (G). Responses are normalized to their respective mean in Rest (represented by the dashed line at 100%). R: Rest condition, SD: 6h sleep deprivation. *$P < 0.05$.

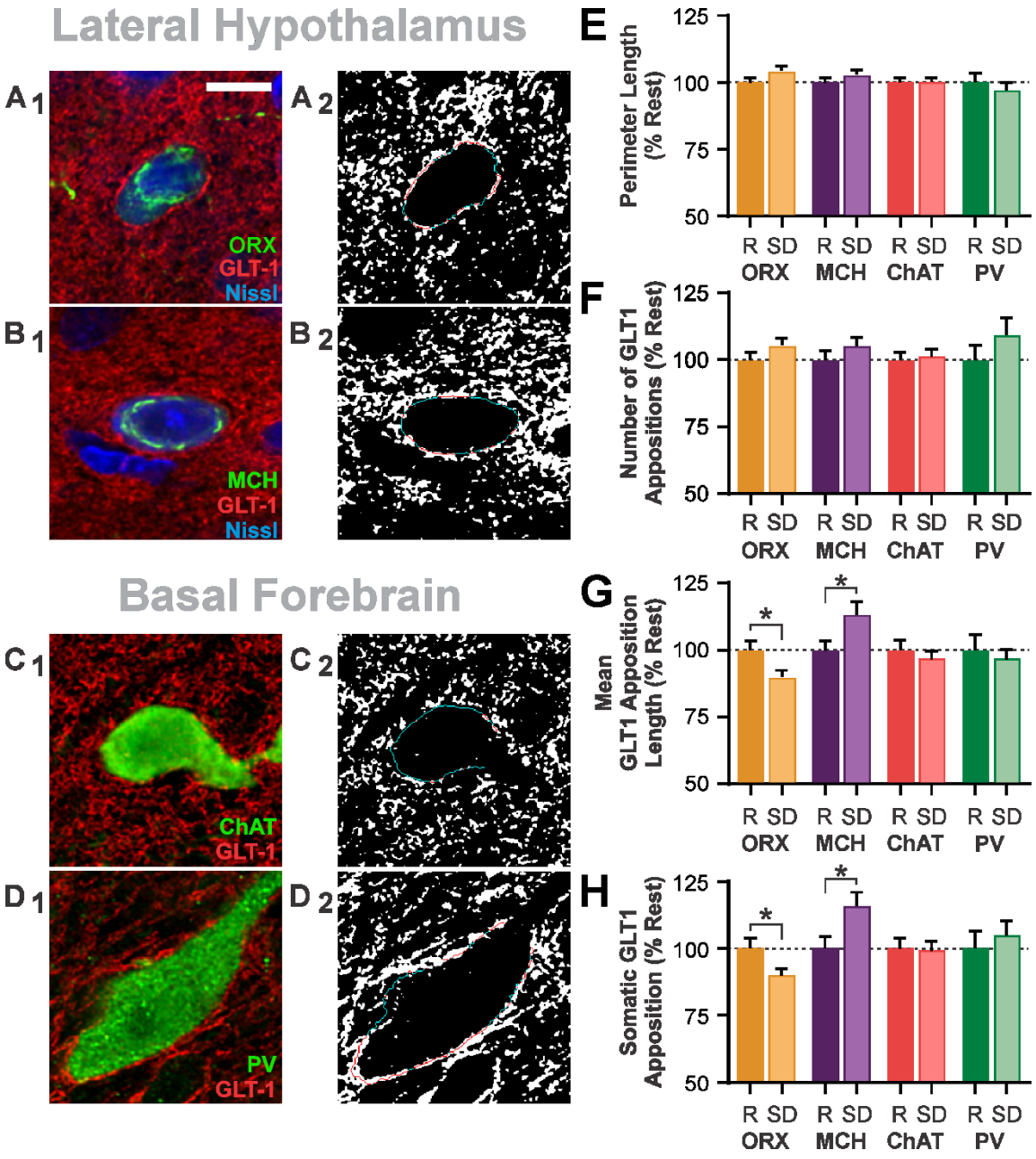
Lateral Hypothalamus
A 1
A 2
ORX
GLT-1
Nissl
B 1
B 2
MCH
GLT-1
Nissl
Basal Forebrain
C 1
C 2
ChAT
GLT-1
D 1
D 2
PV
GLT-1
E
Perimeter Length (% Rest)
125
100
75
50
R SD R SD R SD R SD
ORX MCH ChAT PV
F
Number of GLT1 Appositions (% Rest)
125
100
75
50
R SD R SD R SD R SD
ORX MCH ChAT PV
G
Mean GLT1 Apposition Length (% Rest)
*
*
125
100
75
50
R SD R SD R SD R SD
ORX MCH ChAT PV
H
Somatic GLT1 Apposition (% Rest)
*
*
125
100
75
50
R SD R SD R SD R SD
ORX MCH ChAT PV

Figure 2.3. Correlation analyses of GLT1 apposition measures, indicating that mean contact length is the best predictor of percent apposition in LH neurons. (A,D) Correlations between percent apposition and perimeter length. There is no correlation between these measures for ORX (A) or MCH (D) neurons. (B,E) Correlations between percent apposition and number of GLT1 appositions. There is a positive correlation between these measures for ORX (B) and MCH (E) neurons independent of sleep history. (C,F) Correlations between percent apposition and mean apposition length. There is a positive correlation between these measures for ORX (C) and MCH (F) neurons independent of sleep history. Mean apposition length best accounts for the variation in percent apposition.

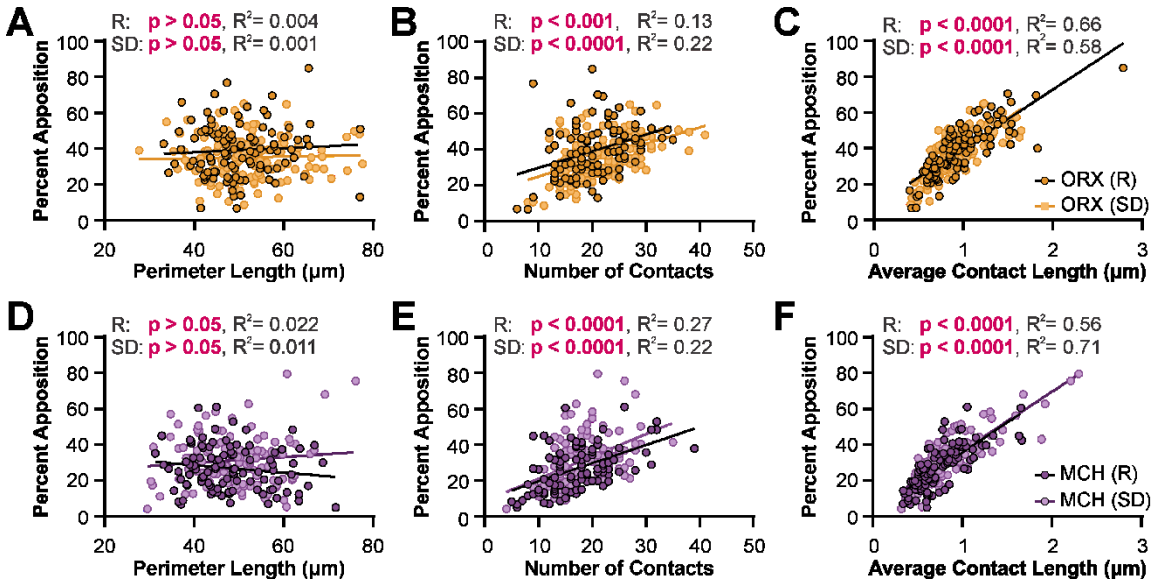
A
R: p > 0.05, R²= 0.004
SD: p > 0.05, R²= 0.001
Percent Apposition
Perimeter Length (µm)
B
R: p < 0.001, R²= 0.13
SD: p < 0.0001, R²= 0.22
Percent Apposition
Number of Contacts
C
R: p < 0.0001, R²= 0.66
SD: p < 0.0001, R²= 0.58
Percent Apposition
Average Contact Length (µm)
ORX (R)
ORX (SD)
D
R: p > 0.05, R²= 0.022
SD: p > 0.05, R²= 0.011
Percent Apposition
Perimeter Length (µm)
E
R: p < 0.0001, R²= 0.27
SD: p < 0.0001, R²= 0.22
Percent Apposition
Number of Contacts
F
R: p < 0.0001, R²= 0.56
SD: p < 0.0001, R²= 0.71
Percent Apposition
Average Contact Length (µm)
MCH (R)
MCH (SD)

Figure 2.4. A 3 h period of sleep opportunity (Recovery, Rec) subsequent to 6 h of SD reverses the effects of SD on GLT1 apposition with ORX and MCH neurons. Extended Recovery (ER) represents the time-matched control group that was left undisturbed during the same period (9 h). (A) Sleep state condition has no effect on somatic perimeter length. (B) Sleep state condition has no effect on number of GLT1 appositions. (C) There is no longer a difference in average GLT1 apposition length following recovery. (D) Following recovery, there is no longer a significant difference in percent somatic apposition with GLT1 relative to the time-matched ER condition. Responses are normalized to their respective mean in ER (represented by the dashed line at 100%).

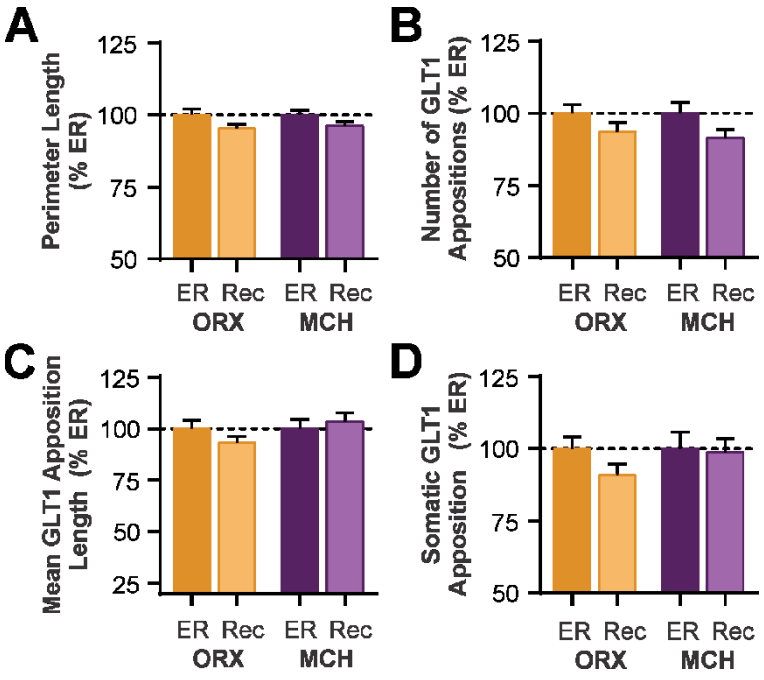
A
Perimeter Length (% ER)
125
100
75
50
ER Rec ER Rec
ORX MCH
B
Number of GLT1 Appositions (% ER)
125
100
75
50
ER Rec ER Rec
ORX MCH
C
Mean GLT1 Apposition Length (% ER)
125
100
75
50
25
ER Rec ER Rec
ORX MCH
D
Somatic GLT1 Apposition (% ER)
125
100
75
50
ER Rec ER Rec
ORX MCH

Figure 2.5. GLT1 prevents the activation of inhibitory presynaptic group III mGluRs in glutamatergic synapses to ORX neurons in the Rest condition. (A) Left: Representative time-effect plot showing the inhibitory effect of DHK (100 μM) in an ORX neuron under Rest. Right: Averaged traces at baseline (a) and during DHK (b), and those scaled to the first EPSC and superimposed show changes in eEPSC amplitude and paired pulse ratio (PPR). (B) DHK has no effect on the decay rate of eEPSCs in Rest. (C) Representative time-effect plot demonstrating that CPPG (200 μM) prevents the effects of DHK in an ORX neuron. (D) Representative time-effect plot showing that L-AP4 (50 μM) mimics and occludes the DHK effects in an ORX neuron. (E) Representative time-effect plot showing that CPPG alone has no effect on an ORX neuron from Rest. (F and G) Bar graphs illustrating the relative changes in eEPSC amplitude (E) and PPR (F) across drug conditions. ‡ $P < 0.05$, ‡‡ $P < 0.01$, ‡‡‡ $P < 0.001$, ‡‡‡‡ $P < 0.0001$ compared to their respective baseline; **$P < 0.01$, ***$P < 0.001$.

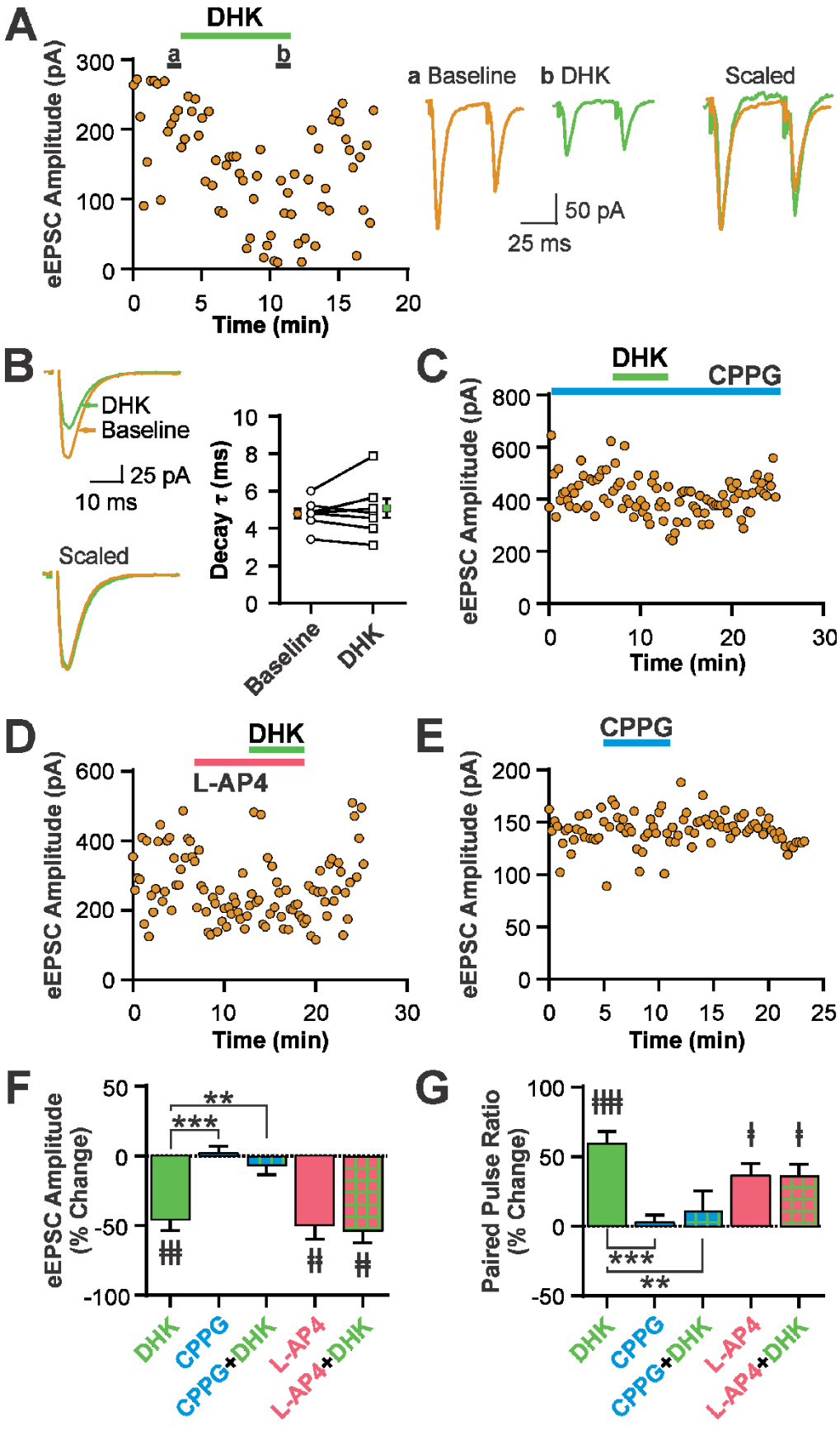
A
DHK
a
b
eEPSC Amplitude (pA)
300
200
100
0
0
5
10
15
20
Time (min)
a Baseline
b DHK
Scaled
50 pA
25 ms
B
DHK
Baseline
25 pA
10 ms
Scaled
Decay τ (ms)
10
8
6
4
2
0
Baseline
DHK
C
DHK
CPPG
eEPSC Amplitude (pA)
800
600
400
200
0
0
10
20
30
Time (min)
D
DHK
L-AP4
eEPSC Amplitude (pA)
600
400
200
0
0
10
20
30
Time (min)
E
CPPG
eEPSC Amplitude (pA)
200
150
100
50
0
0
5
10
15
20
25
Time (min)
F
eEPSC Amplitude (% Change)
50
0
-50
-100
**
***
##
#
#
DHK
CPPG
CPPG+DHK
L-AP4
L-AP4+DHK
G
Paired Pulse Ratio (% Change)
100
50
0
-50
###
‡
‡
***
**
DHK
CPPG
CPPG+DHK
L-AP4
L-AP4+DHK

Figure 2.6. Sleep deprivation decreases release probability at glutamatergic synapses to ORX neurons through GLT1 and group III mGluRs. (A) Paired pulse ratio (PPR) in Rest and SD demonstrating that SD decreases release probability. (B-C) Effects of DHK and CPPG on eEPSC amplitude (B) and PPR (C) by sleep condition. The effect of DHK on eEPSC amplitude and PPR is attenuated or abolished in SD compared to Rest. In contrast, CPPG has no effect in Rest, but increases eEPSC amplitude while decreasing PPR in SD, indicating tonic presynaptic inhibition via group III mGluRs specifically in SD. (D) DHK has no effect on the decay rate of eEPSCs in SD. (E) Left: Representative time-effect plot of eEPSC amplitude from SD. Right: Averaged traces from baseline (a), in the presence of CPPG (b), and CPPG plus DHK (c). Baseline and CPPG traces are scaled to the first eEPSC to show the change in PPR. (F) Left: Representative time-effect plot showing the attenuated inhibitory effects of DHK on eEPSCs in an ORX neuron in the SD condition compared to the Rest condition (cf. Figure 2.5A). Right: Averaged traces from baseline (d) and DHK (e). ‡ $P < 0.05$, ‡‡ $P < 0.01$, ‡‡‡ $P < 0.001$, ‡‡‡‡ $P < 0.0001$ compared to their respective baseline. *$P < 0.05$, ** $P < 0.01$, ****$P < 0.0001$.

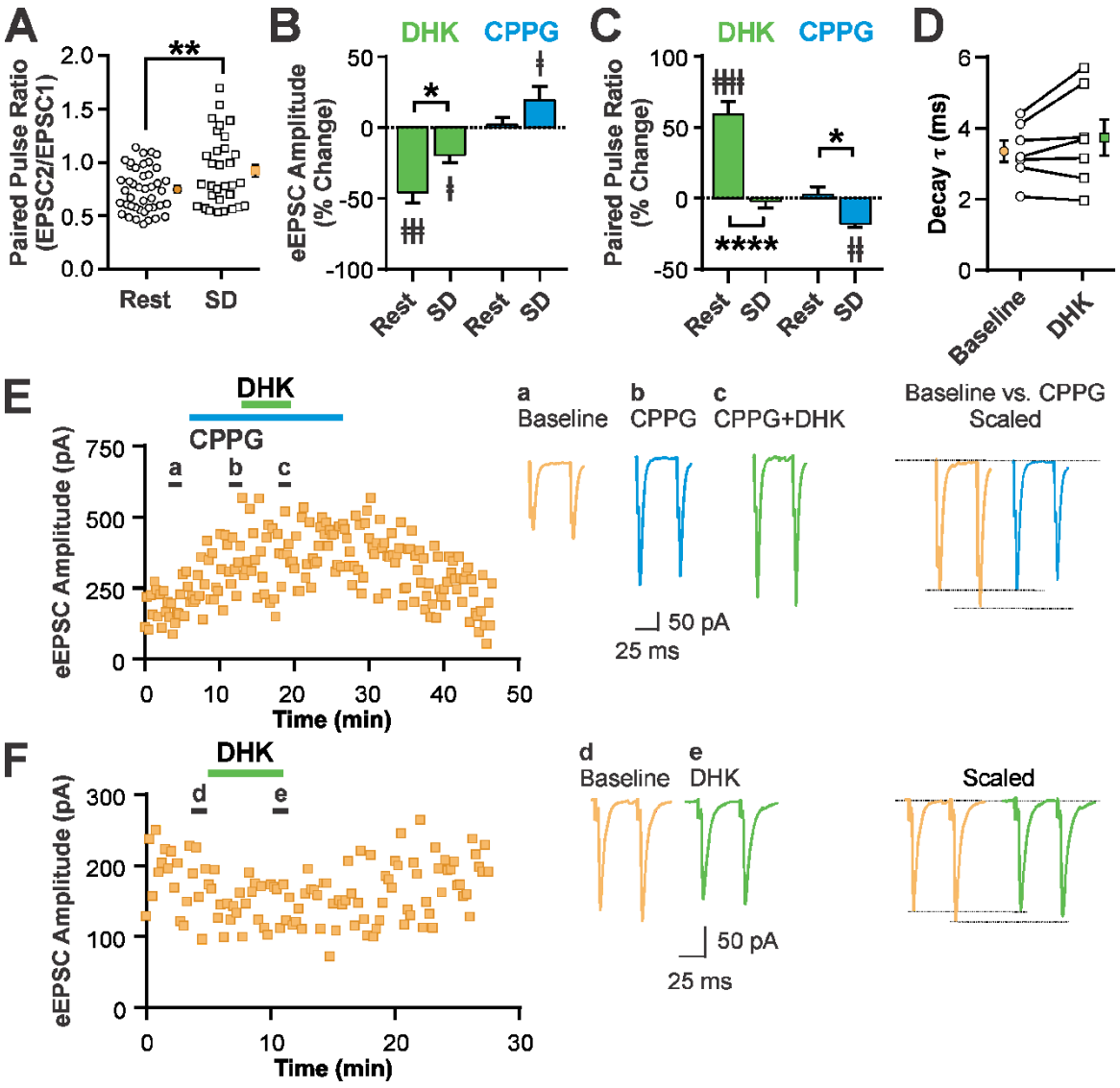
A
Paired Pulse Ratio (EPSC2/EPSC1)
2.0
1.5
1.0
0.5
0.0
**
Rest
SD
B
DHK
CPPG
eEPSC Amplitude (% Change)
50
0
-50
-100
*
Rest
SD
Rest
SD
C
DHK
CPPG
Paired Pulse Ratio (% Change)
100
50
0
-50
*
****
Rest
SD
Rest
SD
D
Decay τ (ms)
6
4
2
0
Baseline
DHK
E
DHK
CPPG
eEPSC Amplitude (pA)
750
500
250
0
a
b
c
0
10
20
30
40
50
Time (min)
a
Baseline
b
CPPG
c
CPPG+DHK
50 pA
25 ms
Baseline vs. CPPG
Scaled
F
DHK
eEPSC Amplitude (pA)
300
200
100
0
d
e
0
10
20
30
Time (min)
d
Baseline
e
DHK
50 pA
25 ms
Scaled

Figure 2.7. Sleep deprivation reduces synaptic depression via GLT1 and group III mGluRs. (A-C) eEPSC amplitude during a train stimulation (20 pulses at 50 Hz), normalized to the amplitude of the first eEPSC (represented by the dashed line at 100%). Differences by sleep condition are shown in panel A. Notice the attenuation in synaptic depression following SD when compared to Rest. In panel B, CPPG (200 μM) shifts the SD response towards the baseline pattern in Rest (cf. panel A). Conversely in panel C, DHK (10 μM) under Rest shifts the response towards the pattern observed under SD (cf. panel A). ‡ $P < 0.05$, ‡‡ $P < 0.01$, ‡‡‡ $P < 0.001$, ‡‡‡‡ $P < 0.0001$ compared to their respective baseline. *$P < 0.05$, ****$P < 0.0001$.

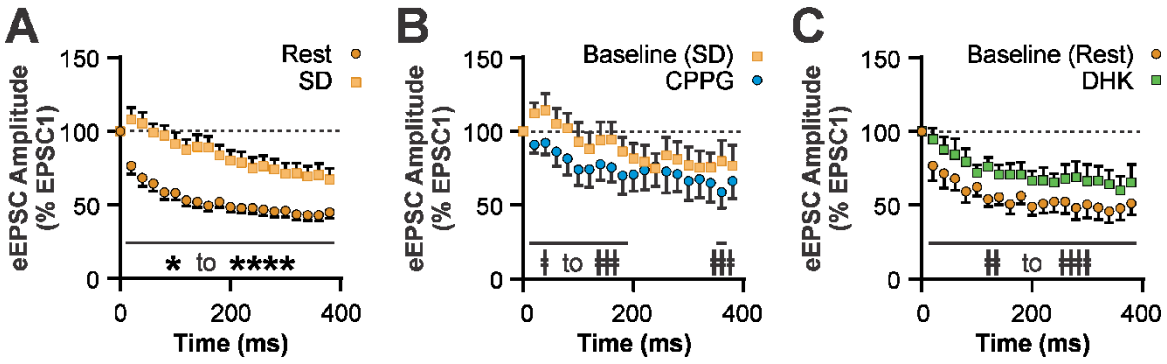
A
Rest
SD
eEPSC Amplitude (% EPSC1)
150
100
50
0
* to ****
0
200
400
Time (ms)
B
Baseline (SD)
CPPG
eEPSC Amplitude (% EPSC1)
150
100
50
0
to
0
200
400
Time (ms)
C
Baseline (Rest)
DHK
eEPSC Amplitude (% EPSC1)
150
100
50
0
to
0
200
400
Time (ms)

Figure 2.8. SD reduces the strength of a slow EPSC induced by train stimulation in MCH neurons independent of presynaptic mechanisms. (A) Paired pulse ratio (PPR) at glutamatergic synapses in MCH neurons by sleep state, demonstrating that SD has no effect on release probability. (B-C) Representative time-effect plot (B) and summary graph (C) showing lack of DHK effect (100 μM) on fast eEPSC amplitude in MCH neurons in Rest. (D, E) DHK has no effect on PPR (D), or the decay rate of eEPSCs (E) in MCH neurons in Rest. (F) Representative scaled average traces from Rest and SD showing fast and slow EPSCs evoked in MCH neurons by train stimulation (20 pulses at 50 Hz). (G) SD has no effect on fast eEPSC amplitude. Responses are normalized to the amplitude of the first fast eEPSC (represented by the dashed line at 100%). (H-I) SD reduces the amplitude (H) and area (I) of the slow EPSC following train stimulation. Responses are normalized to the amplitude of the first fast eEPSC. *$P < 0.05$, **$P < 0.01$.

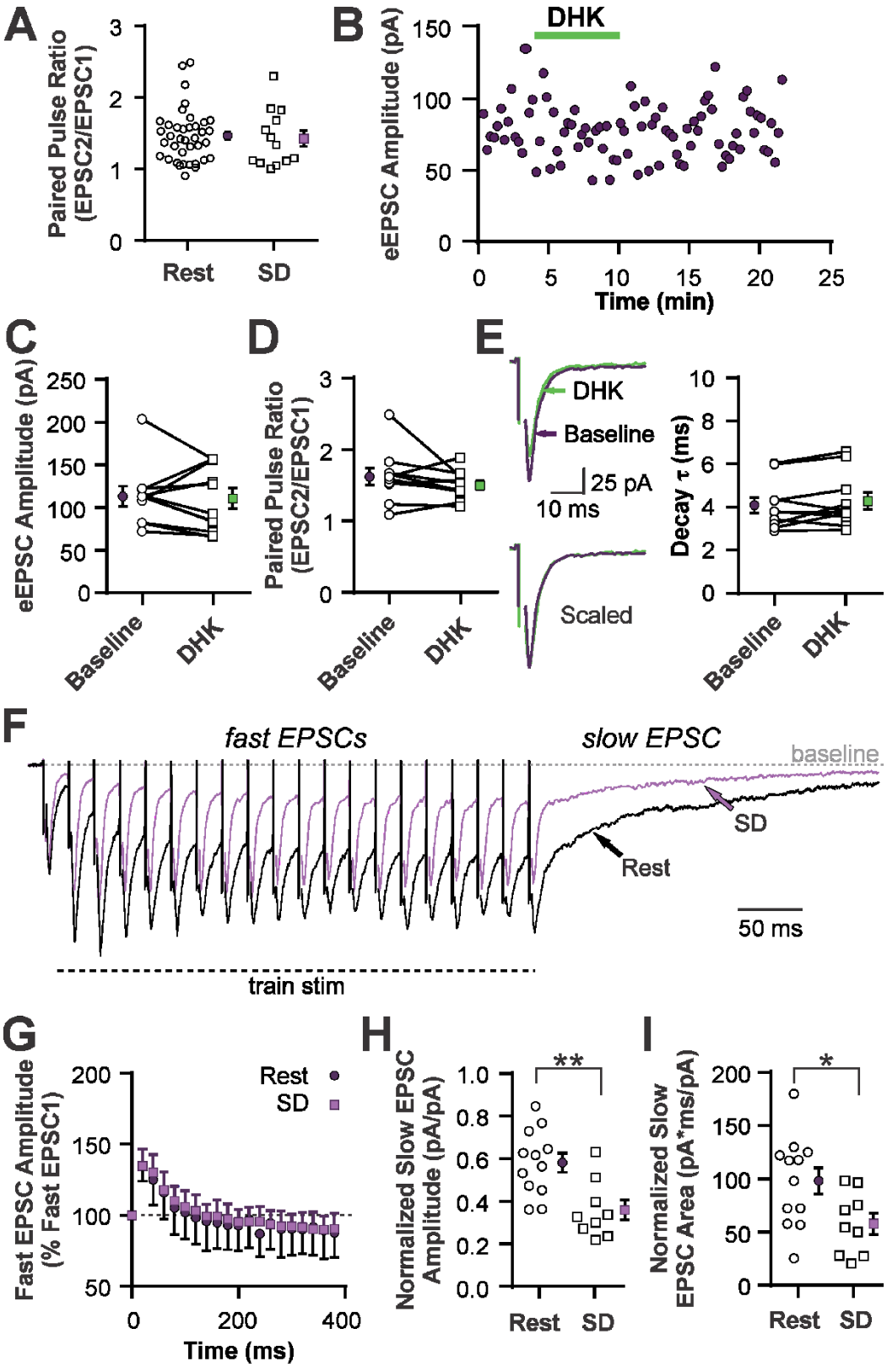
A
Paired Pulse Ratio (EPSC2/EPSC1)
Rest
SD
B
DHK
eEPSC Amplitude (pA)
Time (min)
C
eEPSC Amplitude (pA)
Baseline
DHK
D
Paired Pulse Ratio (EPSC2/EPSC1)
E
DHK
Baseline
25 pA
10 ms
Scaled
Decay τ (ms)
F
fast EPSCs
slow EPSC
baseline
SD
Rest
50 ms
train stim
G
Fast EPSC Amplitude (% Fast EPSC1)
Rest
SD
Time (ms)
H
Normalized Slow EPSC Amplitude (pA/pA)
**
I
Normalized Slow EPSC Area (pA*ms/pA)
*

Figure 2.9. SD has no effect on slow EPSCs in ORX neurons. (A) Representative average traces of the slow inward current induced by train stimulation (20 pulses at 50 Hz) in an ORX neuron from Rest (black) and SD (orange). (B) SD had no effect on the amplitude of this current.

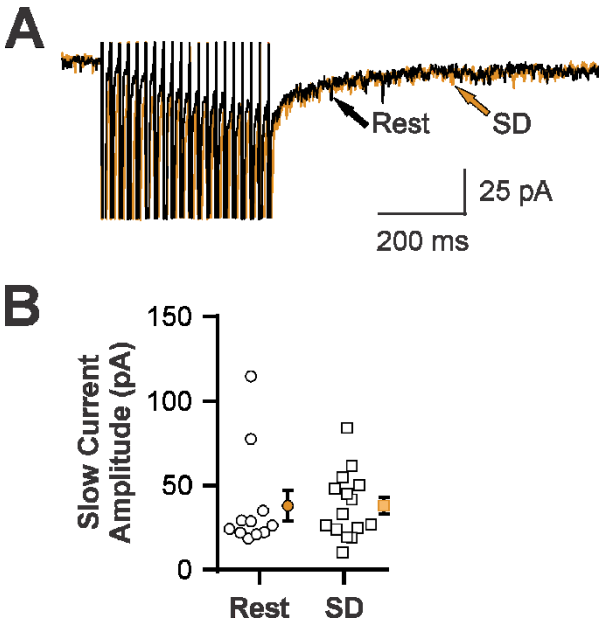
A
Rest
SD
25 pA
200 ms
B
Slow Current Amplitude (pA)
150
100
50
0
Rest
SD

Figure 2.10. Changes in GLT1 apposition with LH neurons have cell type-specific consequences for glutamatergic transmission. **ORX neurons** (wake-active and wake-promoting): Following Rest, a period of neuronal *inactivity* for these neurons, GLT1 apposition is high, limiting glutamate diffusion. There is no detectable activation at presynaptic group III mGluRs under these conditions. When GLT1 is pharmacologically blocked, however, these group III mGluRs are activated, decreasing release probability. GLT1 therefore facilitates excitatory transmission to ORX neurons under Rest, perhaps to expedite transitions to wake. Following SD, a period of neuronal *activity* for these neurons, there is reduced GLT1 apposition. Under these conditions, glutamate diffusion is expected to be greater, causing tonic activation of presynaptic group III mGluRs. This presynaptic inhibition reduces the release probability of excitatory synapses to ORX neurons. Under these conditions, stronger excitatory drive is required to activate ORX neurons, which may represent a synaptic correlate of sleepiness or an increase in homeostatic drive for sleep. **MCH neurons** (REM sleep-active and sleep-promoting): Following Rest, a period of likely neuronal *activity*, GLT1 apposition is low, enabling greater glutamate diffusion. Under these conditions or pharmacological blockade of GLT1, there is no detectable presynaptic inhibition, suggesting that glutamatergic inputs to MCH neurons are not regulated via presynaptic mechanisms as in ORX neurons. However, a large slow EPSC appears following high frequency synaptic activity in these neurons, which may be mediated by ionotropic glutamate receptors (iGluRs) or mGluRs. Following SD, a period of neuronal *inactivity*, this slow EPSC becomes smaller as glutamate diffusion is limited by increased GLT1 apposition. Therefore, in the SD condition excitatory inputs to MCH neurons elicit a weaker response than in the Rest condition, likely permitting wake state maintenance.

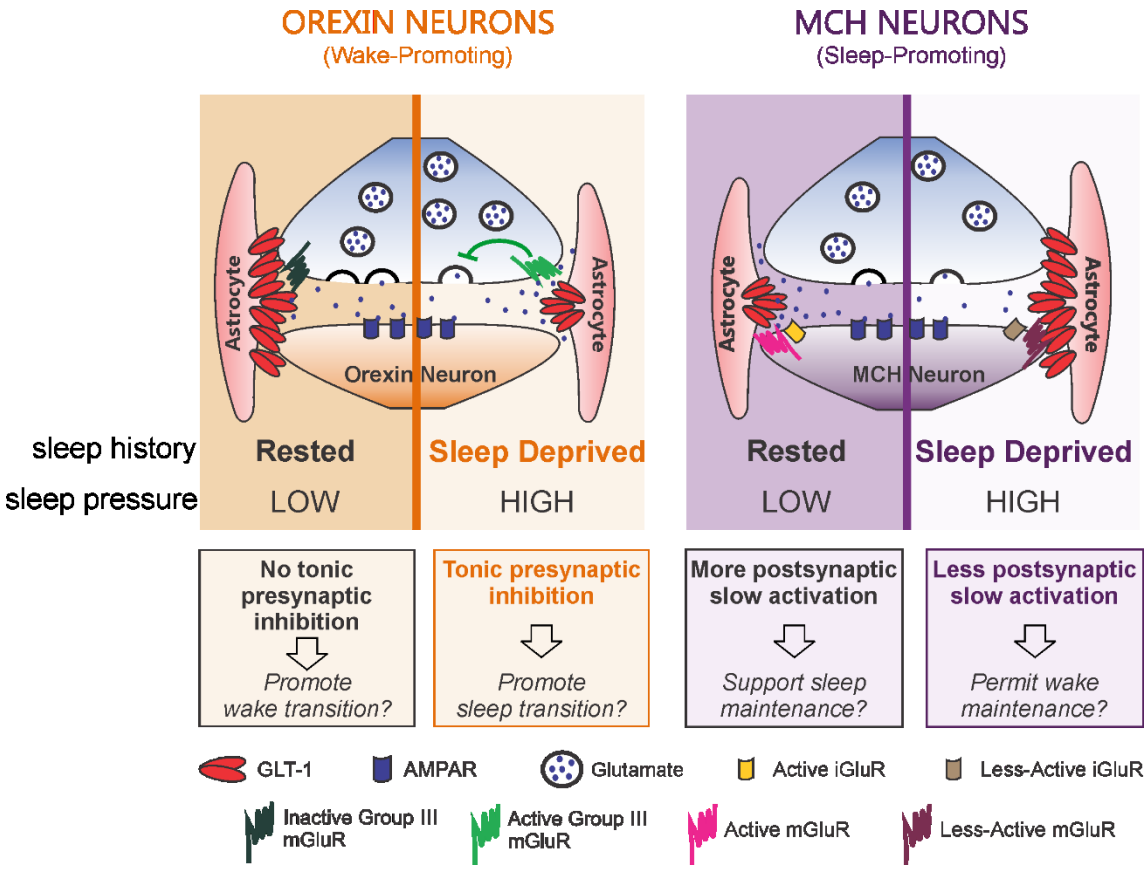
OREXIN NEURONS
(Wake-Promoting)
MCH NEURONS
(Sleep-Promoting)
Astrocyte
Astrocyte
Orexin Neuron
Astrocyte
Astrocyte
MCH Neuron
sleep history
sleep pressure
Rested
LOW
Sleep Deprived
HIGH
Rested
LOW
Sleep Deprived
HIGH
No tonic presynaptic inhibition
Promote wake transition?
Tonic presynaptic inhibition
Promote sleep transition?
More postsynaptic slow activation
Support sleep maintenance?
Less postsynaptic slow activation
Permit wake maintenance?
GLT-1
AMPAR
Glutamate
Active iGluR
Less-Active iGluR
Inactive Group III mGluR
Active Group III mGluR
Active mGluR
Less-Active mGluR

Table 2.1. Properties of GLT1 apposition with sleep/wake regulatory neurons by sleep-history condition.

Lateral Hypothalamus

Orexin Neurons

Variables	Rested*			Sleep Deprivation*			*P* value
	Mean	SEM	*n*	Mean	SEM	*n*	
Somatic perimeter length (μm)	49.97	0.8361	102	52.22	0.8169	135	0.0602
Number of appositions	20.2	0.5697	102	21.32	0.5275	135	0.1532
Average apposition length (μm)	0.962	0.0357	***101***[1]	0.866	0.0227	135	**0.025**
GLT-1 apposition (% somatic perimeter)	39.21	1.475	102	35.24	1.019	135	**0.0281**

Melanin Concentrating Hormone Neurons

Variables	Rested*			Sleep Deprivation*			*P* value
	Mean	SEM	*n*	Mean	SEM	*n*	
Somatic perimeter length (μm)	47.69	0.8886	100	49.07	0.8528	111	0.266
Number of appositions	17.33	0.6273	100	18.25	0.5147	111	0.2535
Average apposition length (μm)	0.7397	0.0277	100	0.8395	0.0350	111	**0.0266**
GLT-1 apposition (% somatic perimeter)	27.03	1.234	100	31.34	1.365	111	**0.021**

Basal Forebrain

Choline Acetyltransferase Neurons

Variables	Rested*			Sleep Deprivation*			*P* value
	Mean	SEM	*n*	Mean	SEM	*n*	
Somatic perimeter length (μm)	53.34	1.034	100	53.48	0.8726	123	0.9182
Number of appositions	17.87	0.5319	100	18.09	0.4739	123	0.7581
Average apposition length (μm)	0.967	0.0366	***99***[1]	0.935	0.0297	***121***[1]	0.4982
GLT-1 apposition (% somatic perimeter)	32.36	1.246	100	32.11	1.122	123	0.8845

Parvalbumin Neurons

Variables	Rested*			Sleep Deprivation*			*P* value
	Mean	SEM	*n*	Mean	SEM	*n*	
Somatic perimeter length (μm)	57.03	2.048	59	55.33	1.68	62	0.5213
Number of appositions	20.54	1.093	59	22.47	1.294	62	0.2602
Average apposition length (μm)	0.986	0.0583	59	0.952	0.0374	62	0.6115
GLT-1 apposition (% somatic perimeter)	35.98	2.386	59	37.76	1.912	62	0.559

* There were 12 rats per behavioural state for each neuronal population

[1] Outliers that were more than 4 standard deviations from the mean were excluded from analysis.

Table 2.2. Properties of GLT1 apposition with sleep/wake regulatory neurons by sleep-history condition: Recovery.

Lateral Hypothalamus	Orexin Neurons						
	Extended Rest*			Recovery*			
Variables	Mean	SEM	*n*	Mean	SEM	*n*	*P* value
Somatic perimeter length (µm)	55.73	1.142	67	53.05	0.9323	70	0.0705
Number of appositions	21.34	0.6584	67	19.67	0.6593	70	0.0752
Average apposition length (µm)	0.9269	0.0386	67	0.8619	0.0324	70	0.1974
GLT-1 apposition (% somatic perimeter)	35.06	1.442	67	31.81	1.353	70	0.1029
	Melanin Concentrating Hormone Neurons						
	Extended Rest*			Recovery*			
Variables	Mean	SEM	*n*	Mean	SEM	*n*	*P* value
Somatic perimeter length (µm)	50.52	0.8647	62	48.59	0.729	82	0.0881
Number of appositions	17.44	0.6612	62	15.94	0.4991	82	0.0675
Average apposition length (µm)	0.7284	0.0321	62	0.7529	0.0307	82	0.5864
GLT-1 apposition (% somatic perimeter)	25.34	1.44	62	24.98	1.249	82	0.8495

*There were 6 rats per behavioural state for each neuronal population

CHAPTER 3

GLUTAMATE TRANSPORTER 1 MODULATES MCH NEURON KAINATE RECEPTORS

3.1 INTRODUCTION

Growing evidence implicates neuron-glia interactions in brain function. One population of glial cells, namely astrocytes, influences neuronal activity in several important ways, via ion buffering, metabolic support, and the release of neuroactive molecules (Parsons, 2010; Larsen et al., 2014; Pan et al., 2015). Astrocytes are also involved in the quick reuptake of synaptically released glutamate and GABA through high-affinity transporters, thus terminating their action (Zhou and Danbolt, 2013). One such transporter, glial glutamate transporter 1 (GLT1), modulates diffusion and spillover of synaptically-released glutamate, thereby regulating the activation of synaptic and/or extrasynaptic receptors (Rusakov and Kullmann, 1998; Oliet et al., 2001; Zheng et al., 2008). Consequently, changes in GLT1 properties, expression, or localization modulate synaptic transmission in many regions throughout the central nervous system such as the supraoptic nucleus (Oliet et al., 2001), the hippocampus (Huang et al., 2004; Omrani et al., 2009), the cerebellum (Marcaggi et al., 2003), the cerebral cortex (Genoud et al., 2006), and the spinal cord (Weng et al., 2007).

The studies reported in Chapter 2 demonstrated that anatomical plasticity of GLT1 occurs in the lateral hypothalamus (LH), where GLT1 juxtaposition with sleep/wake neuronal populations was altered by acute (6 h) sleep deprivation (SD; Chapter 2). One such population is melanin concentrating hormone (MCH) neurons, which are active during the rapid eye movement (REM) sleep and inactive during both spontaneous wake and SD (Modirrousta et al., 2005; Hassani et al., 2009). Specifically, SD resulted in an increase in perisomatic GLT1 apposition with MCH neurons (Figure 2.2H). This was accompanied by a decrease in high-frequency stimulation-induced slow excitatory postsynaptic currents (EPSCs; Figure 2.8H,I), likely a result of reduced glutamate diffusion following SD (Chapter 2). However, the question of which postsynaptic receptors were mediating this slow EPSC remained unexplored.

In the present study, we used whole-cell patch-clamp electrophysiology to investigate which type or types of glutamatergic receptors mediate slow EPSCs in MCH neurons and how GLT1 regulates the activation of these receptors (e.g. whether intense neuronal activity such as high-frequency stimulation is required, whether GLT1 prevents AP-independent activation of these receptors, etc.). We determined that GLT1 regulates a

basal glutamate tone and glutamate spillover during intense synaptic activity, preventing the activation of kainate receptors in MCH neurons. The efficacy of GLT1 to modulate kainate receptor-mediated slow EPSC is altered by SD, in agreement with the anatomical change in perisomatic GLT1 apposition shown in Chapter 2. Together with Chapter 2, these results demonstrate that GLT1 modulates kainate receptor activity in sleep-promoting MCH neurons depending on prior sleep history.

3.2 METHODS

3.2.1 ANIMALS

All procedures were conducted in accordance with the Canadian Council on Animal Care and were approved by the Memorial University Institutional Animal Care Committee. The source, age, housing conditions and behavioral manipulations (SD or Rest) of model animals were the same as in the electrophysiological studies reported in Chapter 2, Section 2.3. Briefly, Male Sprague Dawley rats were obtained from the breeding colony at Memorial University or from Charles River Canada (St. Constant, QC, Canada). Animals were housed in pairs under a 12 h light/12 h dark cycle (lights on at 08:00) in a colony room. Food and water were available ad libitum. Experiments were performed on brain slices from rats aged 29 to 58 days old.

Rats were randomly assigned to one of two treatment groups at 08:00, and individually housed during behavioural treatment; one group underwent 6 h of sleep opportunity (Rest), and the other was subjected to 6 h of SD by gentle handling as previously described (Deurveilher et al., 2011). Both groups were euthanized immediately after the respective conditions at 14:00 and brain slices were generated (see below). A total of 62 cells from 47 rats were included in the analyses reported in this study.

3.2.2 IN VITRO ELECTROPHYSIOLOGY

The artificial cerebrospinal fluid (ACSF), slice preparation conditions, internal solution, and patch-clamp recording conditions were the same as in Chapter 2. Briefly, rats were deeply anesthetized with isoflurane and decapitated, and brains were quickly

removed. Coronal brain slices (250 μm thick) through the hypothalamus were cut in ice-cold artificial cerebrospinal fluid (ACSF) containing (in mM): 126 NaCl, 2.5 KCl, 1.2 NaH_2PO_4, 1.2 $MgCl_2$, 18 $NaHCO_3$, 2.5 glucose, 2 $CaCl_2$. Slices were then incubated in ACSF at 33-34 °C for 30-45 mins and then at room temperature until recording. ACSF was continuously bubbled with O_2 (95%) and CO_2 (5%).

Patch-clamp recordings were performed on hemisected hypothalamic slices superfused with 30-34 °C ACSF at 2-2.5 ml/min. Under a differential interference contrast microscope (DM LFSA; Leica Microsystems), LH neurons that were located dorsomedial to the fornix and had a soma diameter of 10-20 μm were selected for recording. Recordings were performed using a Multiclamp 700B amplifier and pClamp 10.3 software (Molecular Devices, Sunnyvale, CA). The whole-cell internal solution contained (in mM): 123 potassium gluconate, 2 $MgCl_2$, 8 KCl, 10 Hepes, 0.2 EGTA, 5 Na2-ATP, 0.3 Na2-GTP, adjusted to pH 7.29-7.30 with KOH. Biocytin (0.1-0.2%) was added to the internal solution to label recorded cells. Filled recording electrodes had a tip resistance of 3-7 MΩ.

Once whole-cell access was achieved, a series of hyperpolarizing and depolarizing current steps (300 or 600 ms each) was applied to the cell to characterize its electrophysiological properties. Since the LH also contains other neuronal populations, MCH neurons were tentatively identified by their well-established properties; MCH neurons exhibit spike adaptation upon positive current injection, have a hyperpolarized resting membrane potential (RMP), lack spontaneous firing in vitro, lack H-current, and lack rebound depolarization upon relief from a hyperpolarizing current (Alberto et al., 2011) (Figure 3.1Aa). Only cells displaying each electrophysiological characteristic typical of MCH neurons (Alberto et al., 2011) were included in these experiments. A subset of cells was filled with biocytin and the brain slices were processed for post-hoc immunohistochemistry to confirm the neurochemical identity of recorded cells (see below).

Experimental current-clamp recordings were performed at a holding current of 0 pA to record RMP. Every 30 seconds, a series of hyperpolarizing and depolarizing current steps (300 ms each) was applied to the cell to assess excitability. For voltage clamp recordings, neurons were held at -70 mV. Membrane currents were filtered at 1

kHz, digitized at 5-10 kHz and stored for offline analysis. To study evoked EPSCs, a bipolar tungsten stimulating electrode was placed within the LH lateral to the recorded cell. Paired pulses were applied at 25 Hz every 15 s, and the amplitude of the slow EPSC was measured 25 ms after the final stimulation artifact. Train stimulation consisted of 20 pulses at 50 Hz every 30 s, and the amplitude of the fast evoked EPSC following each pulse (within 10 ms) was measured, along with the subsequent slow EPSC, which was measured for 750 ms beginning 25 ms after the final stimulation artifact. A 20-mV hyperpolarizing pulse (100 ms) was applied every 15-30 s, and the steady-state and capacitive currents were monitored as measures of input resistance and series/access resistance, respectively. Cells that showed significant change (>20%) in these parameters during electrophysiological recordings were excluded from analysis.

Recordings were performed during the remainder of the light phase, and were discontinued prior to the beginning of the dark phase at 20:00. Neither time-since-dissection (Appendix B), nor age of the rat (Appendix C), were correlated with measures in this study.

3.2.3 POST-HOC IMMUNOHISTOCHEMISTRY

Post-hoc immunohistochemistry was conducted as in Chapter 2. Immediately following recording, brain slices containing biocytin-filled cells were placed in 10% formalin and fixed for >24 h at 4 °C. To confirm the transmitter phenotype of recorded cells, fixed slices were individually incubated with a cocktail of goat anti-orexin A (1:2000; sc-8070; Santa Cruz Biotechnology, Dallas, TX) and rabbit anti-MCH (1:2000; H-070-47; Phoenix Pharmaceuticals, Belmont, CA) antibodies for 3 days at 4 °C. Next, slices were incubated with secondary antibodies (1:500; Alexa 594-conjugated donkey anti-goat IgG, and Alexa 488-conjugated donkey anti-rabbit IgG) as well as Alexa 350-conjugated streptavidin to visualize biocytin in recorded cells. Stained slices were examined with an epifluorescence microscope to examine for co-localization of biocytin with MCH (or orexin-A, another prominent LH neuropeptide). In the biocytin-positive cells, immunohistochemical phenotype confirmed the electrophysiological MCH phenotype in 92.2% of cases (47 out of 51 cell). In the remaining cases, the

immunohistochemistry was ambiguous. In no case was the electrophysiological MCH phenotype mismatched with the orexin-A immunohistochemical phenotype.

3.2.4 Drugs

All drugs were bath-perfused at final concentrations indicated, by diluting stock solutions in the ACSF immediately before use. Picrotoxin and biocytin were purchased from Sigma Aldrich Canada (Oakville, ON, Canada); DHK, MPEP, LY367685, DNQX, and GYKI52466 were purchased from Tocris Bioscience (Minneapolis, MN); and TTX was purchased from Alomone Labs (Jerusalem, Israel).

3.2.5 Data Analysis

RMP, latency to 1st spike, evoked EPSCs, and DHK-induced inward current were analyzed using Clampfit 10.3 software (Molecular Devices, Sunnyvale, CA). RMP and threshold potential values were corrected for the liquid junction potential (Neher, 1992), which was +15.2 mV in our preparation. Statistical analyses were conducted with GraphPad Prism 6 (GraphPad Software, La Jolla, CA). For the drug effect compared to baseline, paired t-tests or two-way repeated measures ANOVA was used as appropriate. For group comparisons of drug effects, the drug effect was normalized to its respective baseline before comparison by independent t-test or a one-way ANOVA. The Holm-Sidak post hoc test was used for all post-hoc multiple comparisons. P values < 0.05 were considered statistically significant. Values are expressed as means ± SEM.

3.3 Results

3.3.1 GLT1 Restricts the Excitability of MCH Neurons

We first examined the endogenous role of GLT1 on MCH neuron excitability in the Rest condition by using the GLT1-specific transport blocker dihydrokainate (DHK; Figure 3.1A). MCH neurons had a RMP of -83.51 ± 2.77 mV and typically did not fire APs in response to a 100 pA current step (n = 5; Figure 3.1Aa). DHK (100 μM) induced a large depolarization of MCH neurons (+20.08 ± 2.30 mV, $P = 0.0010$, paired *t*-test;

Figure 3.1B), although this was not sufficient to induce spontaneous APs in any of the cells tested. Nonetheless, DHK increased the number of APs induced by each positive current step ($P < 0.0001$ for drug effect, 2-way repeated measures ANOVA; Figure 3.1C). Furthermore, DHK decreased the latency between stimulus onset and the first AP for both the 200 and 300 pA current steps ($P < 0.0028$ for drug effect, 2-way repeated measures ANOVA; Figure 3.1D).

Together these data demonstrate that GLT1 continuously limits the excitability of MCH neurons.

3.3.2 GLT1 Restricts MCH Neuron Excitability after Both Rest and SD

GLT1 apposition with MCH neurons is increased following SD (Chapter 2, Figure 2.2H). We therefore sought to determine whether GLT1 is more effective at reducing MCH neuron excitability following SD compared to Rest. DHK induced a large depolarization in MCH neurons following SD, but its magnitude was similar to that observed after Rest ($P = 0.8756$, unpaired t-test; Figure 3.2A). DHK also increased AP numbers during positive current steps following SD),but there was no difference in the DHK-dependent increase in the number of APs between the Rest and SD conditions ($P = 0.2201$ for sleep state, 2-factor mixed model ANOVA; Figure 3.2B). Finally, DHK had a similar effect on latency to 1st spike in both the Rest and SD conditions (n = 5 cells for Rest, and n = 6 cells for SD; $P = 0.6323$ for sleep state, 2-factor mixed model ANOVA; Figure 3.2C). Interestingly, two out of six MCH neurons fired spontaneous APs in the SD condition when DHK was present. While this contrasts with a total lack of spontaneous firing following Rest in the presence of DHK, little can be concluded due to the small sample sizes.

These data demonstrate that blocking GLT1 has similar effects regardless of sleep-state conditions.

3.3.3 GLT1 Limits MCH Neuron Excitability during intense excitatory synaptic activation Primarily by Preventing the Activation of Postsynaptic Kainate Receptors

The effect of DHK in MCH neurons was visible in voltage clamp as a slow inward current (Figure 3.3A). This slow current was similar in the Rest and SD conditions ($P = 0.5519$, unpaired t-test; Figure 3.3B, Table 3.1), in accordance with similar effects on neuronal excitability in both sleep-state conditions.

We next blocked action potentials with tetrodotoxin (TTX; 1 μM), a sodium channel blocker, to determine whether the DHK-induced slow current requires neuronal firing. TTX also had no effect on this current ($P = 0.6081$, unpaired t-test, DHK vs. TTX+DHK; Figure 3.3E,F), indicating that AP-dependent glutamate release is not necessary for sufficient accumulation of extracellular glutamate to activate extrasynaptic glutamate receptors in the absence of GLT1 activity.

To determine which postsynaptic receptors were mediating the large slow current induced by blocking GLT1, we pretreated the tissue with several glutamate receptor antagonists prior to applying DHK (100 μM) in the Rest condition. First, a combination of the mGluR5 antagonist MPEP (20 μM) and the $mGluR1_a$ antagonist LY367385 (LY; 100 μM) did not appear to prevent the DHK-induced slow current ($P = 0.6702$, one way ANOVA, DHK vs. MPEP+LY+DHK; Figure 3.3C, Table 3.1). Likewise, the AMPA receptor-specific inhibitor GYKI52466 (GYKI; 100 μM) did not prevent the DHK-induced slow current ($P = 0.2397$, one way ANOVA, DHK vs. GYKI+DHK; Figure 3.3C, Table 3.1). In contrast, DNQX (10 μM), an antagonist to both AMPA receptors and kainate (KA) receptors, reduced the amplitude of the DHK-induced slow current by 74.6% ($P < 0.0001$, one way ANOVA, DHK vs. DNQX+DHK; Figure 3.3C,D, Table 3.1). Because blocking AMPA receptors alone had no effect on the DHK-induced slow current, the effect of DNQX on blocking DHK current is likely explained by antagonism at KA receptors. These KA receptors are not tonically active when GLT1 is properly functioning, as DNQX alone without DHK had no effect on holding current in MCH neurons (not shown).

DHK is structurally similar to kainic acid and may directly activate KA receptors. We therefore tested a non-specific glutamate transporter inhibitor that is structurally

dissimilar to kainic acid and DHK, L-*trans*-2,4-PDC (PDC), to ensure that the observed DHK effects were due to impaired glutamate uptake. Like DHK, PDC induced an inward current in MCH neurons in a dose-dependent manner ($P = 0.0004$, unpaired t-test, 300 μM vs. 900 μM PDC; Figure 3.3F, Table 3.1). There was no difference in the magnitude of inward current induced by DHK and by 900 μM PDC ($P = 0.0698$, unpaired t-test, DHK vs. 900 μM PDC; Figure 3.3F, Table 3.1). This result suggests that glutamate transporters play a significant role in limiting the effect of endogenous glutamate on KA receptors.

Together, these data indicate that GLT1 is actively maintaining a low level of endogenous extracellular glutamate tone, thereby preventing the activation of postsynaptic KA receptors and limiting excitability in MCH neurons. The magnitude of KA receptor-mediated current induced by blocking GLT1-alone is unaffected by prior sleep history, suggesting that KA receptors on MCH neurons are insensitive to behavioral states.

3.3.4 Postsynaptic Kainate Receptors Mediate the Slow EPSC during Intense Synaptic Activity in MCH Neurons

A previous report had demonstrated that slow EPSCs in mouse MCH neurons are regulated by glutamate transport (Huang and van den Pol, 2007). We sought to confirm whether glutamate transport also modified the slow EPSCs in rats. We found that a paired pulse protocol was sufficient to uncover a slow EPSC in MCH neurons from the Rest condition (Figure 3.4A). DHK had no effect on fast EPSCs in MCH neurons (Chapter 2, Figure 2.8B-E), but it reduced the amplitude of the slow EPSC evoked by the paired pulse protocol (n = 10 cells; $P = 0.0001$, paired t-test; Figure 3.4A, B), likely by occluding the effects of evoked glutamate release on postsynaptic receptors.

To test whether the postsynaptic receptors mediating the activity-dependent slow EPSC were indeed the same as those mediating the DHK-induced slow current, we employed a train-stimulation protocol to induce a robust slow EPSC (20 pulses at 50 Hz; Figure 3.5A) and tested the effects of GYKI or DNQX. 100 μM GYKI reduced fast EPSC amplitude by 54.2%, indicating that fast EPSCs are primarily mediated by AMPA receptors (n = 5 cells; $P = 0.0005$, baseline vs. GYKI, main drug effect, 2-way repeated

measures ANOVA; Figure 3.5B,E). DNQX also decreased fast EPSC amplitude ($P <$ 0.0001, baseline vs. DNQX, main drug effect, 2-way repeated measures ANOVA; Figure 3.5B,E), reducing it by a further 20.5% beyond the effect of GYKI ($P = 0.01$ to < 0.0001, GYKI vs. DNQX, post-hoc comparisons, 2-way repeated measures ANOVA; Figure 3.5B,E). This indicates that AMPA and KA receptors are mediating a large portion of fast EPSC.

GYKI alone also reduced slow EPSC amplitude (n = 5 cells; $P = 0.0169$, baseline vs. GYKI, one-way repeated measures ANOVA; Figure 3.5C,F), but the effect was much smaller than that on fast EPSC amplitude ($P = 0.0062$, % baseline fast vs. slow EPSC amplitude, unpaired t-test; Figure 3.5E,F). Furthermore, GYKI had no effect on slow EPSC area ($P = 0.0750$, baseline vs. GYKI, one-way repeated measures ANOVA; Figure 3.5D,G), suggesting that AMPA receptors play a small role in mediating the slow EPSC. Interestingly, DNQX almost doubled the effect of GYKI on slow EPSC amplitude ($P =$ 0.0169, GYKI vs. DNQX, one-way repeated measures ANOVA; Figure 3.5C,F). Additionally, DNQX also reduced slow EPSC area by 27.8% beyond the GYKI effect ($P = 0.0496$, baseline vs. DNQX; $P = 0.0496$, GYKI vs DNQX, one-way repeated measures ANOVA; Figure 3.5D,G), suggesting that KA receptors play a larger role than AMPA receptors in mediating the slow EPSC.

Together these data illustrate that while the fast EPSCs induced by evoking synaptic glutamate release onto MCH neurons are primarily mediated by AMPA receptors, KA receptors mediate a larger portion of the slow EPSC than AMPA receptors. Synaptic activity-dependent slow EPSCs are mediated by a similar mechanism to DHK-induced slow currents.

3.4 Discussion

We demonstrate that GLT1 plays a role in maintaining the hyperpolarized RMP of MCH neurons by preventing the activation of KA receptors. It does so by maintaining a low glutamate tone in the extracellular space. Perisomatic apposition of GLT1 with MCH neurons is increased by SD compared to Rest (Chapter 2; Figure 2.2H), suggesting that MCH neurons may be even less excitable following SD. However, we did not observe a change in RMP following SD. Additionally, DNQX does not induce a change in holding

current in MCH neurons in the Rest condition when GLT1 apposition is lower, suggesting that KA receptors are not tonically active following Rest. These data indicate that in both sleep state conditions, GLT1 activity is sufficient to regulate the background glutamate tone and prevent tonic activation of KA receptors. Consistently, blocking GLT1 with DHK depolarizes MCH neurons (by roughly 20 mV under the current experimental conditions), increases the number of APs induced by positive current steps, reduces the latency to first AP, and induces an inward current of similar magnitude in both the Rest and SD conditions. Additionally, KA receptors mediate the slow EPSC induced by train stimulation, a current that is sensitive to prior sleep history (Chapter 2, Figure 2.8) and modulated by GLT1.

The large depolarizing current induced by DHK is primarily mediated by KA receptors, as it was largely blocked by the AMPA/KA receptor antagonist DNQX but not by the AMPA receptor-specific antagonist GYKI52466. However, DHK structurally resembles the KA receptor agonist kainic acid, potentially confounding our interpretation of the results. At the concentration used in this study, DHK may be interacting with KA receptors directly (Møllerud et al., 2016). Yet, in addition to DHK binding affinity at KA receptors, there remain the questions of its potency at KA receptors (Coyle, 1983), and particularly the nature of its action (e.g., agonistic or antagonistic). DHK has been treated as a potential AMPA/KA receptor inhibitor by others conducting GLT1-related research, but no such effects were observed (e.g. Deng et al., 2003). In our hands, DHK induced a large KA receptor-dependent current; therefore, weak direct inhibition of this receptor by DHK would simply indicate that the observed KA receptor-dependent current is an underestimate of true KA-receptor current induced by blocking GLT1. If DHK is acting as a direct agonist at KA receptors, the observed effect may be independent of GLT1. While these possibilities remain unresolved, the effect of DHK was mimicked by the non-specific competitive glutamate transport inhibitor L-*trans*-2,4-PDC, demonstrating that an inhibition of glutamate uptake results in KA receptor activation. This is further supported by a report showing that the non-specific, non-transportable glutamate transport inhibitor TBOA increases slow EPSC in mouse MCH neurons (Huang and van den Pol, 2007).

The KA receptor-dependent DHK current persisted in the presence of the AP blocker TTX, indicating that neuronal firing is not necessary for the increase in

extracellular glutamate induced by blocking GLT1. While action potential-independent glutamate release from neurons cannot be ruled out, the background glutamate tone may be maintained by astrocytes themselves; several studies suggest that astrocytes can release glutamate in response to cytosolic [Ca^{2+}] increases resulting from astrocytic mGluR5 activation (Fellin et al., 2004; D'Ascenzo et al., 2007). However, in our study the mGluR5 antagonist MPEP did not prevent the inward current induced by DHK, and a recent report suggests that astrocytic expression of mGluR5 is largely absent from murine astrocytes after the third postnatal week (Sun et al., 2013). Instead, other signals that can increase cytosolic [Ca^{2+}] in astrocytes might be involved in the background astrocytic glutamate release, such as nitric oxide (Bal-Price et al., 2002; Ida et al., 2008), purines (Jeremic et al., 2001; Fumagalli et al., 2003), or endocannabinoids (Navarrete and Araque, 2008). While astrocytes can also release glutamate via reversal of glutamate transporters like GLT1 following injury or in pathological conditions (McAdoo et al., 2000; Rossi et al., 2000), this explanation is unlikely as DHK is a non-transportable blocker that prevents glutamate transport in either direction (Levy et al., 1998; McAdoo et al., 2000).

While the source of glutamate may be different for the DHK-induced slow current and the evoked slow EPSC, they may be mediated by the same set of postsynaptic receptors. Indeed, slow EPSC evoked with a paired pulse protocol was diminished by DHK (Figure 3.4A,B), which is likely explained by DHK occluding the effects of evoked glutamate release. Furthermore, we observed that like the DHK current, evoked slow EPSC is in part mediated by KA receptors.

A similar slow EPSC was described by another group using train stimulation with mouse MCH neurons (Huang and van den Pol, 2007). This current was shown to be mediated primarily by group I mGluRs (60%), and modulated by glutamate transporters (Huang and van den Pol, 2007). While in our study KA receptors mediate the bulk of the DHK current (75.3%), they were responsible for only 19.8% of the amplitude, or 27.8% of the area of slow EPSCs induced by train stimulation. Group I mGluRs may be mediating the remaining slow EPSC. Intriguingly, the work done by Huang and van den Pol (2007) with mouse MCH neurons illustrated that 39.2% of the slow EPSC was insensitive to group I mGluRs, and this may therefore be mediated by KA receptors.

The difference in proportion of the KA receptor current component (75.3 % for DHK-induced and 19.8% for train stimulation-induced) may be a matter of different subcellular distributions of KA receptors and group I mGluRs in MCH neurons and their relative proximity to excitatory afferents. As blocking glutamate uptake results in a large KA receptor-mediated current that does not require neuronal firing, many KA receptors may be extrasynaptic. This is supported by our results demonstrating that in MCH neurons, GLT1 does not modulate synaptic receptor activation (Chapter 2, Figure 2.8B-E). Little is known about KA receptors in MCH neurons, yet in the hippocampus, there is ample evidence for extrasynaptic KA receptors (Eder et al., 2003; Liu et al., 2004; Yang et al., 2006), and some are specifically activated by non-synaptic, astrocyte-derived glutamate (Liu et al., 2004). Astrocytes may therefore modulate the excitability of MCH neurons directly through such a population of KA receptors. On the other hand, AP-dependent and -independent glutamate release from neurons, as reflected in train stimulation-induced slow EPSCs, would primarily result in activation of receptors proximal to synapses, especially with an abundance of GLT1 limiting further diffusion. The relative densities of KA receptors and group I mGluRs in this space may favour the metabotropic receptors. These differences in subcellular localization of glutamate receptors may underlie the sensitivity of synaptically evoked slow EPSCs to GLT1 plasticity induced by SD.

Finally, in organotypic slices from the rat LH containing both MCH neurons and orexin neurons, another sleep/wake regulatory cell population (Lee et al., 2005; Adamantidis et al., 2007), MCH neurons were significantly more sensitive to kainic acid cytotoxicity than orexin neurons (Katsuki and Akaike, 2004). Quantal excitatory transmission to orexin neurons is mediated by AMPA but not KA receptors (Alberto and Hirasawa, 2010). Further, the slow EPSC in orexin neurons is much smaller than in MCH neurons, and is not altered by prior sleep history (Chapter 2, Figure 2.9), indicating that KA receptor may play a particularly meaningful role in regulating the excitability of MCH neurons across sleep and wake states.

3.5 CONCLUSIONS

In conclusion, this study demonstrates that astrocytes modulate the activity of KA receptors in REM sleep-active MCH neurons via GLT1-mediated glutamate transport. GLT1 actively maintains a low level of background extracellular glutamate tone to prevent the activation of these receptors. Astrocytes thus maintain the hyperpolarized RMP of MCH neurons. KA receptors in MCH neurons become activated during repetitive synaptic activity and mediate slow EPSCs, which were previously demonstrated to be modulated by glutamate transporters, and sensitive to prior sleep history. This could have significant impact on synaptic integration and overall excitability of these neurons. KA receptors therefore play an important role in regulating MCH neurons and, likely, sleep and wake states.

Figure 3.1. Blocking GLT1 increases the excitability of MCH neurons in the Rest condition. (**A**) Top: Representative current clamp trace showing the effect of DHK (100 μM) on an MCH neuron following Rest. MCH neurons did not fire spontaneously in vitro; therefore a series of 300 ms hyperpolarizing and depolarizing current steps were applied every 30 seconds to assess neuron excitability. Bottom: current step traces from baseline (**a**), with DHK (**b**) and during wash (**c**). (**B**) DHK depolarized MCH neurons. (**C**) DHK increases the number of action potentials in response to positive current steps. (**D**) DHK decreases latency to fire in response to positive current steps. ## $P < 0.001$, ### $P < 0.0001$, compared to respective baseline.

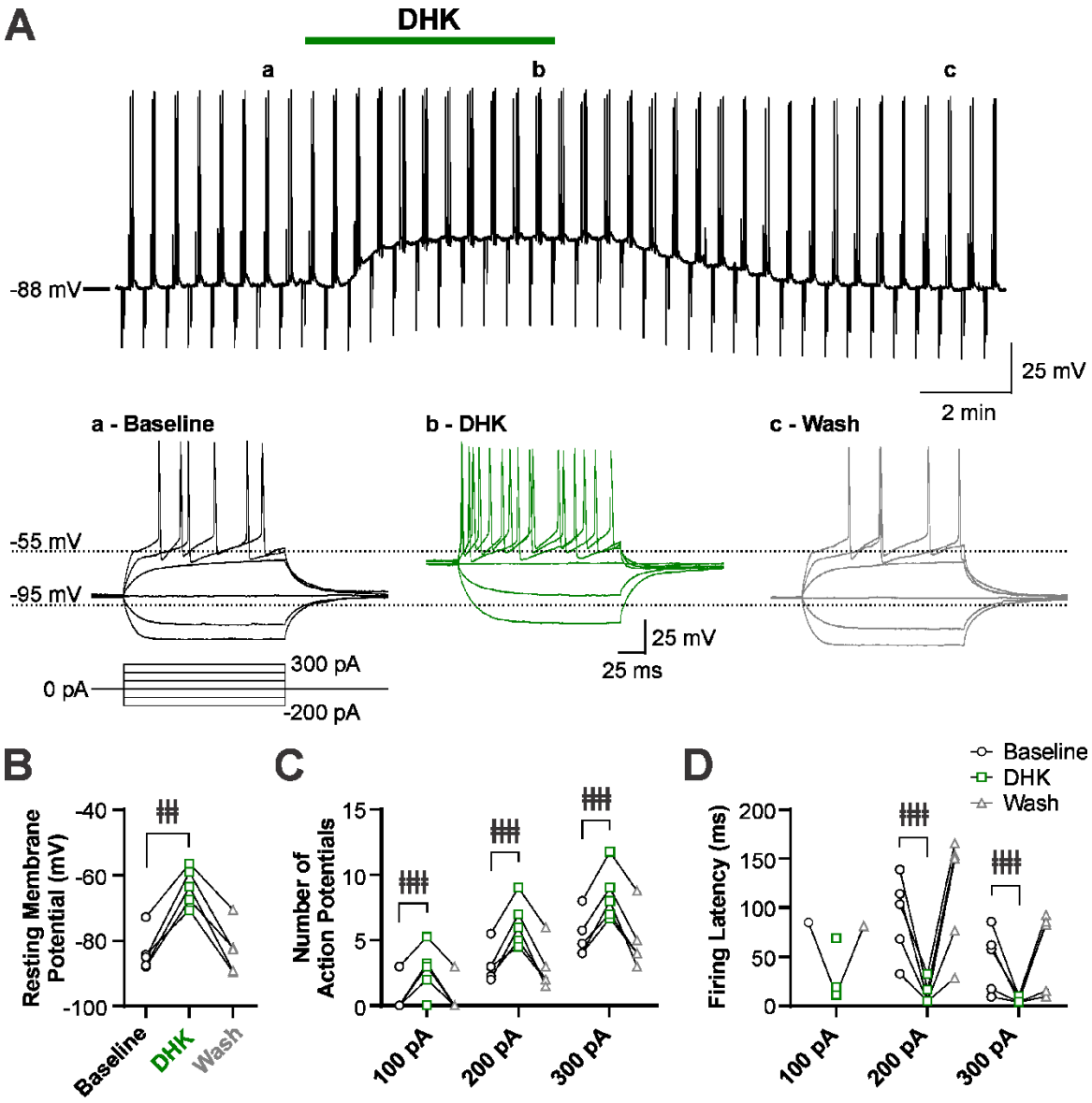
A
DHK
a
b
c
-88 mV
25 mV
2 min
a - Baseline
b - DHK
c - Wash
-55 mV
-95 mV
25 mV
25 ms
0 pA
300 pA
-200 pA
B
Resting Membrane Potential (mV)
-40
-60
-80
-100
###
Baseline
DHK
Wash
C
Number of Action Potentials
15
10
5
0
###
100 pA
200 pA
300 pA
D
Baseline
DHK
Wash
Firing Latency (ms)
200
150
100
50
0
###
100 pA
200 pA
300 pA

Figure 3.2. SD does not alter the effect of DHK on MCH neuron excitability. (A) SD has no effect on the change in resting membrane potential induced by DHK. (B) SD has no effect on increased MCH neuron firing in response to DHK. (C) SD has no effect on decreased firing latency in response to DHK.

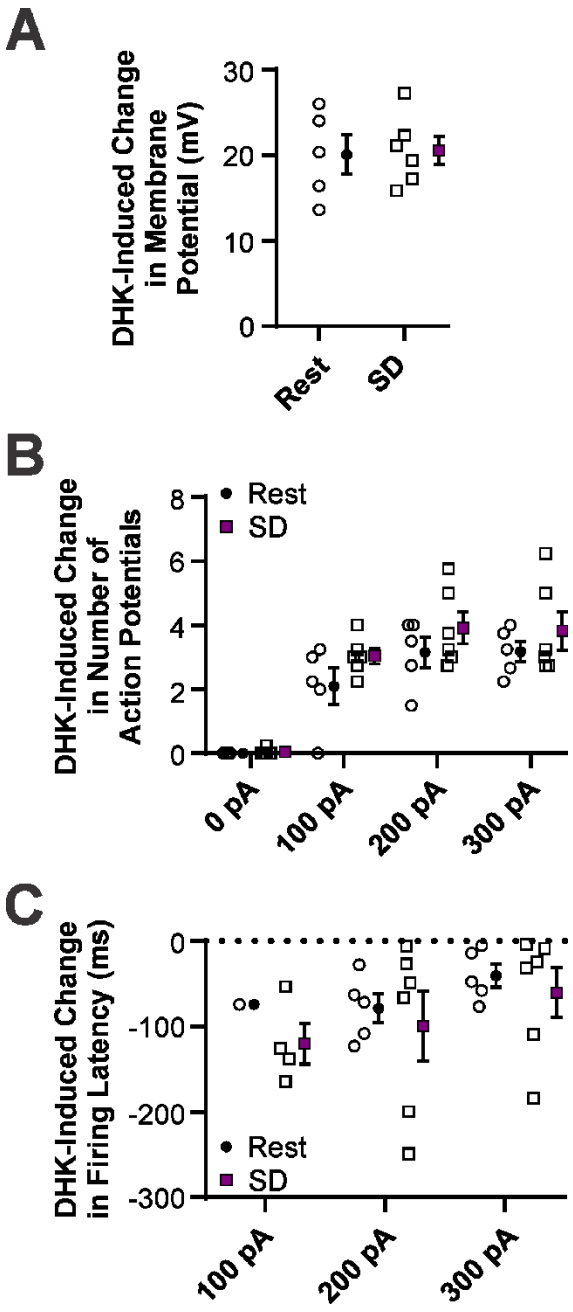
A
DHK-Induced Change in Membrane Potential (mV)
30
20
10
0
Rest
SD
B
DHK-Induced Change in Number of Action Potentials
Rest
SD
8
6
4
2
0
0 pA
100 pA
200 pA
300 pA
C
DHK-Induced Change in Firing Latency (ms)
0
-100
-200
-300
Rest
SD
100 pA
200 pA
300 pA

Figure 3.3. DHK induces a slow reversible current in MCH neurons that is primarily mediated by kainate receptors. (A) Representative voltage clamp trace showing the effect of DHK (100 μM) on an MCH neuron following Rest. (B) DHK induces an equivalent slow current in MCH neurons following Rest and SD. (C) The inward current induced by DHK is primarily mediated by KA receptors. Group I mGluR antagonists MPEP & LY367385 (LY) do not block the DHK effect. GYKI52466 (GYKI) does not block the DHK effect, while DNQX significantly reduces the current induced by DHK, suggesting that KA receptors mediate the bulk of this current. (D) Representative trace demonstrating that DNQX largely prevents the inward current induced by DHK. (E) Representative trace demonstrating that TTX has no effect on the inward current induced by DHK. (F) The current induced by DHK persists unchanged in the presence of TTX, implying that neuronal firing was not necessary for the effect. Additionally, a non-selective glutamate transport inhibitor, L-*trans*-PDC, induces a dose-dependent current, mimicking the effects of DHK. The dashed line represents the mean current induced by DHK alone (from panel C). *$P < 0.05$, **$P < 0.01$, ***$P < 0.001$.

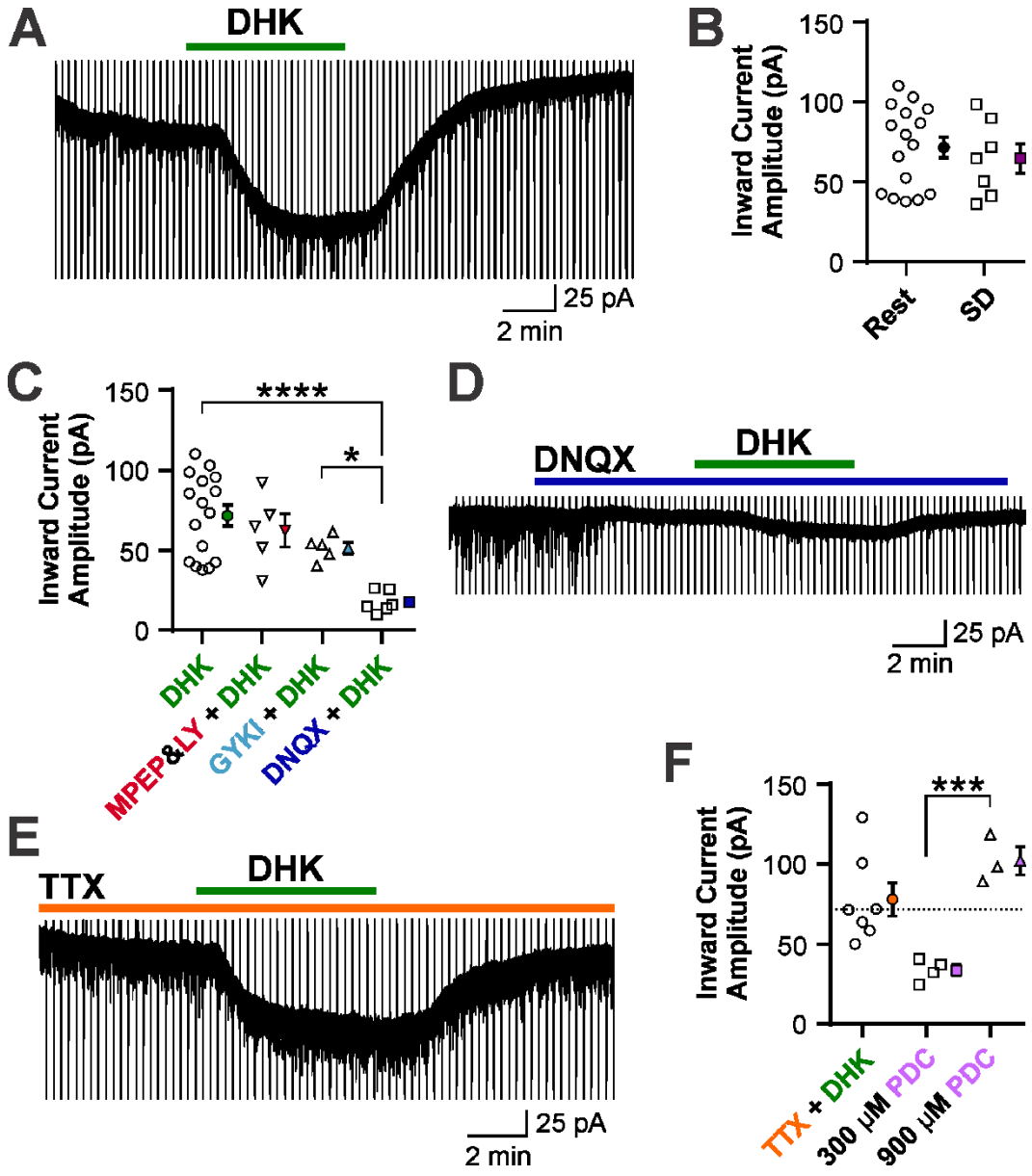
A
DHK
25 pA
2 min
B
Inward Current Amplitude (pA)
150
100
50
0
Rest
SD
C
Inward Current Amplitude (pA)
****
*
DHK
MPEP&LY + DHK
GYKI + DHK
DNQX + DHK
D
DNQX
DHK
25 pA
2 min
E
TTX
DHK
25 pA
2 min
F
Inward Current Amplitude (pA)
***
TTX + DHK
300 µM PDC
900 µM PDC

Figure 3.4. GLT1 modulates the evoked slow EPSC in MCH neurons. (A) Representative average traces showing the effect of DHK on the slow EPSC induced by evoking presynaptic glutamate release. (B) DHK occludes the slow EPSC induced by evoking presynaptic glutamate release. ### $P < 0.0001$ compared to baseline.

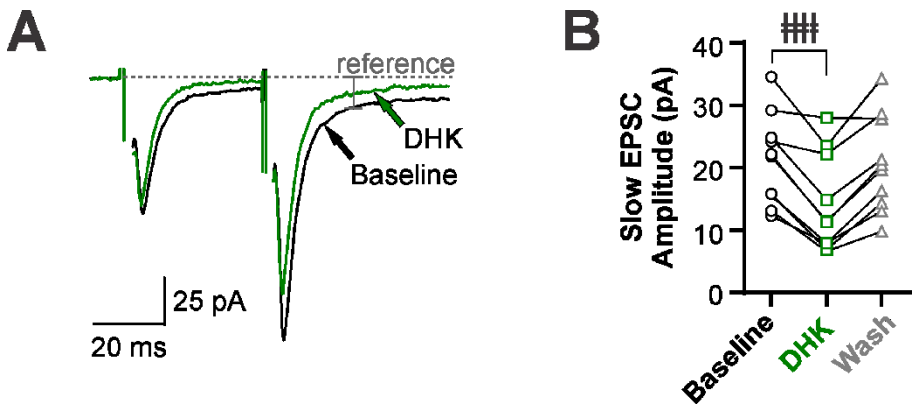
A
reference
DHK
Baseline
25 pA
20 ms
B
###
Slow EPSC Amplitude (pA)
40
30
20
10
0
Baseline
DHK
Wash

Figure 3.5. The slow EPSC induced by train stimulation is also mediated by kainate receptors. (A) Representative average traces from baseline, in the presence of GYKI52466, and in the presence of DNQX showing fast and slow EPSCs evoked in MCH neurons by train stimulation (20 pulses at 50 Hz). (B) Fast EPSC amplitudes during the 20 pulses. The fast EPSCs are primarily mediated by AMPA receptors (C,D) blocking KA receptors reduces the amplitude (C) and area (D) of the slow EPSC following train stimulation. (E-G) Proportion of remaining evoked current following blockade of AMPA receptors or AMPA/KA receptors for the fast EPSC (E), slow EPSC amplitude (F), and slow EPSC area (G). ǂ $P < 0.05$, ǂǂ $P < 0.01$, ǂǂǂ $P < 0.0001$ compared to baseline.

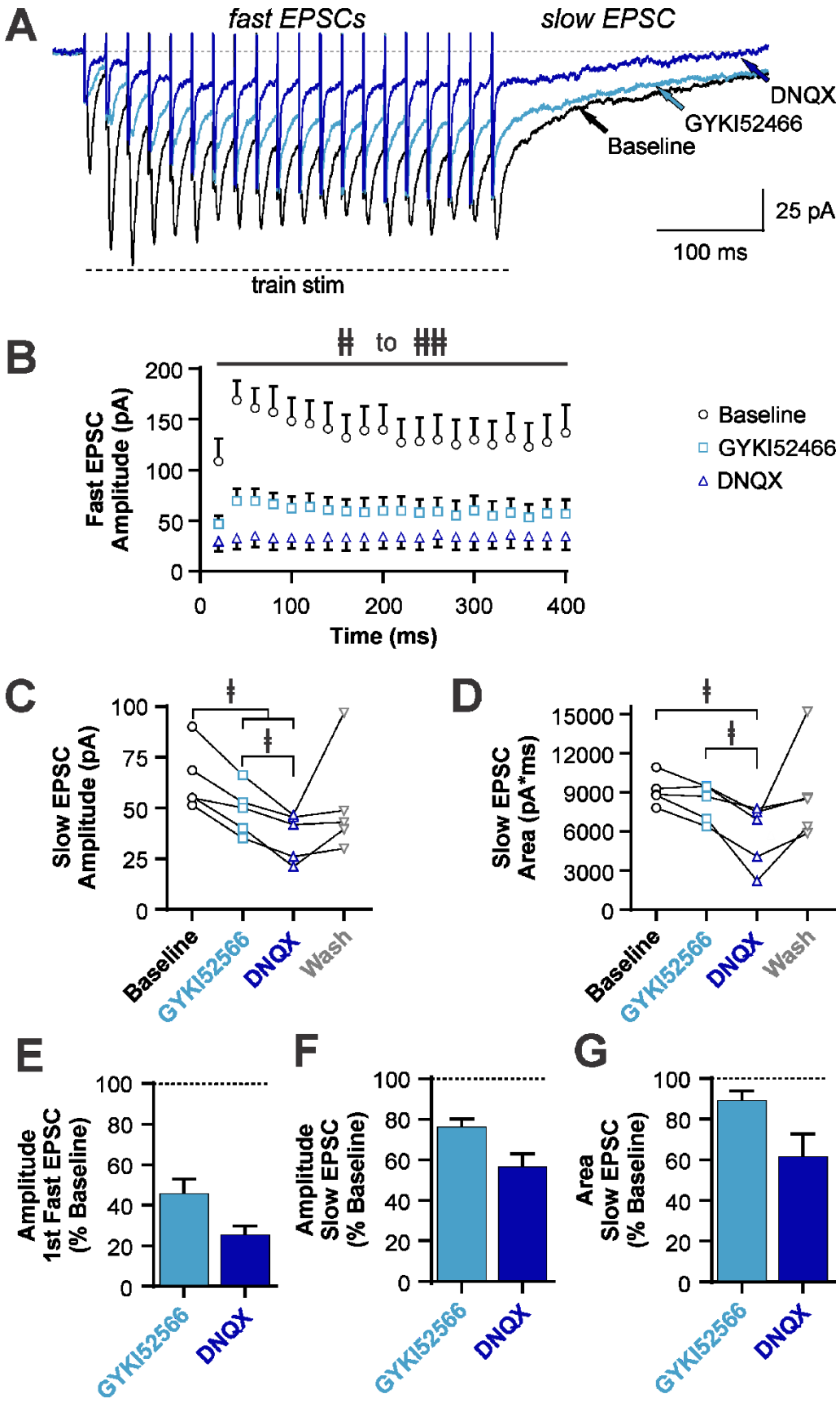
A
fast EPSCs
slow EPSC
DNQX
GYKI52466
Baseline
25 pA
100 ms
train stim
B
to
Fast EPSC Amplitude (pA)
200
150
100
50
0
0
100
200
300
400
Time (ms)
Baseline
GYKI52466
DNQX
C
Slow EPSC Amplitude (pA)
100
75
50
25
0
Baseline
GYKI52566
DNQX
Wash
D
Slow EPSC Area (pA*ms)
15000
12000
9000
6000
3000
0
Baseline
GYKI52566
DNQX
Wash
E
Amplitude 1st Fast EPSC (% Baseline)
100
80
60
40
20
0
GYKI52566
DNQX
F
Amplitude Slow EPSC (% Baseline)
100
80
60
40
20
0
GYKI52566
DNQX
G
Area Slow EPSC (% Baseline)
100
80
60
40
20
0
GYKI52566
DNQX

Table 3.1. Inward current induced by glutamate transport blockers in MCH neurons.

	Rested				Sleep Deprivation				Rest versus SD
Drugs	Δ pA	SEM	*n*	*P* value*	Δ pA	SEM	*n*	*P* value*	*P* value
DHK	71.62	6.49	16	< 0.0001	64.66	9.01	7	0.0004	0.5519
DHK (over MPEP + LY367385)	62.30	10.29	5	0.0038					
DHK (over GYKI52466)	51.33	3.55	5	0.0001					
DHK (over DNQX)	17.67	2.75	6	0.0014					
DHK (over TTX)	71.12	11.27	8	0.0004					
PDC (300 μM)	33.50	3.46	4	0.0023					
PDC (900 μM)	102.0	8.71	3	0.0072					

*** Compared to respective baseline values.**

CHAPTER 4

SLEEP DEPRIVATION INCREASES THE INTRINSIC EXCITABILITY OF MCH AND ORX NEURONS: PARADOXICAL IMPLICATIONS FOR SLEEP HOMEOSTASIS

4.1 INTRODUCTION

Regulation of sleep/wake behaviour involves alternate activation of sleep- and wake-promoting neurons (Saper et al., 2010; Weber and Dan, 2016). The reciprocal activity of these neuronal populations is coordinated in part by changes to their synaptic afferents (Weber and Dan, 2016). Within the lateral hypothalamus (LH), there is a mutually-inhibiting circuit comprised of sleep-promoting melanin concentrating hormone (MCH) neurons (Modirrousta et al., 2005; Hassani et al., 2009) and wake-promoting orexin (ORX) neurons (Lee et al., 2005; Modirrousta et al., 2005). The distributions of MCH and ORX neuron perikarya overlap (Hahn, 2010), and both populations receive monosynaptic inputs from similar cell populations outside the LH (González et al., 2016). Excitatory synaptic transmission to both neuronal populations is modulated by prior sleep history (Chapters 2 and 3). The activation of MCH neurons promotes sleep (Konadhode et al., 2013; Blanco-Centurion et al., 2016), particularly rapid eye movement (REM) sleep (Jego et al., 2013; Vetrivelan et al., 2016), and these neurons are indirectly inhibited by ORX neurons (Apergis-Schoute et al., 2015). ORX neurons, conversely, promote wake (Adamantidis et al., 2007) and are inhibited by MCH (Rao et al., 2008).

In addition to synaptic afferents, changes to the intrinsic membrane properties of ORX and MCH neurons could contribute to the reciprocal activity patterns of these neuronal populations, a concept known as intrinsic plasticity (Sehgal et al., 2013). For example, sleep fragmentation, a model for sleep disturbances associated with sleep apnea, decreases the intrinsic excitability of hippocampal CA1 neurons by reducing input resistance (Tartar et al., 2010). On the other hand, acute REM sleep deprivation increases the intrinsic excitability of pyramidal neurons in the medial prefrontal cortex through an unknown mechanism (Winters et al., 2011). Yet, other than sleep deprivation (SD) resulting in a mild depolarization in ORX neurons (Liu et al., 2011), very little is known regarding if and how sleep and wake states, and sleep need, impact the intrinsic excitability of MCH and ORX neurons.

In this study, by applying whole-cell patch-clamp electrophysiology in acute hypothalamic slices prepared from rats that either underwent 6 h of SD or were left to sleep undisturbed for the same period (Rest), we revealed that SD induces intrinsic plasticity in both MCH and ORX neurons. SD paradoxically increases the intrinsic

excitability of MCH neurons and a subset of ORX neurons through separate mechanisms. These findings have implications for the homeostatic and non-homeostatic regulation of sleep/wake behaviour.

4.2 METHODS

4.2.1 ANIMALS

All procedures were conducted in accordance with the Canadian Council on Animal Care and were approved by the Memorial University Institutional Animal Care Committee. The source, age, housing conditions and behavioral manipulations (SD or Rest) of rats were the same as in Chapter 2, as described in Section 2.3. Briefly, male Sprague Dawley rats were obtained from the breeding colony at Memorial University or from Charles River Canada (St. Constant, QC, Canada). Animals were housed in pairs under a 12 h light/12 h dark cycle (lights on at 08:00) in a colony room. Food and water were available ad libitum. Experiments were performed on brain slices from rats aged 29 to 58 days old.

Rats were randomly assigned to one of two treatment groups at 08:00; one group underwent 6 h of sleep opportunity (Rest), and the other was subjected to 6 h of SD by gentle handling as previously described (Deurveilher et al., 2011) . Both groups were euthanized immediately after the respective conditions at 14:00 and brain slices were generated (see below). A total of 314 cells from 111 rats were included in the analyses reported in this study.

4.2.2 IN VITRO ELECTROPHYSIOLOGY

The artificial cerebrospinal fluid (ACSF), slice preparation conditions, internal solution, and patch-clamp recording conditions were the same as in Chapter 2. Briefly, rats were deeply anesthetized with isoflurane and decapitated, and brains were quickly removed. Coronal brain slices (250 µm thick) through the hypothalamus were cut in ice-cold ACSF containing (in mM): 126 NaCl, 2.5 KCl, 1.2 NaH_2PO_4, 1.2 $MgCl_2$, 18 $NaHCO_3$, 2.5 glucose, 2 $CaCl_2$. Slices were then incubated in ACSF at 33-34 °C for 30-

45 mins and then at room temperature until recording. ACSF was continuously bubbled with O_2 (95%) and CO_2 (5%).

Patch-clamp recordings were performed on hemisected hypothalamic slices superfused with 30-34 °C ACSF at 2-2.5 ml/min. Picrotoxin (50 μM) was always present in the bath to block $GABA_A$ receptors. Under a differential interference contrast microscope (DM LFSA; Leica Microsystems), LH neurons that were located dorsomedial to the fornix and had a soma diameter of 10-20 μm were selected for recording. Recordings were performed using a Multiclamp 700B amplifier and pClamp 10.3 software (Molecular Devices, Sunnyvale, CA). The whole-cell internal solution contained (in mM): 123 potassium gluconate, 2 $MgCl_2$, 8 KCl, 10 Hepes, 0.2 EGTA, 5 Na2-ATP, 0.3 Na2-GTP, adjusted to pH 7.29-7.30 with KOH. Biocytin (0.1-0.2%) was added to the internal solution to label recorded cells. Filled recording electrodes had a tip resistance of 3-7 MΩ.

Once whole-cell access was achieved, a series of hyperpolarizing and depolarizing current steps (300 or 600 ms each) was applied to the cell to characterize its electrophysiological properties. ORX and MCH neurons, which have overlapping anatomical distributions (Hahn, 2010), were tentatively identified by their well-established electrophysiological properties. MCH neurons are not spontaneously active in vitro, have a hyperpolarized RMP, lack H-current and rebound depolarization, and display spike-adaptation upon positive current injection (Alberto et al., 2011; Figure 4.1A). ORX neurons are spontaneously active, have a depolarized resting membrane potential (RMP), display H-current when hyperpolarized, display rebound depolarization when hyperpolarizing current is removed, and have a uniphasic afterhyperpolarizing potential (Eggermann et al., 2003; Parsons et al., 2012a; Linehan et al., 2015; Figure 4.2A) . All cells were filled with biocytin and the brain slices were processed for post-hoc immunohistochemistry to confirm the neurochemical identity of recorded cells (see below).

Recordings were performed during the remainder of the light phase, and were discontinued prior to the beginning of the dark phase at 20:00. Neither time-since-dissection (Appendix B), nor age of the rat (Appendix C), were correlated with measures in this study.

4.2.3 Post-hoc Immunohistochemistry

Post-hoc immunohistochemistry was conducted as in Chapter 2. Immediately following recording, brain slices containing biocytin-filled cells were placed in 10% formalin and fixed for >24 h at 4 °C. To confirm the transmitter phenotype of recorded cells, fixed slices were individually incubated with a cocktail of goat anti-orexin A (1:2000; sc-8070; Santa Cruz Biotechnology, Dallas, TX) and rabbit anti-MCH (1:2000; H-070-47; Phoenix Pharmaceuticals, Belmont, CA) antibodies for 3 days at 4 °C. Next, slices were incubated with secondary antibodies (1:500; Alexa 594-conjugated donkey anti-goat IgG, and Alexa 488-conjugated donkey anti-rabbit IgG) as well as Alexa 350-conjugated streptavidin to visualize biocytin in recorded cells. Stained slices were examined with an epifluorescence microscope to examine for co-localization of biocytin with MCH or orexin-A. The immunohistochemical phenotype was confirmed for all cells included in this study.

4.2.4 Drugs

Picrotoxin and biocytin were purchased from Sigma Aldrich Canada (Oakville, ON, Canada).

4.2.5 Data Analysis

Membrane capacitance and membrane resistance were measured using Clampex 10.3 software (Molecular Devices, Sunnyvale, CA). Spontaneous action potential (AP) frequency, spike frequency adaptation (SFA) ratio, and AP waveform parameters were measured using MiniAnalysis 6.0 software (Synaptosoft, Decatur, GA). All other measures were analyzed using Clampfit 10.3 software (Molecular Devices, Sunnyvale, CA). Investigations of AP waveform parameters were done by averaging the last four complete APs (beginning from the threshold potential) during the 200 pA current step. RMP and threshold potential values were corrected for the liquid junction potential (Neher, 1992), which was +15.2 mV in our preparation. Statistical analyses were conducted with GraphPad Prism 6 (GraphPad Software, La Jolla, CA). The Holm-Sidak

post hoc test was used for all multiple comparisons. P values < 0.05 were considered statistically significant. Values are expressed as means ± SEM.

4.3 RESULTS

4.3.1 SD INCREASES THE INTRINSIC EXCITABILITY OF MCH NEURONS COMPARED TO REST

We examined the effects of acute SD on the intrinsic electrophysiological properties of MCH neurons compared to Rest. SD had no effect on either membrane capacitance or membrane resistance (Table 4.1). SD also had no effect on RMP (n = 115 cells for Rest, and n = 55 cells for SD; $P = 0.2362$, unpaired t-test; Figure 4.1B), which is consistent with the much smaller dataset in Chapter 3 (Figure 3.2A).

In both Rest and SD conditions, not a single MCH neuron fired spontaneous APs. We next measured the effects of SD on MCH neuron excitability using a series of current steps (600 ms; Figure 4.1A). MCH neurons fired significantly more APs in response to positive current steps following SD compared to Rest (n = 96 cells for Rest, and n = 40 cells for SD; $P = 0.0066$ for sleep state, 2-factor mixed model ANOVA; Figure 4.1C). Increased AP numbers following SD were not due to a shift in the AP threshold potential (Table 4.1). Many MCH neurons failed to respond with a single AP to the 50 pA current injection in both the Rest and SD conditions. Nonetheless, the ratio of MCH neurons that did respond to the 50 pA current step increased following SD (n = 14 for successes, and n = 80 for failures in Rest, and n = 14 for successes, and n = 26 for failures in SD; $P = 0.0116$, Fisher's exact test; Figure 4.1D). Several neurons also failed to respond with an AP to 100 pA and 150 pA current injections, but there was no difference between sleep-state conditions (Figure 4.1D). In the neurons that responded with APs, there was a decrease in latency to the first spike from the onset of positive current injections of 100, 150, and 200 pA in the SD condition (P ranged from 0.0039 to 0.0092, multiple unpaired t-tests corrected for multiple comparisons; Figure 4.1E). There was no difference in the latency to respond to 50 pA injections among the neurons fired an AP ($P = 0.7910$, unpaired t-test; Figure 4.1E). These results are consistent with a decrease in A-type potassium current (Carrasquillo and Nerbonne, 2014) following SD. Finally, to determine

whether changes in AP number following SD might also be due to a change in spike adaptation, we calculated the SFA ratio. This ratio was obtained by dividing the initial frequency calculated from the interval between the first two APs by the final frequency calculated from the interval between the last two APs (Venance and Glowinski, 2003). A minimum of three APs are therefore required to calculate this ratio. There was no difference in SFA ratio between Rest and SD in the neurons where SFA could be calculated ($P > 0.076$, multiple unpaired t-tests corrected for multiple comparisons; Figure 4.1F).

Together, these data indicate that the intrinsic excitability of MCH neurons is increased following SD compared to Rest, specifically via a reduction in latency to spike, likely due to a reduction in A-current.

4.3.2 SD INCREASES THE INTRINSIC EXCITABILITY OF ORX NEURONS COMPARED TO REST

We next examined the effects of acute SD on the intrinsic electrophysiological properties of ORX neurons. Again, SD had no effect on membrane capacitance or membrane resistance (Table 4.2). SD also had no effect on ORX neuron RMP (n = 83 cells for Rest, and n = 61 cells for SD; $P = 0.8964$, unpaired t-test; Figure 4.2B). While ORX neurons fire spontaneously in vitro, there was no difference in the basal firing rate between Rest and SD (Table 4.2). To further examine the effects of SD on ORX neuron excitability, we used a series of current steps (600 ms; Figure 4.2A). ORX neurons fired significantly more APs in response to positive current injection following SD compared to Rest (n = 83 cells for Rest, and n = 61 cells for SD; $P = 0.0001$ for interaction effect, mixed model ANOVA; Figure 4.2C).

Together, these data indicate that the intrinsic excitability of ORX neurons is increased following SD compared to Rest.

4.3.3 INCREASED ORX NEURON EXCITABILITY FOLLOWING SD IS DUE TO A REDUCTION IN AFTERHYPERPOLARIZATION.

Increased AP numbers following SD were not due to a change in latency to the first spike from the stimulus onset ($P = 0.5291$ for sleep state, 2-factor mixed model ANOVA; Figure 4.2D), indicating that the mechanism for increased excitability is different between ORX and MCH neurons. The increase in AP numbers following SD compared to Rest in ORX neurons was predominantly apparent during the 200 pA current step (Figure 4.2C). We therefore compared various AP waveform parameters at this current intensity to determine whether there were any changes between sleep-state conditions. Following SD, there was no change in AP threshold potential (Table 4.2), amplitude (n = 81 cells for Rest, and n = 61 cells for SD; $P = 0.2287$, unpaired t-test; Figure 4.3A) or half-width ($P = 0.1774$, unpaired t-test; Figure 4.3B). We performed regression analyses on the grouped data for each measure to determine whether these measures were indeed independent of AP numbers. There was no correlation between AP amplitude and AP number (Figure 4.3E). However, there was a positive correlation between AP half-width and AP number (Figure 4.3F). In contrast, SD had a significant effect on the afterhyperpolarizing potential (AHP) compared to Rest; it reduced AHP amplitude ($P = 0.0126$, unpaired t-test; Figure 4.3C) and AHP area ($P = 0.0008$, unpaired t-test; Figure 4.3D). Again, we performed regression analyses to compare these measures with number of APs. Both AHP amplitude (Figure 4.3G) and AHP area (Figure 4.3H) were negatively correlated with number of APs induced with a 200 pA current step.

These data indicate that the AHP is smaller following SD compared to Rest in ORX neurons. This reduction in AHP is likely underlying the increase in number of APs observed at 200 pA following SD.

4.3.4 SD INCREASES THE INTRINSIC EXCITABILITY OF D-TYPE, BUT NOT H-TYPE, ORX NEURONS.

ORX neurons have previously been subdivided into two groups based on their electrophysiological properties (Williams et al., 2008; Schöne et al., 2011). D-type ORX neurons display depolarization capped with APs upon relief from a hyperpolarizing current (Figure 4.4A - left) while H-type ORX neurons display A-like current upon relief

of a hyperpolarizing current that delays the return of spontaneous APs (Schöne et al., 2011; Figure 4.4A - right). In our hands, D-type and H-type ORX neurons had several other differences independent of sleep-state history; H-type neurons had a significantly larger membrane capacitance and AHP amplitude during spontaneous APs than did D-type neurons, while D-type neurons had a significantly faster spontaneous firing rate and larger AP half-width during spontaneous APs than H-type neurons (Table 4.3). They did not differ in RMP, membrane resistance, or spontaneous AP amplitude (Table 4.3). There were previously no known differences between D-type and H-type ORX neurons in their roles in the regulation of sleep/wake states.

Sleep-state conditions did not significantly affect the ratio of D-type versus H-type neurons, at 1.96 (53/27) after Rest, and 1.07 (37/29) after SD ($P = 0.0855$, Fisher's exact test; Figure 4.4B), with D-type neurons accounting for 60% of all ORX neurons recorded. We next examined whether the observed increases in ORX neuron excitability following SD occurred similarly between D-type and H-type neurons. In the Rest condition, D-type ORX neurons fired more APs than H-type neurons in response to a 200 pA current step (2-factor mixed model ANOVA, D-type Rest versus H-type Rest, $P > 0.0344$ for post hoc analysis; Figure 4.5A). SD selectively increased AP numbers in D-type ORX neurons (2-factor mixed model ANOVA, D-type Rest versus D-type SD, $P = 0.01544$ at 150 pA, and $P = 0.0024$ at 200 pA for post hoc analysis; Figure 4.5A) without affecting H-type ORX neurons compared to Rest (2-factor mixed model ANOVA, H-type Rest versus H-type SD, $P > 0.4$ for post hoc analysis; Figure 4.5A). SD had no effect on latency to first spike in either D-type or H-type ORX neurons (Figure 4.5C), which was different by ORX neuron subtype (Figure 4.5B,C). Because H-type ORX neurons display A-current (Schöne et al., 2011), we also examined their latency to respond following removal of a hyperpolarizing current (Figure 4.4A). SD had no effect on this latency ($P = 0.2396$, unpaired t-test; Figure 4.5D).

We next compared various parameters of the AP waveform at 200 pA, where D-type ORX neurons alone had increased AP numbers in the SD condition (Figure 4.5A and Figure 4.6A). SD had no effect on the threshold potential for AP induction (Figure 4.5E), AP amplitude (Figure 4.6B), or half-width in either subtype (Figure 4.6C). However, D-type ORX neurons had a larger AP half-width than H-type ORX neurons ($P = 0.0379$, 2-

way ANOVA, main effect for ORX subtype; Figure 4.6C), similar to their spontaneous APs (Table 4.3). SD induced a decrease in AHP amplitude ($P = 0.0054$, 2-way ANOVA with post hoc analysis; Figure 4.6A,D) and area ($P = 0.0011$, 2-way ANOVA with post hoc analysis; Figure 4.6E) in D-type ORX neurons, while there was no change in AHP amplitude ($P = 0.7673$, 2-way ANOVA with post hoc analysis; Figure 4.6D) or area ($P = 0.3136$, 2-way ANOVA with post hoc analysis; Figure 4.6E) in H-type ORX neurons. Changes in AHP can be accompanied by changes in spike frequency adaptation (Faber, 2009; Ji et al., 2009). We therefore investigated SFA in D-type ORX neurons (Figure 4.6A), as described above. SD decreased SFA ratio compared to Rest ($P = 0.0083$ for sleep-history, 2-factor mixed model ANOVA; Figure 4.6A,F), thus permitting more spikes to occur.

Together, these data indicate that SD specifically increases the intrinsic excitability of D-type ORX neurons with no effect on H-type ORX neurons. In the SD condition, D-type ORX neurons fire more APs during positive current steps, exhibit less AHP, and have less SFA than in the Rest condition.

4.4 DISCUSSION

We demonstrate that acute (6 h) SD increases the intrinsic excitability of both sleep-promoting MCH neurons and a subset of wake-promoting ORX neurons through different mechanisms. Following a period of neuronal inactivity (SD; Modirrousta et al., 2005; Hassani et al., 2009), MCH neurons exhibit fewer failures to respond and a reduced latency to first spike during positive current steps, thus permitting an increase in APs, likely due to a smaller A-current. Contrastingly, following a period of neuronal activity (SD; Lee et al., 2005; Modirrousta et al., 2005), D-type ORX neurons exhibit reduced AHP and spike adaptation, permitting more APs during positive current steps. These results indicate that intrinsic plasticity in LH neurons is occurring with SD, which may alter future synaptic activity (Sehgal et al., 2013), and may therefore be involved in sleep/wake regulation.

MCH neurons appear to exhibit a reduction in A-current following SD compared to Rest. A-current is a voltage-dependent, rapidly inactivating potassium current that counters membrane depolarization, thus transiently delaying firing (Nadin and

Pfaffinger, 2010). It is well-recognized for its role in regulating the excitability of a variety of neurons (Carrasquillo and Nerbonne, 2014). Several other sleep/wake regulatory populations exhibit A-current (Kamondi et al., 1992; Pan et al., 1994; Kim et al., 2009; Ishibashi et al., 2016), including ORX neurons (H-type; Burdakov et al., 2004; Schöne et al., 2011). In H-type ORX neurons, SD induced no detectable change in A-current, suggesting that a reduction in A-current following SD is specific to MCH neurons. A-current in MCH neurons could be positively or negatively regulated by a variety of neuromodulators that change their tones with sleep/wake state. For example, histamine has been shown to increase A-current (Sethi et al., 2011). However, the neuronal population containing this neurotransmitter is most active during wake (Takahashi et al., 2006) when A-current in MCH neurons is reduced, suggesting that another mechanism likely explains our results. One such possibility is via an increase in A-current during Rest (rather than a decrease in A-current during SD) through an endocannabinoid-dependent mechanism (Tang et al., 2005; Zou et al., 2016). MCH neurons release endocannabinoids upon depolarization (Huang et al., 2007), and this could occur during REM sleep or in the Rest condition, when MCH neurons are active (Hassani et al., 2009). Finally, MCH neurons express both orexin receptors and the κ-opioid receptor (Parks et al., 2014b). Orexin-A and KOR agonists can decrease A-current (McDermott and Schrader, 2011; Ishibashi et al., 2016), suggesting that abundant ORX neuron activity during SD could be driving the observed decrease in A-current in MCH neurons via orexin and/or its cotransmitter dynorphin, a KOR agonist (Chou et al., 2001; Muschamp et al., 2014). This increase in excitability of sleep-promoting MCH neurons following prolonged wake could promote transition to sleep, and may be a novel mechanism for the homeostatic regulation of sleep/wake behaviour.

D-type ORX neurons also displayed increased intrinsic excitability following SD, with no change in H-type ORX neurons. These two subpopulations have overlapping but distinct distributions within the orexinergic field of the LH (Williams et al., 2008). Williams et al. reported a D-type to H-type ratio of about 2.5, while we observed a D-type to H-type ratio of about 1.5. Of interest is their relative distribution along the mediolateral axis; D-type ORX neurons are more abundant medially, whereas H-type ORX neurons are more frequent laterally (Williams et al., 2008). Yet, whether these two ORX neuron

subpopulations are truly distinct, or whether ORX neurons can switch between the two phenotypes, is unknown. It has previously been postulated that medial ORX neurons may be involved in arousal while lateral ORX neurons may be involved in reward (Harris and Aston-Jones, 2006). Several studies have since provided support for this hypothesis. Lateral, but not medial, ORX neurons support the learned association of environmental context with drug reward (Harris et al., 2007), are preferentially activated by morphine preference in a learned context (Richardson and Aston-Jones, 2012), and are activated by the lateral septum during drug context learning (Sartor and Aston-Jones, 2012). Medial and perifornical, but not lateral ORX neurons show a significant correlation between expression of the immediate early gene Fos and diurnal rhythms (Estabrooke et al., 2001). The neurons recorded in my study were located dorsomedial to the fornix, and are therefore a population likely to be involved in sleep/wake regulation. Indeed, our data further supports this mediolateral distinction, where medial (more frequently D-type) ORX neurons are particularly implicated in sleep/wake regulation and lateral ORX neurons may be implicated in reward. Whether D-type and H-type ORX neurons located laterally demonstrate similar changes following SD is not known.

One previous report illustrated that SD has an excitatory effect on ORX neurons, inducing a mild depolarization of their RMP through increased intracellular ATP (Liu et al., 2011). We did not observe a change in RMP in ORX neurons following SD, but this could be due to a difference in methodology. Liu et al. employed perforated patch clamp, whereas we used the whole-cell patch clamp configuration. Due to the continuous environment between the cytosol and the pipette solution in our setup, any small differences in ATP concentration would be lost through diffusion. Nonetheless we did see a decrease in AHP and spike adaptation in D-type ORX neurons following SD, which may be due to a reduction in calcium-dependent potassium conductance. Both BK and SK channels are calcium activated potassium channels that can mediate the AHP and spike adaptation (Sah and Faber, 2002; Stocker, 2004). BK, or big conductance, channels also influence AP half-width (Sah and Faber, 2002). AP half-width was unaffected in D-type neurons following SD (Figure 4.6C), indicating that another channel may be responsible for the observed changes. SK, or small conductance, channels generally do not affect AP half-width (Sah and Faber, 2002). Like A-current (discussed above), SK-current is

sensitive to a variety of factors that change with sleep/wake states such as serotonin or noradrenaline. Both of these neuromodulators can reduce SK-current via the 5-HT_{1A} receptor and α_1/β adrenergic receptors, respectively (Wagner et al., 2001; Grunnet et al., 2004; Maingret et al., 2008). ORX neurons express the 5-HT_{1A} receptor (Muraki et al., 2004), and at least a subset of ORX neurons express the α_1 adrenergic receptor (Modirrousta et al., 2005; Yamanaka et al., 2006), The neuronal populations releasing serotonin and noradrenaline in the LH are primarily active during wake (Takahashi et al., 2010; Sakai, 2011).

Finally, glutamate can reduce SK-current via activation of group I metabotropic glutamate receptors (mGluRs) in cortical neurons (Sourdet et al., 2003). ORX neurons receive glutamatergic afferents from a variety of sources, including other wake-promoting brain areas (Henny and Jones, 2006a, 2006b; Yoshida et al., 2006) and local neurons (Li et al., 2002; Acuna-Goycolea et al., 2004; Yamanaka et al., 2010). ORX neurons are directly activated by agonists to group I mGluRs (Huang and van den Pol, 2007), indicating that this is another potential pathway for the reduction in SK current in D-type ORX neurons following SD. Glial glutamate transporter 1 (GLT1) is reduced around ORX neurons following SD (Figure 2.2H), resulting in increased activation of presynaptic glutamate receptors (Figure 2.6 and Figure 2.7). It is therefore possible that SD-dependent changes in glial GLT1 localization around ORX neurons recruits both presynaptic and postsynaptic glutamate receptors, thus impacting both synaptic transmission (Chapter 2) and intrinsic excitability (this Chapter). This increase in excitability of wake-promoting ORX neurons following SD may be a novel mechanism facilitating the maintenance of wake, when necessary, with mounting sleep pressure.

4.5 CONCLUSIONS

In conclusion, these data indicate that SD paradoxically increases the intrinsic excitability of both sleep-promoting MCH neurons and wake-promoting D-type ORX neurons through a reduction in different potassium currents. These unexpected findings indicate that in addition to synaptic plasticity at glutamatergic afferents, there is also plasticity of membrane excitability in MCH and D-type ORX neurons with sleep and

wake states. This intrinsic plasticity has implications for both homeostatic and non-homeostatic regulation of sleep/wake behaviour.

Figure 4.1. Sleep deprivation increases the intrinsic excitability of MCH neurons by reducing firing latency. (A) Representative traces of an MCH neuron from Rest and SD with similar RMPs. A series of 600 ms hyperpolarizing and depolarizing current steps were applied to assess neuron excitability. Measures for panels B-to-F were obtained from these recordings. (B) SD has no effect on RMP in MCH neurons. (C) SD increases the number of action potentials (APs) in response to positive current steps compared to Rest. (D) The percentage of MCH neurons responding to current injections with at least one AP, by sleep-state condition. (E) The latency between current onset and the first AP is reduced in MCH neurons at 100, 150, and 200 pA. (F) Spike-frequency adaptation is unchanged following SD compared to Rest. *$P < 0.05$, **$P < 0.01$ for sleep-state condition.

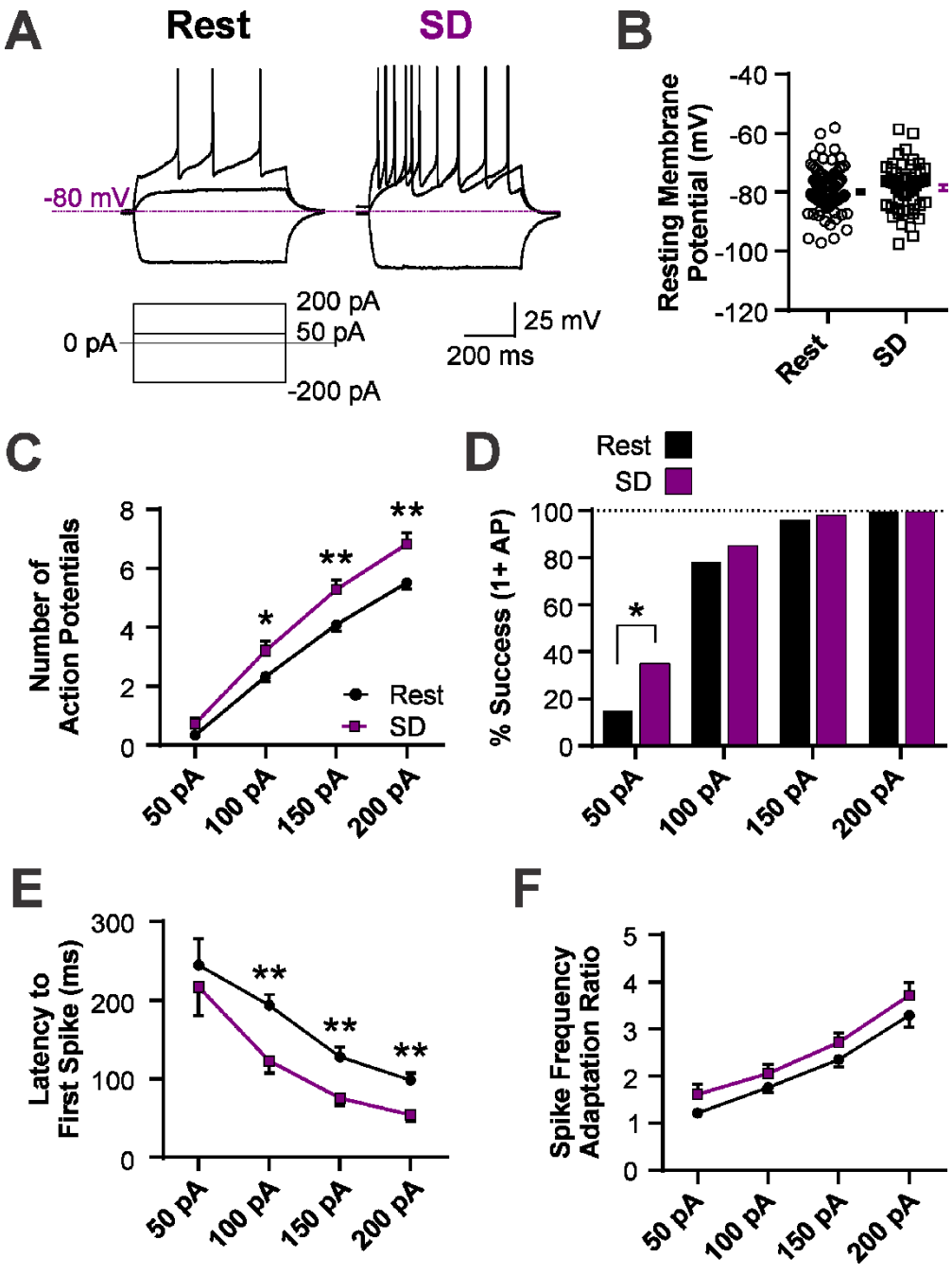
A
Rest
SD
-80 mV
200 pA
50 pA
0 pA
-200 pA
25 mV
200 ms
B
Resting Membrane Potential (mV)
-40
-60
-80
-100
-120
Rest
SD
C
Number of Action Potentials
8
6
4
2
0
*
**
**
Rest
SD
50 pA
100 pA
150 pA
200 pA
D
Rest
SD
% Success (1+ AP)
100
80
60
40
20
0
*
50 pA
100 pA
150 pA
200 pA
E
Latency to First Spike (ms)
300
200
100
0
**
**
**
50 pA
100 pA
150 pA
200 pA
F
Spike Frequency Adaptation Ratio
5
4
3
2
1
0
50 pA
100 pA
150 pA
200 pA

Figure 4.2. Sleep deprivation increases the intrinsic excitability of ORX neurons. (A) Representative traces of an ORX neuron from Rest and SD with similar RMPs. A series of 600 ms hyperpolarizing and depolarizing current steps were applied to assess neuron excitability. (B) Sleep deprivation has no effect on RMP in ORX neurons. (C) SD increases the number of action potentials (APs) in response to positive current steps. (D) Unlike in MCH neurons, there is no change in latency to first spike in ORX neurons. *P < 0.05 for sleep-state condition.

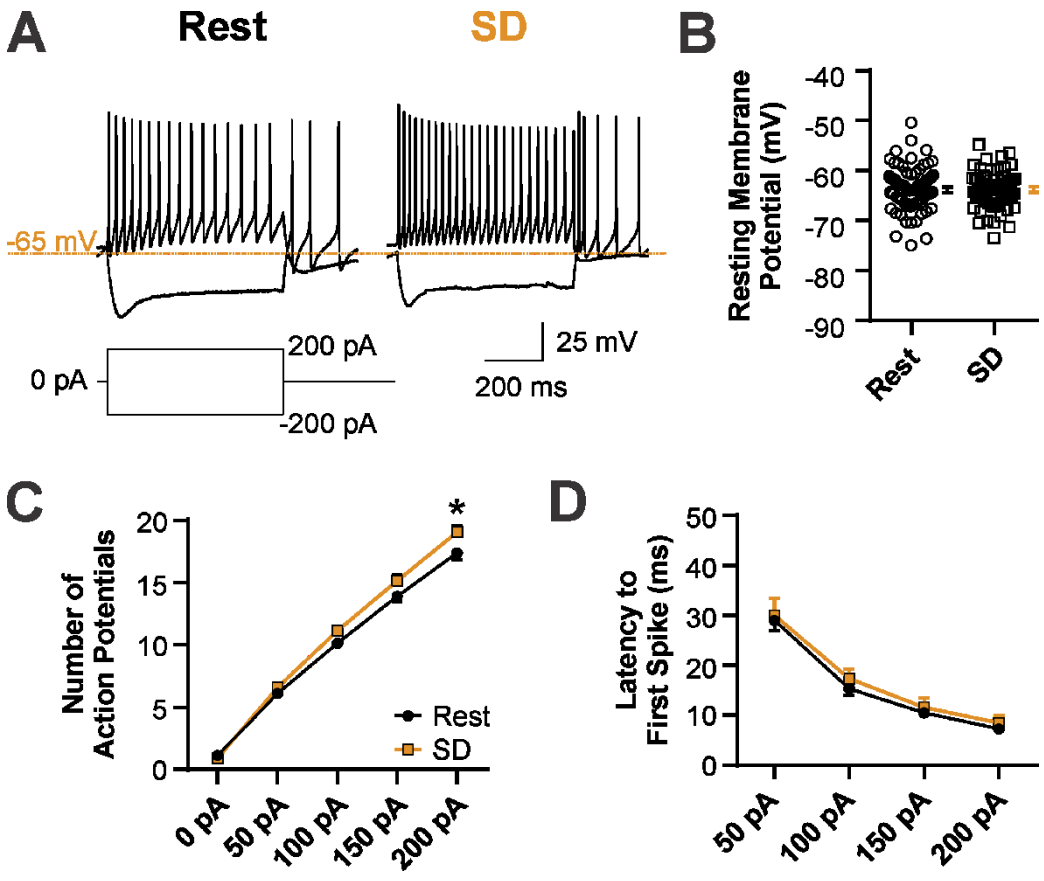
A
Rest
SD
-65 mV
200 pA
0 pA
-200 pA
25 mV
200 ms
B
Resting Membrane Potential (mV)
-40
-50
-60
-70
-80
-90
Rest
SD
C
Number of Action Potentials
20
15
10
5
0
*
Rest
SD
0 pA
50 pA
100 pA
150 pA
200 pA
D
Latency to First Spike (ms)
50
40
30
20
10
0
50 pA
100 pA
150 pA
200 pA

Figure 4.3. Sleep deprivation reduces the afterhyperpolarization in ORX neurons at a 200 pA depolarizing current. SD has no effect on AP amplitude (A) or half-width (B). SD decreases both the AHP amplitude (C) and the AHP area (D). (E) Regression analysis demonstrating a lack of correlation between the number of APs and AP amplitude. (F) Regression analysis demonstrating that the number of APs and AP half-width are positively correlated. (G, H) Regression analyses demonstrating that both AHP amplitude (G) and AHP area (H) are negatively correlated with number of APs. *$P < 0.05$, ***$P<0.001$ for sleep-state condition.

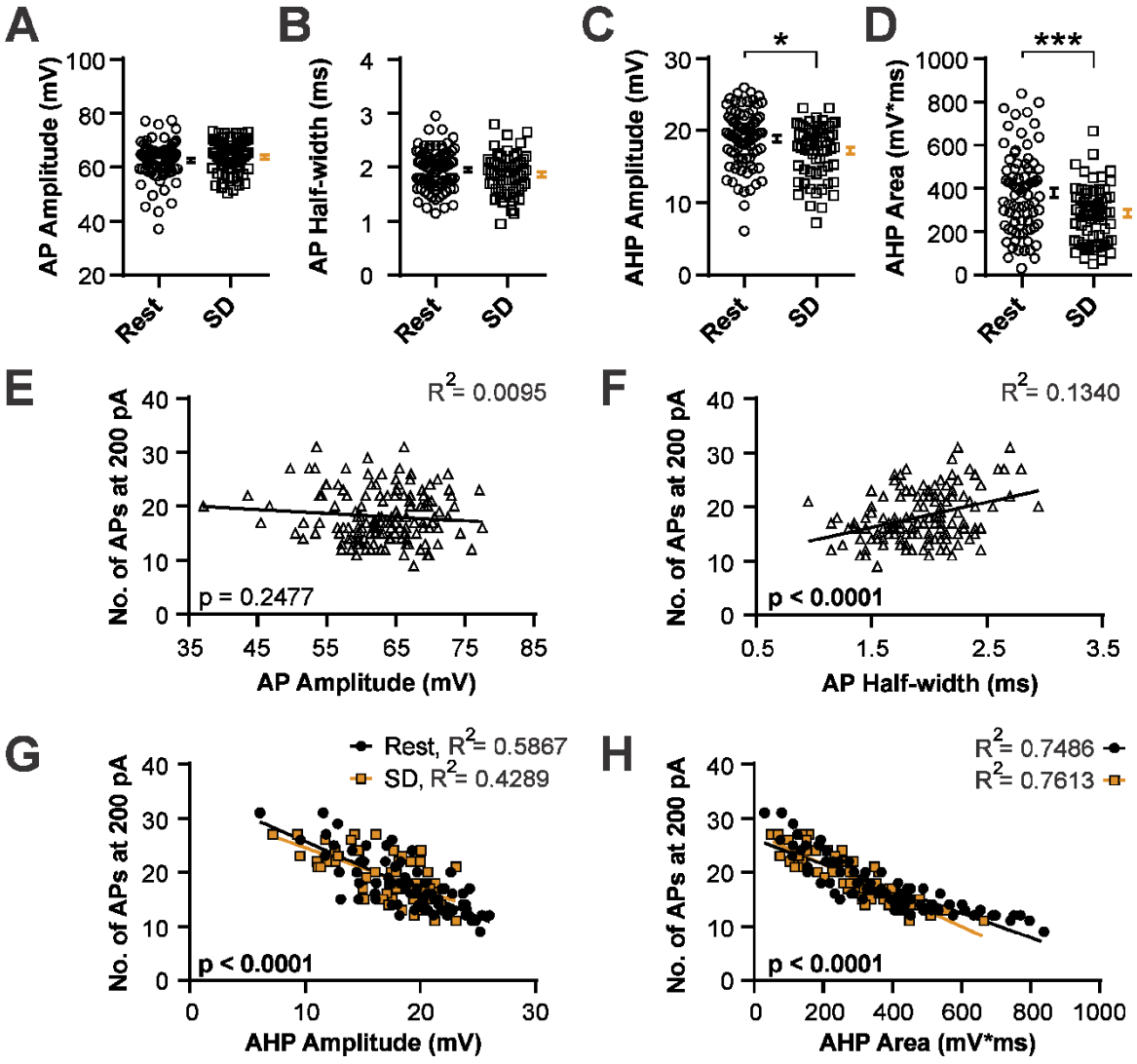
A
AP Amplitude (mV)
100
80
60
40
20
Rest
SD
B
AP Half-width (ms)
4
3
2
1
0
C
AHP Amplitude (mV)
30
20
10
0
*
D
AHP Area (mV*ms)
1000
800
600
400
200
0
***
E
No. of APs at 200 pA
R2= 0.0095
p = 0.2477
35
45
55
65
75
85
AP Amplitude (mV)
F
R2= 0.1340
p < 0.0001
0.5
1.5
2.5
3.5
AP Half-width (ms)
G
Rest, R2= 0.5867
SD, R2= 0.4289
p < 0.0001
AHP Amplitude (mV)
H
R2= 0.7486
R2= 0.7613
p < 0.0001
AHP Area (mV*ms)

Figure 4.4. Sleep deprivation does not change the ratio of D-type and H-type ORX neurons. (A) Representative traces from a D-type ORX neuron (left), and an H-type ORX neuron (right). They are easily distinguishable by their firing behaviour immediately upon relief from a hyperpolarizing current. (B) There is no difference in the ratio between D-type and H-type ORX neurons in response to SD.

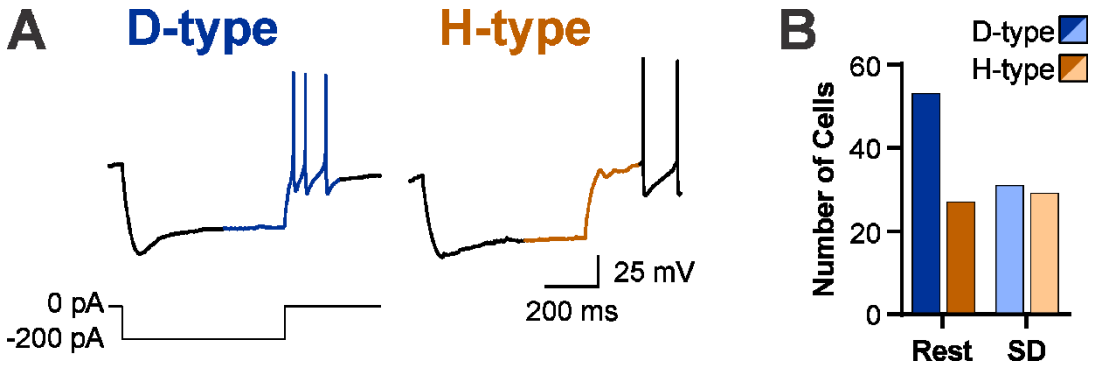
A
D-type
H-type
0 pA
-200 pA
25 mV
200 ms
B
D-type
H-type
Number of Cells
60
40
20
0
Rest
SD

Figure 4.5. Sleep deprivation increases the intrinsic excitability of D-type, but not H-type, ORX neurons. (A) SD increases firing with current injection in D-type ORX neurons. (B) Representative trace from a D-type ORX neuron (blue) and an H-type ORX neuron (orange) demonstrating their first spike in response to a 50 pA depolarizing current. Inset: The APs are lined up by their threshold potential. The vertical scale bar represents 20 mV and the horizontal scale bar represents 2 ms. (C) SD has no effect on latency to first spike for either ORX subpopulation. D-type neurons have a significantly shorter firing latency than H-type ORX neurons. (D) Latency to first spike following a 200 pA hyperpolarizing current (see Figure 4.4A) in H-type ORX neurons. (E) SD has no effect on AP threshold potential either ORX neuron subpopulation. *$P < 0.05$, **$P<0.01$ for sleep-state condition. $^{\#}P < 0.05$, $^{\#\#\#}P <0.001$ for ORX neuron subpopulation.

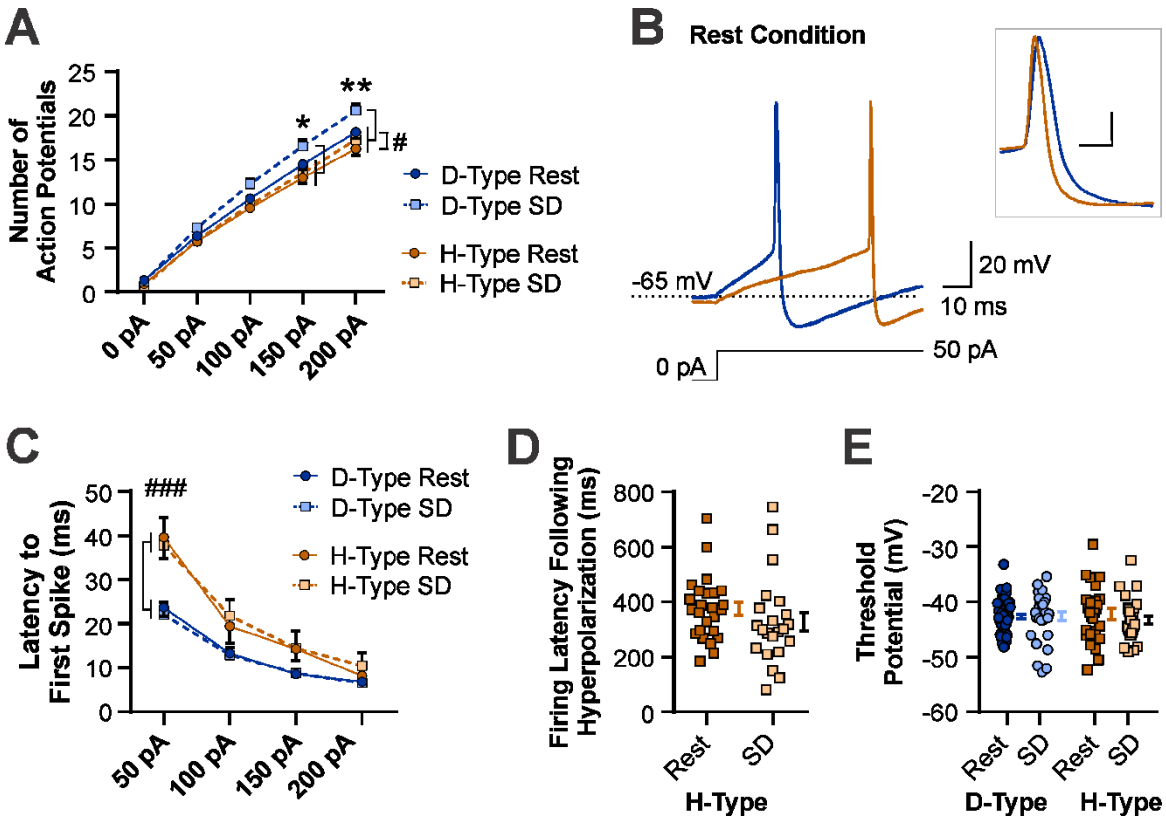
A
Number of Action Potentials
25
20
15
10
5
0
0 pA
50 pA
100 pA
150 pA
200 pA
*
**
#
D-Type Rest
D-Type SD
H-Type Rest
H-Type SD
B
Rest Condition
-65 mV
20 mV
10 ms
0 pA
50 pA
C
Latency to First Spike (ms)
50
40
30
20
10
0
###
50 pA
100 pA
150 pA
200 pA
D-Type Rest
D-Type SD
H-Type Rest
H-Type SD
D
Firing Latency Following Hyperpolarization (ms)
800
600
400
200
0
Rest
SD
H-Type
E
Threshold Potential (mV)
-20
-30
-40
-50
-60
Rest
SD
Rest
SD
D-Type
H-Type

Figure 4.6. A decrease in both AHP and spike adaptation underlie the increase in intrinsic excitability in D-type ORX neurons following sleep deprivation. (A-F) Analysis of APs induced by a 200 pA depolarizing current step. (A) Representative traces from D-type ORX neurons following Rest (top) and SD (bottom). Inset: The APs are lined up by their threshold potential. The vertical scale bar represents 20 mV and the horizontal scale bar represents 5 ms. (B) SD has no effect on AP amplitude. (C) SD has no effect on AP half-width in either ORX subpopulation. (D,E) SD decreases AHP amplitude (D) and area (E) specifically in D-type ORX neurons. (F) SD also decreases SFA in D-type ORX neurons (visible in A). *$P < 0.05$, **$P<0.01$ for sleep-state condition. $^{\#}P < 0.05$ for ORX neuron subpopulation.

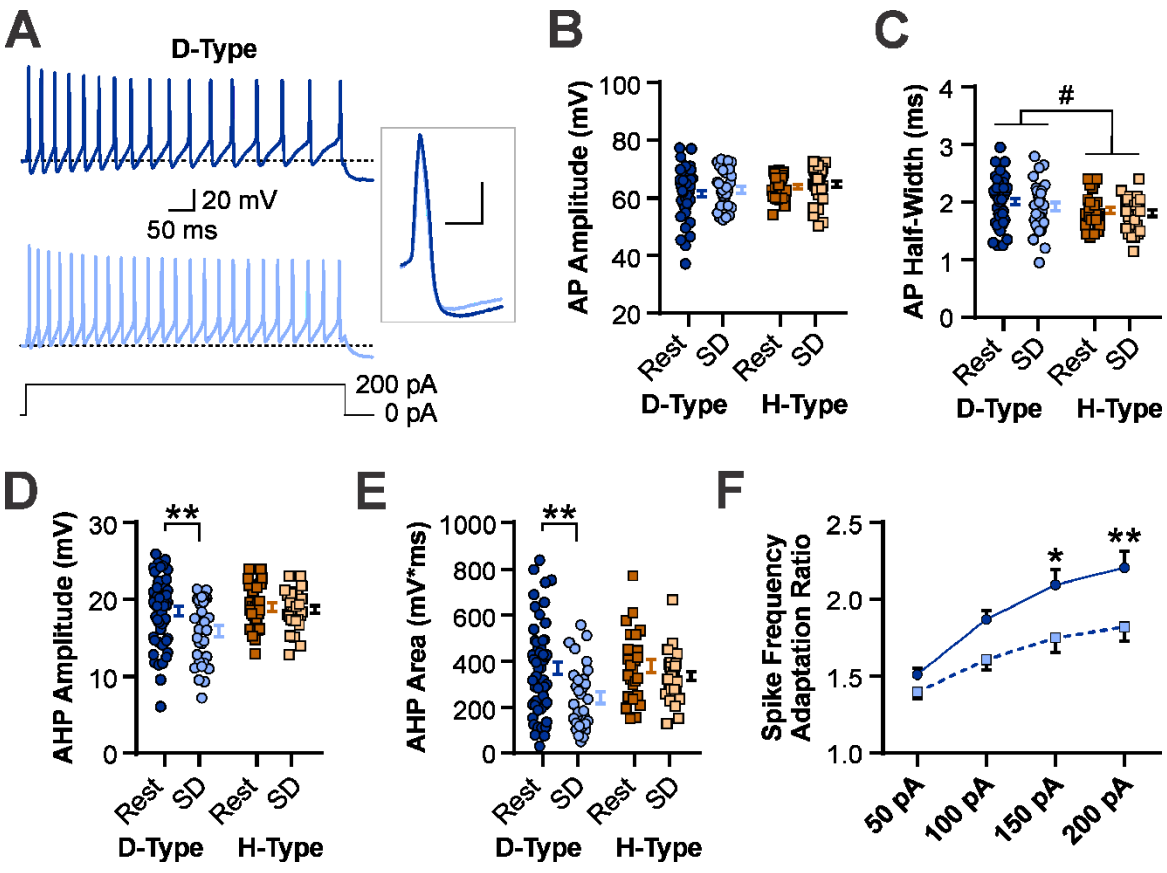
A
D-Type
20 mV
50 ms
200 pA
0 pA
B
AP Amplitude (mV)
100
80
60
40
20
Rest
SD
Rest
SD
D-Type
H-Type
C
AP Half-Width (ms)
4
3
2
1
0
#
Rest
SD
Rest
SD
D-Type
H-Type
D
AHP Amplitude (mV)
30
20
10
0
**
Rest
SD
Rest
SD
D-Type
H-Type
E
AHP Area (mV*ms)
1000
800
600
400
200
0
**
Rest
SD
Rest
SD
D-Type
H-Type
F
Spike Frequency Adaptation Ratio
2.5
2.0
1.5
1.0
*
**
50 pA
100 pA
150 pA
200 pA

Table 4.1. Membrane properties of MCH neurons by sleep-state condition.

	Rest			Sleep Deprived			
Variables	Mean	SEM	*n*	Mean	SEM	*n*	*P* value
Membrane Capacitance (pF)	93.17	2.15	110	87.54	2.17	53	0.1042
Membrane Resistance (MΩ)	348.2	16.87	62	367.2	19.3	34	0.4804
AP Threshold Potential (mV)	-40.87	0.41	91	-41.19	0.46	40	0.6408

Table 4.2. Membrane properties of MCH neurons by sleep-state condition.

	Rest			Sleep Deprived			
Variables	Mean	SEM	*n*	Mean	SEM	*n*	*P* value
Membrane Capacitance (pF)	62.86	1.52	74	62.92	1.77	52	0.9795
Membrane Resistance (MΩ)	373.2	18.38	74	341.1	21.06	52	0.257
AP Threshold Potential (mV)	-43.72	0.45	81	-43.92	0.53	61	0.7917
Spontaneous Firing Rate (Hz)	3.75	0.16	55	3.92	0.26	37	0.5763

Table 4.3. Intrinsic properties of D-type and H-type ORX neurons by sleep-state condition.

	D-Type							H-Type							D- vs. H-Type
	Rest			Sleep Deprived				Rest			Sleep Deprived				
Variables	Mean	SEM	*n*	Mean	SEM	*n*	*P* value*	Mean	SEM	*n*	Mean	SEM	*n*	*P* value*	*P* value!
Membrane Capacitance (pF)	62.22	1.807	48	60.65	1.955	28	0.8419	66.41	2.737	23	66.08	3.117	23	0.9302	**0.0472**
Membrane Resistance (MΩ)	367.0	22.52	48	373.8	29.69	28	0.8538	396.8	35.38	23	306.2	29.47	23	0.1005	0.5251
Membrane Potential (mV)	-63.61	0.46	53	-63.03	0.65	31	0.7338	-64.14	1.04	27	-64.88	0.664	29	0.7338	0.0848
Spontaneous Action Potentials															
Frequency (Hz)	3.903	0.2246	37	4.273	0.3736	23	0.5101	3.442	0.1656	18	3.326	0.2509	14	0.8088	**0.0201**
Threshold (mV)	-44.59	0.5011	47	-44.13	0.7931	31	0.6235	-44.02	1.1044	24	-45.64	0.5473	22	0.3201	0.5348
Amplitude (mV)	75.86	0.9001	47	77.72	1.126	31	0.4032	76.83	1.483	24	78.28	1.586	22	0.4632	0.5391
Half-Width (ms)	1.36	0.0439	47	1.21	0.0557	31	**0.0280**	1.102	0.0393	24	1.132	0.0432	22	0.7099	**0.0009**
AHP Amplitude (mV)	22.21	0.6423	47	22.24	0.7957	31	0.9994	24.8	0.7957	24	23.91	0.5839	22	0.6823	**0.0039**
AHP Area (mV)	2311.8	92.538	47	2365.0	91.334	31	0.6651	2582.4	86.676	24	2437.5	84.204	22	0.5856	0.0868

*** 2-way ANOVA, post hoc comparison for sleep state condition**
! 2-way ANOVA, main effect for ORX subpopulation

CHAPTER 5

GENERAL DISCUSSION

There are three major findings in this thesis. First, acute SD (6 h) alters GLT1 juxtaposition with the somata of sleep/wake regulatory neurons of the LH, but not the BF. The change in juxtaposition between GLT1 and ORX and MCH neuron somata following SD is opposite for these wake- and sleep-promoting LH neurons, and is reversible by a subsequent 3 h period of sleep opportunity (Chapter 2). Second, excitatory synaptic transmission to both ORX and MCH neurons is altered by SD in a manner consistent with the changes in GLT1 distribution. SD decreases GLT1 juxtaposition with ORX neurons while decreasing release probability at excitatory afferents to these neurons. This is due to tonic presynaptic inhibition via group III mGluRs, and results in metaplasticity at these synapses following SD (Chapter 2). Meanwhile, SD increases GLT1 juxtaposition with MCH neurons, and reduces the amplitude of a KA receptor-mediated slow EPSC induced by train stimulation (Chapter 2 and Chapter 3).

Third, acute SD induces intrinsic plasticity in LH neurons. It increases the excitability of both MCH and D-type ORX neurons by altering different membrane properties (Chapter 4). MCH neurons exhibit an increase in AP firing during positive current injections due to a decrease in latency to first spike, indicating a likely reduction in A-current following SD. D-type ORX neurons also demonstrate increased AP firing during positive current injections, but this is due to a decrease in AHP and a reduction in spike adaptation, potentially indicating a reduction in SK-current following SD (Chapter 4). Intrinsic excitability in H-type ORX neurons was unchanged. This cell subtype selectivity contrasts with the synaptic plasticity following SD (Chapter 2); release probability was reduced in excitatory afferents to both D-type and H-type ORX neurons following SD (Figure D.1).

Of note, while GLT1 juxtaposition with sleep/wake neurons was examined in Wistar rats, electrophysiological studies were performed using Sprague Dawley rats (Chapters 2 and 3). I was able to confirm that an increase in PPR in excitatory afferents to ORX neurons following SD in Wistar rats (Appendix E, Figure E.1) was very similar to that observed in Sprague-Dawley rats (Figure 2.6A). It is therefore unlikely that strain differences would confound the interpretation of the results.

Together, these data establish that acute SD induces synaptic and intrinsic plasticity in both ORX and MCH neurons via distinct presynaptic and postsynaptic

mechanisms. These findings have important implications for the homeostatic regulation of sleep.

5.1 Redistribution of GLT1 During SD

As briefly discussed in Section 2.5, GLT1 remodelling during SD could occur through a variety of mechanisms including GLT1 redistribution within astrocytic processes, or structural withdrawal or protrusion of astrocytic processes themselves.

5.1.1 GLT1 Redistribution Within Astrocytic Processes

If GLT1 is redistributing within astrocytic processes, the most likely mechanism is via glutamate-mediated motility and trafficking. GLT1 juxtaposition is lowest in both ORX and MCH neurons following periods of higher neuronal activity (Chapter 2), when the drive from excitatory afferents is stronger. Both GLT1 motility within the plasma membrane (Murphy-Royal et al., 2015), and GLT1 trafficking between the membrane and intracellular compartments (Nakagawa et al., 2008), may be involved and can both be initiated and promoted by glutamate itself, as previously demonstrated.

GLT1 internalization and degradation have also been reported to be mediated by protein kinase C (PKC; González et al., 2005; Sheldon et al., 2008; García-Tardón et al., 2012) independent of glutamate. A variety of neuromodulators that are released during wake can activate PKC in astrocytic cell cultures, including NA (Drouva et al., 1991; Juric et al., 2008), HA (Lipnik-Stangelj and Carman-Krzan, 2004; Wang et al., 2013), 5-HT (Li et al., 2008), and orexin peptides (Shu et al., 2014, 2016). Thus, these neuromodulators could also mediate SD-dependent GLT1 redistribution via PKC signaling within astrocytic processes.

5.1.2 Structural Plasticity of Astrocytic Processes

SD-induced structural plasticity of astrocytic processes is another likely explanation for changes in GLT1 juxtaposition with LH neurons. Structural plasticity of astrocytes has previously been demonstrated in other hypothalamic areas. In the SCN, astrocytic coverage of circadian pacemaker neurons changes in a rhythmic manner over

the 24 h circadian period (Becquet et al., 2008). In the supraoptic nucleus (SON), astrocytic coverage of magnocellular neurons decreases with a variety of homeostatic challenges such as parturition, lactation, and dehydration (Theodosis and Poulain, 1993). During lactation, this structural plasticity results in reduced GLT1 efficacy, increased glutamate diffusion and presynaptic inhibition in the SON (Oliet et al., 2001). These changes in excitatory transmission are similar to those I observed with ORX neurons following acute SD. It is therefore plausible that similar changes in astrocytic coverage are occurring in the LH in response to acute SD.

Astrocytic processes that associate with synapses are particularly motile, changing in shape, orientation, and location on the order of minutes (Haber et al., 2006). This has primarily been demonstrated in the hippocampus (Haber et al., 2006; Bernardinelli et al., 2014; Perez-Alvarez et al., 2014; Krzisch et al., 2015), but is also known to occur in the barrel cortex (Perez-Alvarez et al., 2014). I examined GLT1 juxtaposition with LH neuron somata, not dendrites or dendritic spines where most excitatory synapses usually occur (Sheng and Hoogenraad, 2007). Yet, ORX neurons are unconventional in that they receive more than five excitatory synapses for every inhibitory synapse to their somata (Horvath and Gao, 2005). Therefore, changes in somatic juxtaposition with GLT1 may be highly impactful in these neurons. Whether MCH neurons have a similar input distribution is currently unknown.

Structural plasticity of astrocytic processes occurs through actin remodelling downstream of astrocyte Ca^{2+} transients (Haber et al., 2006; Molotkov et al., 2013). Actin remodelling in astrocytes can occur rapidly through redistribution of pre-existing proteins rather than de novo protein synthesis (Safavi-Abbasi et al., 2001), consistent with the fast rate of astrocyte process remodelling in the hippocampus (Haber et al., 2006). Again, several neuromodulators with changing tones across sleep and wake may be initiating such structural plasticity. For one, NA results in propagating Ca^{2+} waves in astrocytes in awake mice (Ding et al., 2013). It has been proposed that NA release during wake, which typically occurs through non-synaptic (i.e., volume) transmission in the cortex (Cohen et al., 1997), changes the astrocyte network "gain" to make astrocytes more responsive to local neuronal activity (Paukert et al., 2014). While it is possible that NA during forced wake is facilitating opposite effects on astrocyte process juxtaposition with wake-active

ORX neurons and REM sleep-active MCH neurons, other signals may more readily account for the opposite changes observed following SD.

One possibility is another neuromodulator, acetylcholine (ACh). ACh induces Ca^{2+} signaling in astrocytes (Shelton and McCarthy, 2000; Takata et al., 2011; Chen et al., 2012). Unlike NA neurons, cholinergic neurons in the BF and the mesopontine tegmentum are active during both wake and REM sleep (Hassani et al., 2009a; Boucetta et al., 2014). While BF cholinergic neurons make few to no synaptic contacts with LH neurons (Henny and Jones, 2006a, 2006b; Agostinelli et al., 2016), the LH receives significant cholinergic projections from the mesopontine tegmentum (Bayer et al., 1999), and axonal cholinergic varicosities were commonly observed in the LH (Henny and Jones, 2006b). Like NA, ACh can be released through volume transmission (Picciotto et al., 2012) and may also tune astrocyte network "gain" to be responsive to local neuronal activity. Thus, cholinergic input to the LH could prime astrocytes to respond with structural remodelling of their processes to ORX neuron activity during wake (Lee et al., 2005) and MCH neuron activity during REM sleep (Hassani et al., 2009b), thereby facilitating the observed differences in GLT1 apposition with these two neuronal populations. Finally, other sleep/wake neuromodulators such as HA (Shelton and McCarthy, 2000) and 5-HT (Schipke et al., 2011) induce Ca^{2+} signalling in astrocytes, and may also be involved in wake-dependent structural plasticity in astrocytes.

ORX and MCH neurons are intermingled throughout the LH (Hahn, 2010), yet whether single astrocytes are juxtaposed with both ORX neurons and MCH neurons is unknown. Astrocytes in the neocortex and hippocampus are distributed in a tile-like pattern with non-overlapping territories (Bushong et al., 2002; Halassa et al., 2007). Within a single astrocyte, microdomains of astrocytic processes are capable of responding to and modulating synaptic activity in their vicinity (Grosche et al., 1999; Panatier et al., 2011; Shigetomi et al., 2013). If astrocytes in the LH also have non-overlapping territories, a single astrocyte could be exclusively juxtaposed with both ORX and MCH neurons, and exhibit opposite changes in GLT1 apposition with these neurons during SD. Alternatively, different subpopulations of astrocytes within the LH could be regulating ORX or MCH neurons. For example, in the basal ganglia, different subpopulations of astrocytes differentially respond to and regulate two intermingled populations of medium

spiny neurons (Martín et al., 2015). Further, in the hippocampus, different subpopulations of astrocytes responded to different combinations of neuromodulators that change their tone with sleep and wake (Shelton and McCarthy, 2000). If such subpopulations of astrocytes are also present in the LH, and express receptors to different neuromodulators, they could explain the opposite changes in GLT1 apposition with ORX and MCH neurons during acute SD.

5.1.3 Other Considerations

In addition to the mechanisms discussed above, there may be other explanations for changes in GLT1 juxtaposition with ORX and MCH neurons during SD. A previous report demonstrated that acute SD by gentle handling (4 h), or acute and chronic administration of modafinil, a wake promoting pharmaceutical that is used to treat narcolepsy, increased the frequency of miniature EPSCs (mEPSCs) in mouse ORX neurons (Rao et al., 2007). In the same study, chronic treatment with modafinil increased the number of anatomically-identified excitatory synapses on ORX neuron somata (Rao et al., 2007). A change in synapse number during SD could change the proportion of the somatic surface in apposition with GLT1 in LH neurons. While I have not done ultrastructural analyses, I did examine mEPSCs in both ORX and MCH neurons following Rest and SD in the rat (Appendix F). SD (6 h) had no effect on mEPSC frequency in ORX neurons compared to Rest (Figure F.1C). The discrepancy between my data and those from Rao et al. could be due to species differences, or it could be due to progressive changes occurring during prolonged wake. For example, following 4 hours of SD, Rao et al. observed an increase in mEPSC frequency in ORX neurons, potentially due to an increase in the number of excitatory synapses on their somata. Following 6 hours of SD, I did not observe a change in mEPSC frequency compared to Rest, while paired pulse ratio was increased (Figure 2.6A). It is possible that a decrease in release probability begins between 4 and 6 hours of SD to compensate for an earlier increase in synapse number, thus leading to no net change in mEPSC frequency following 6 hours of SD. Regardless, these data give little indication to whether changes in synapse number could be contributing to changes in GLT1 apposition with ORX neurons.

In MCH neurons, acute SD (6 h) did increase the frequency of mEPSCs compared to Rest (Figure F.1E) without a change in release probability (Figure 2.8A), suggesting that MCH neurons may receive more excitatory synapses following SD than following Rest. This is opposite to what one would predict based on GLT1 apposition, as GLT1 apposition with MCH neurons is higher, not lower, following SD (Figure 2.2H). The distribution of excitatory synapses on MCH neurons is not currently known. An increase in synapse number could be occurring within the dendritic arbor rather than on the soma. However, GLT1 is primarily located in astrocytic membranes facing synapses (Chaudhry et al., 1995). Therefore, increased somatic glutamatergic synapse number following SD could lead to increased GLT1 apposition.

5.2 Other Possible Consequences of Changes in GLT1 Juxtaposition

Alterations in juxtaposition of glutamate transporters with LH neurons could have implications beyond glutamatergic synaptic transmission. For example, neuronal and glial glutamate transport via EAAC1 and GLAST has been shown to modulate GABAergic transmission in many brain regions. In the midbrain periaqueductal gray, blocking the neuronal glutamate transporter EAAC1 results in presynaptic inhibition of GABAergic transmission (Drew et al., 2008). In the cerebellum, blocking the glial glutamate transporter GLAST has the opposite effect, increasing GABAergic transmission to Purkinje neurons through activation of presynaptic NMDA receptors (Huang and Bordey, 2004).

GLT1 has also specifically been implicated in modulating fast inhibitory transmission. In the dorsal horn of the spinal cord, blocking GLT1 decreases evoked inhibitory postsynaptic current (IPSC) amplitude, and decreases miniature IPSC amplitude and frequency (Jiang et al., 2012). In the hippocampus and SON, GLT1 prevents presynaptic inhibition of GABAergic transmission by preventing the activation of group III mGluRs on GABAergic terminals (Semyanov and Kullmann, 2000; Piet et al., 2003, 2004). A decrease in astrocytic coverage of SON neurons during lactation increased heterosynaptic signalling from excitatory synapses to inhibitory synapses due to increased glutamate diffusion (Piet et al., 2004). This led to the inhibition of GABAergic

transmission through activation of presynaptic group III mGluRs (Piet et al., 2004). GABAergic afferents to the SON also express KA receptors, and their impact on inhibitory synaptic transmission changes from facilitation to inhibition during lactation, due to increased concentrations of extracellular glutamate (Bonfardin et al., 2010).

Due to the wide array of glutamate receptors that can be present on GABAergic synaptic terminals, changes in GLT1 juxtaposition with LH neurons during SD may facilitate or inhibit GABAergic transmission to these neurons as well.

5.3 Integrating Synaptic and Intrinsic Plasticity in Response to SD

I have determined that a variety of changes in synaptic transmission and intrinsic excitability occurred in ORX and MCH neurons following SD compared to Rest (summarized in Table G.1). Importantly, measures that were altered by SD were not affected by how long the brain tissue was kept in vitro (Time-Since-Dissection; Appendix B), indicating that the effects of SD did not dissipate in vitro and that circadian influences were minimal over the experimental window. Likewise, these measures were not impacted by the age of the rat (Appendix C).

In wake-promoting ORX neurons, the decrease in glutamate release from excitatory afferents following SD may promote homeostatic transition to sleep. Yet, D-type ORX neurons concurrently demonstrate an increase in intrinsic excitability that would promote maintenance of the wake state. Following SD, MCH neurons also display an increase in intrinsic excitability that may contribute to sleep homeostasis. They also have a higher frequency of mEPSCs following SD, which also appears homeostatic. Yet, SD decreases the slow EPSC in these neurons, reducing the temporal summation of excitatory signals and favouring wake maintenance. While many SD-dependent changes appear contradictory, they could work together effectively to control the output of these sleep/wake neuronal populations according to behavioural need. After all, the specific output of a neuron is determined by the integration of its synaptic input and its intrinsic membrane properties (Sehgal et al., 2013).

In the next several sections, I will discuss each combination of neuronal population and sleep-state condition in turn, and propose how these seemingly disparate changes could work together for the appropriate control of sleep and wake.

5.3.1 ORX NEURONS DURING REST

In the Rest condition, ORX neurons and many neuronal populations that send excitatory afferents to them would be inactive (see Table A.1). Under this behavioral state, ORX neurons are under tonic inhibition from GABAergic neurons in the preoptic area (Koyama and Hayaishi, 1994; Suntsova et al., 2002; Saito et al., 2013), from MCH neurons (Rao et al., 2008) and likely from non-MCH GABAergic neurons from the LH (Hassani et al., 2010). GLT1 apposition is high, limiting glutamate diffusion (Figure 2.2). Excitatory afferents to ORX neurons have a high release probability due to the absence of inhibitory tone through presynaptic mGluRs (Figure 2.6). Under these conditions, should wake-promoting excitatory signals arrive, they would likely stimulate ORX neurons efficiently. Further, because excitatory terminals synapsing onto ORX neuron somata outnumber the inhibitory terminals by over five to one (Horvath and Gao, 2005), excitatory input in this area may quickly overcome the sleep-promoting GABAergic tone, activating ORX neurons, and facilitating transitions to wake.

5.3.2 ORX NEURONS DURING SD

In the SD condition, ORX neurons and many of their excitatory afferents would be active (see Table A.1). GLT1 apposition is low permitting increased glutamate diffusion from release sites (Figure 2.2). Consequently, excitatory afferents to ORX neurons have a reduced release probability due to tonic presynaptic inhibition through presynaptic group III mGluRs (Figure 2.6). Under these conditions, sparse wake-promoting signals would be selectively suppressed. This may be a neuronal correlate of sleepiness, which aids transitions from wake to sleep.

However, ORX neurons maintain the ability to promote wake following acute SD, should the need to maintain wake be sufficiently strong. For one, short-term synaptic depression during high frequency transmission at excitatory synapses is reduced

following SD (Figure 2.7), indicating that high intensity excitatory input can reliably drive ORX neurons in this condition. Second, D-type ORX neurons have increased intrinsic excitability following SD. Nonetheless, Strong synaptic excitatory drive would be required for this increase in excitability to become apparent, as it was only observed when large positive current injections were applied to these neurons (Figure 4.4).

The ability of ORX neurons to increase firing in response to strong excitatory input could be important for sustaining wake against mounting sleep pressure. ORX neurons can drive other wake-promoting neurons by releasing the excitatory transmitters glutamate and orexin peptides (Hagan et al., 1999; Brown et al., 2002; Arrigoni et al., 2010; Schöne et al., 2012, 2014); however, ORX neurons only release the wake-promoting orexin peptides under fast firing frequencies (Schöne et al., 2014). Because the same excitatory stimulus induces faster firing in D-type ORX neurons during SD than in Rest, D-type ORX neurons would more readily reach firing frequencies necessary for orexin peptide release in response to less synaptic excitatory drive following acute SD. This extra excitatory push may temporarily rebuff the inhibitory effects of increasing extracellular adenosine (Section 1.2.5) when there is an imperative need to maintain wake and alertness.

5.3.3 MCH Neurons during Rest

In the Rest condition, MCH neurons are active (see Table A.1). GLT1 apposition is low, permitting glutamate diffusion (Figure 2.2). In this condition, train stimulation results in a large slow EPSC (Figure 2.8). This indicates that there is robust temporal summation of excitatory currents in the Rest condition that could effectively depolarize MCH neurons. MCH neurons can release endocannabinoids when depolarized which results in the disinhibition of MCH neurons through the presynaptic inhibition of GABAergic transmission (Huang et al., 2007). Decreased GLT1 apposition during Rest could therefore strengthen excitatory transmission to MCH neurons through KA receptor-mediated slow EPSCs (Figure 3.5), and potentially result in decreased inhibitory input through retrograde endocannabinoid signalling, both of which would promote MCH neuron firing, likely contributing to sleep maintenance.

However, MCH neurons also have a large A-like current which becomes more prominent during Rest. There is consequently a low likelihood that small depolarizing currents will result in APs (Figure 4.1). These results suggest that while excitatory afferents can activate MCH neurons more efficiently during Rest, as excitatory drive to MCH neurons decreases with sleep satiety, activity of these neurons would become sparse, perhaps facilitating homeostatic transitions to Wake.

5.3.4 MCH NEURONS DURING SD

In the SD condition, MCH neurons are inactive (see Table A.1). GLT1 apposition is high, limiting glutamate diffusion (Figure 2.2). In this condition, train stimulation results in a reduced slow EPSC (Figure 2.8). This indicates that during SD, there is less temporal summation of excitatory currents than during Rest. However, since there is an increase in mEPSC frequency in these neurons during SD that is unaccompanied by a change in paired pulse ratio (See Figure 2.8A and Figure F.1E), there are likely more excitatory synapses on these neurons following acute SD. This could negate the effects of reduced temporal summation of excitatory currents.

Additionally, intrinsic excitability of MCH neurons increases during SD due to a reduction in A-like current. This raises the likelihood that sleep-promoting MCH neurons will fire APs in response to small and/or brief depolarizing currents (Figure 4.1). This intrinsic plasticity in MCH neurons may increasingly promote sleep as wake progresses.

Many forms of synaptic and intrinsic plasticity were observed in ORX and MCH neurons following acute SD compared to Rest. However, my interpretations of their effects on sleep/wake activity are constrained, because it is not known whether all or some of these changes occur simultaneously, or whether some precede (and inform) subsequent changes. This is especially true for MCH neurons. For example, does temporal summation of KA receptor currents increase in Rest to maintain MCH neuron output as excitatory synapses become less numerous or to overcome an increase in A-like current? Or does A-like current increase to counter a rise in temporal summation of KA receptor currents? The SD-dependent changes in ORX neurons appear more congruous

than those in MCH neurons; they are consistent with homeostatic sleep regulation, yet maintain the capacity of ORX neurons to further sustain wake under strong wake-promoting signals. Yet, as discussed in Section 5.1.3, there is also indication that SD-dependent changes in ORX neurons may occur sequentially. It will be important to determine how and when these changes are occurring to fully comprehend their roles in the homeostatic process of sleep regulation.

5.4 CONCLUSIONS

The research contained in this thesis suggests that both synaptic and intrinsic plasticity in sleep/wake regulatory neurons in the LH may be involved in the homeostatic process of sleep regulation. The glial glutamate transporter GLT1 differentially underlies synaptic plasticity in intermingled sleep-promoting MCH neurons and wake-promoting ORX neurons in the LH in a manner dependent on prior sleep history and largely consistent with the homeostatic regulation of sleep. In addition, acute SD paradoxically increases the intrinsic excitability of both neuronal populations with complex implications for sleep regulation. These results further our knowledge on the regulation of sleep and wake under normal physiological conditions, will inform future research, and will hopefully lead to improved interventions and therapeutics to reduce the negative impact of sleep loss and to improve health.

REFERENCES

Abel T, Havekes R, Saletin J, Walker M (2013) Sleep, Plasticity and Memory from Molecules to Whole-Brain Networks. Current Biology 23:R774–R788.

Acuna-Goycolea C, Li Y, van den Pol AN (2004) Group III metabotropic glutamate receptors maintain tonic inhibition of excitatory synaptic input to hypocretin/orexin neurons. The Journal of Neuroscience 24:3013–3022.

Adamantidis A, Zhang F, Aravanis A, Deisseroth K, de Lecea L (2007) Neural substrates of awakening probed with optogenetic control of hypocretin neurons. Nature 450:420–424.

Agostinelli LJ, Ferrari LL, Mahoney CE, Mochizuki T, Lowell BB, Arrigoni E, Scammell TE (2016) Descending Projections from the Basal Forebrain to the Orexin Neurons in Mice. The Journal of Comparative Neurology. ePub ahead of print.

Alberto CO, Trask RB, Hirasawa M (2011) Dopamine acts as a partial agonist for α2A adrenoceptor in melanin-concentrating hormone neurons. The Journal of Neuroscience 31:10671–10676.

Alberto C, Hirasawa M (2010) AMPA receptor-mediated miniature EPSCs have heterogeneous time courses in orexin neurons. Biochemical and Biophysical Research Communications 400:707–712.

Anaclet C, Parmentier R, Ouk K, Guidon G, Buda C, Sastre J-PP, Akaoka H, Sergeeva OA, Yanagisawa M, Ohtsu H, Franco P, Haas HL, Lin J-SS (2009) Orexin/hypocretin and histamine: distinct roles in the control of wakefulness demonstrated using knock-out mouse models. The Journal of Neuroscience 29:14423–14438.

Apergis-Schoute J, Iordanidou P, Faure C, Jego S, Schöne C, Aitta-Aho T, Adamantidis A, Burdakov D (2015) Optogenetic evidence for inhibitory signaling from orexin

to MCH neurons via local microcircuits. The Journal of Neuroscience 35:5435–5441.

Arrigoni E, Chamberlin NL, Saper CB, McCarley RW (2006) Adenosine inhibits basal forebrain cholinergic and noncholinergic neurons in vitro. Neuroscience 140:403–413.

Arrigoni E, Mochizuki T, Scammell TE (2010) Activation of the basal forebrain by the orexin/hypocretin neurones. Acta Physiologica 198:223–235.

Bak L, Schousboe A, Waagepetersen H (2006) The glutamate/GABA-glutamine cycle: aspects of transport, neurotransmitter homeostasis and ammonia transfer. The Journal of Neurochemistry 98:641–653.

Bal-Price A, Moneer Z, Brown GC (2002) Nitric oxide induces rapid, calcium-dependent release of vesicular glutamate and ATP from cultured rat astrocytes. Glia 40:312–323.

Basheer R, Porkka-Heiskanen T, Stenberg D, McCarley RW (1999) Adenosine and behavioral state control: adenosine increases c-Fos protein and AP1 binding in basal forebrain of rats. Molecular Brain Research 73:1–10.

Basner M, Dinges DF (2011) Maximizing sensitivity of the psychomotor vigilance test (PVT) to sleep loss. Sleep 34:581–591.

Bayer L, Eggermann E, Serafin M, Grivel J, Machard D, Muhlethaler M, Jones BE (2005) Opposite effects of noradrenaline and acetylcholine upon hypocretin/orexin versus melanin concentrating hormone neurons in rat hypothalamic slices. Neuroscience 130:807–811.

Bayer L, Risold PY, Griffond B, Fellmann D (1999) Rat diencephalic neurons producing melanin-concentrating hormone are influenced by ascending cholinergic projections. Neuroscience 91:1087–1101.

Beaulé C, Granados-Fuentes D, Marpegan L, Herzog ED (2011) In vitro circadian rhythms: imaging and electrophysiology. Essays in Biochemistry 49:103–117.

Bechtholt-Gompf AJ, Walther HV, Adams MA, Carlezon WA, Ongür D, Cohen BM (2010) Blockade of astrocytic glutamate uptake in rats induces signs of anhedonia and impaired spatial memory. Neuropsychopharmacology 35:2049–2059.

Becquet D, Girardet C, Guillaumond F, François-Bellan A, Bosler O (2008) Ultrastructural plasticity in the rat suprachiasmatic nucleus. Possible involvement in clock entrainment. Glia 56:294–305.

Bernardinelli Y, Randall J, Janett E, Nikonenko I, König S, Jones E, Flores C, Murai K, Bochet C, Holtmaat A, Muller D (2014) Activity-Dependent Structural Plasticity of Perisynaptic Astrocytic Domains Promotes Excitatory Synapse Stability. Current Biology 24:1679–1688.

Bjorness TE, Dale N, Mettlach G, Sonneborn A, Sahin B, Fienberg AA, Yanagisawa M, Bibb JA, Greene RW (2016) An Adenosine-Mediated Glial-Neuronal Circuit for Homeostatic Sleep. The Journal of Neuroscience 36:3709–3721.

Bjorness TE, Greene RW (2009) Adenosine and sleep. Current Neuropharmacology 7:238–245.

Blanco-Centurion C, Liu M, Konadhode RP, Zhang X, Pelluru D, van den Pol AN, Shiromani PJ (2016) Optogenetic activation of melanin-concentrating hormone neurons increases non-rapid eye movement and rapid eye movement sleep during the night in rats. The European Journal of Neuroscience 44:2846–2857.

Bonfardin VDJ, Fossat P, Theodosis DT, Oliet SHR (2010) Glia-dependent switch of kainate receptor presynaptic action. The Journal of Neuroscience 30:985–995.

Borbély AA (1982) A two process model of sleep regulation. Human Neurobiology 1:195–204.

Borbély AA, Daan S, Wirz-Justice A, Deboer T (2016) The two-process model of sleep regulation: a reappraisal. The Journal of Sleep Research 25:131–143.

Boucetta S, Cissé Y, Mainville L, Morales M, Jones BE (2014) Discharge profiles across the sleep-waking cycle of identified cholinergic, GABAergic, and glutamatergic

neurons in the pontomesencephalic tegmentum of the rat. The Journal of Neuroscience 34:4708–4727.

Brown R, Basheer R, McKenna J, Strecker R, McCarley R (2012) Control of sleep and wakefulness. Physiological Reviews 92:1087–1187.

Brown R, Sergeeva O, Eriksson K, Haas H (2002) Convergent excitation of dorsal raphe serotonin neurons by multiple arousal systems (orexin/hypocretin, histamine and noradrenaline). The Journal of Neuroscience 22:8850–8859.

Burdakov D, Alexopoulos H, Vincent A, Ashcroft FM (2004) Low-voltage-activated A-current controls the firing dynamics of mouse hypothalamic orexin neurons. European Journal of Neuroscience 20:3281–3285.

Bushong EA, Martone ME, Jones YZ, Ellisman MH (2002) Protoplasmic astrocytes in CA1 stratum radiatum occupy separate anatomical domains. The Journal of Neuroscience 22:183–192.

Bélanger M, Allaman I, Magistretti PJ (2011) Brain energy metabolism: focus on astrocyte-neuron metabolic cooperation. Cell Metabolism 14:724–738.

Büttner D, Wollnik F (1984) Strain-differentiated circadian and ultradian rhythms in locomotor activity of the laboratory rat. Behavior Genetics 14:137–152.

Cain SW, Silva EJ, Chang A-MM, Ronda JM, Duffy JF (2011) One night of sleep deprivation affects reaction time, but not interference or facilitation in a Stroop task. Brain and Cognition 76:37–42.

Carnes K, Fuller T, Price J (1990) Sources of presumptive glutamatergic/aspartatergic afferents to the magnocellular basal forebrain in the rat. The Journal of Comparative Neurology 302:824–852.

Carrasquillo Y, Nerbonne JM (2014) IA channels: diverse regulatory mechanisms. Neuroscientist 20:104–111.

Carter ME, Yizhar O, Chikahisa S, Nguyen H, Adamantidis A, Nishino S, Deisseroth K, de Lecea L (2010) Tuning arousal with optogenetic modulation of locus coeruleus neurons. Nature Neuroscience 13:1526–1533.

Chaudhry F, Lehre K, van Campagne M, Ottersen O, Danbolt N, Storm-Mathisen J (1995) Glutamate transporters in glial plasma membranes: Highly differentiated localizations revealed by quantitative ultrastructural immunocytochemistry. Neuron 15:711–720.

Chen N, Sugihara H, Sharma J, Perea G, Petravicz J, Le C, Sur M (2012) Nucleus basalis-enabled stimulus-specific plasticity in the visual cortex is mediated by astrocytes. Proceedings of the National Academy of Science of the United States of America 109:E2832–41.

Chiu C, Prober D (2013) Regulation of zebrafish sleep and arousal states: current and prospective approaches. Frontiers in Neural Circuits 7:58.

Chou TC, Lee CE, Lu J, Elmquist JK, Hara J, Willie JT, Beuckmann CT, Chemelli RM, Sakurai T, Yanagisawa M, Saper CB, Scammell TE (2001) Orexin (hypocretin) neurons contain dynorphin. The Journal of Neuroscience 21:RC168.

Cirelli C, Pompeiano M, Tononi G (1995) Sleep deprivation and c-fos expression in the rat brain. Journal of Sleep Research 4:92–106.

Cohen Z, Molinatti G, Hamel E (1997) Astroglial and vascular interactions of noradrenaline terminals in the rat cerebral cortex. Journal of Cerebral Blood Flow and Metabolism 17:894–904.

Colwell C (2011) Linking neural activity and molecular oscillations in the SCN. Nature Reviews Neuroscience 12:553–569.

Coyle JT (1983) Neurotoxic action of kainic acid. Journal of Neurochemistry 41:1–11.

Cronk J, Derecki N, Kipnis J (2012) Measurement of neuron soma size by fluorescent Nissl stain. Nature Protocol Exchange. doi:10.1038/protex.2012.022

Cui R, Li B, Suemaru K, Araki H (2008) Psychological stress-induced changes in sleep patterns and their generation mechanism. Yakugaku Zasshi 128:405–411.

Czeisler, Duffy, Shanahan, Brown, Mitchell, Rimmer, Ronda, Silva, Allan, Emens, Dijk, Kronauer (1999) Stability, precision, and near-24-hour period of the human circadian pacemaker. Science 284:2177–2181.

Czisch M, Wetter TC, Kaufmann C, Pollmächer T, Holsboer F, Auer DP (2002) Altered processing of acoustic stimuli during sleep: reduced auditory activation and visual deactivation detected by a combined fMRI/EEG study. Neuroimage 16:251–258.

Daan S, Beersma DG, Borbély AA (1984) Timing of human sleep: recovery process gated by a circadian pacemaker. The American Journal of Physiology 246:R161–83.

Danbolt NC (2001) Glutamate uptake. Progress in Neurobiology 65:1–105.

Danbolt NC, Furness DN, Zhou (2016) Neuronal vs glial glutamate uptake: Resolving the conundrum. Neurochemistry International 98:29–45.

Deng W, Rosenberg PA, Volpe JJ, Jensen FE (2003) Calcium-permeable AMPA/kainate receptors mediate toxicity and preconditioning by oxygen-glucose deprivation in oligodendrocyte precursors. Proceedings of the National Academy of Science of the United States of America 100:6801–6806.

Derecki N, Cronk J, Lu Z, Xu E, Abbott S, Guyenet P, Kipnis J (2012) Wild-type microglia arrest pathology in a mouse model of Rett syndrome. Nature 484:105–109.

Deurveilher S, Rusak B, Semba K (2011) Female reproductive hormones alter sleep architecture in ovariectomized rats. Sleep 34:519–530.

Devera A, Pascovich C, Lagos P, Falconi A, Sampogna S, Chase M, Torterolo P (2015) Melanin-concentrating hormone (MCH) modulates the activity of dorsal raphe neurons. Brain Research 1598:114–128.

Ding F, O'Donnell J, Thrane AS, Zeppenfeld D, Kang H, Xie L, Wang F, Nedergaard M (2013) α1-Adrenergic receptors mediate coordinated Ca2+ signaling of cortical astrocytes in awake, behaving mice. Cell Calcium 54:387–394.

Do JP, Xu M, Lee S-HH, Chang W-CC, Zhang S, Chung S, Yung TJ, Fan JL, Miyamichi K, Luo L, Dan Y (2016) Cell type-specific long-range connections of basal forebrain circuit. Elife 5:13214.

Donlea JM, Pimentel D, Miesenböck G (2014) Neuronal machinery of sleep homeostasis in Drosophila. Neuron 81:860–872.

Doucet J, Lenihan N, May B (2009) Commissural Neurons in the Rat Ventral Cochlear Nucleus. Journal of the Association for Research in Otolaryngology 10:269–280.

Drew GM, Mitchell VA, Vaughan CW (2008) Glutamate spillover modulates GABAergic synaptic transmission in the rat midbrain periaqueductal grey via metabotropic glutamate receptors and endocannabinoid signaling. The Journal of Neuroscience 28:808–815.

Drouva SV, Faivre-Bauman A, Loudes C, Laplante E, Kordon C (1991) Alpha 1-adrenergic receptor coupling with phospholipase-C is negatively regulated by protein kinase-C in primary cultures of hypothalamic neurons and glial cells. Endocrinology 129:1605–1613.

Duque, Balatoni, Detari, Zaborszky (2000) EEG correlation of the discharge properties of identified neurons in the basal forebrain. Journal of Neurophysiology 84:1627–1635.

D'Ascenzo M, Fellin T, Terunuma M, Revilla-Sanchez R, Meaney D, Auberson Y, Moss S, Haydon P (2007) mGluR5 stimulates gliotransmission in the nucleus accumbens. Proceedings of the National Academy of Science of the United States of America 104:1995–2000.

Eder M, Becker K, Rammes G, Schierloh A, Azad SC, Zieglgänsberger W, Dodt H-UU (2003) Distribution and properties of functional postsynaptic kainate receptors on

neocortical layer V pyramidal neurons. The Journal of Neuroscience 23:6660–6670.

Eggermann E, Bayer L, Serafin M, Saint-Mleux B, Bernheim L, Machard D, Jones B, Mühlethaler M (2003) The wake-promoting hypocretin-orexin neurons are in an intrinsic state of membrane depolarization. The Journal of Neuroscience 23:1557–1562.

Elliott A, Huber J, O'Callaghan J, Rosen C, Miller D (2014) A review of sleep deprivation studies evaluating the brain transcriptome. SpringerPlus 3:728.

España R, Reis K, Valentino R, Berridge C (2005) Organization of hypocretin/orexin efferents to locus coeruleus and basal forebrain arousal-related structures. The Journal of Comparative Neurology 481:160–178.

Estabrooke IV, McCarthy MT, Ko E, Chou TC, Chemelli RM, Yanagisawa M, Saper CB, Scammell TE (2001) Fos expression in orexin neurons varies with behavioral state. The Journal of Neuroscience 21:1656–1662.

Faber ES (2009) Functions and modulation of neuronal SK channels. Cell Biochemistry and Biophysics 55:127–139.

Fellin T, Pascual O, Gobbo S, Pozzan T, Haydon PG (2004) Neuronal synchrony mediated by astrocytic glutamate through activation of extrasynaptic NMDA receptors. Neuron 43:729-743

Fenzl T, Romanowski C, Flachskamm C, Honsberg K, Boll E, Hoehne A, Kimura M (2007) Fully automated sleep deprivation in mice as a tool in sleep research. Journal of Neuroscience Methods 166:229–235.

Frank MG (2013) Astroglial regulation of sleep homeostasis. Current Opinion in Neurobiology 23:812–818.

Fujita T, Chen M, Li B, Smith N, Peng W, Sun W, Toner M, Kress B, Wang L, Benraiss A, Takano T, Wang S, Nedergaard M (2014) Neuronal Transgene Expression in Dominant-Negative SNARE Mice. The Journal of Neuroscience 34:16594–16604.

Fumagalli M, Brambilla R, D'Ambrosi N, Volonté C, Matteoli M, Verderio C, Abbracchio MP (2003) Nucleotide-mediated calcium signaling in rat cortical astrocytes: Role of P2X and P2Y receptors. Glia 43:218–03.

Furness DN, Dehnes, Akhtar AQ, Rossi DJ, Hamann, Grutle NJ, Gundersen, Holmseth, Lehre KP, Ullensvang, Wojewodzic, Zhou, Attwell, Danbolt NC (2008) A quantitative assessment of glutamate uptake into hippocampal synaptic terminals and astrocytes: New insights into a neuronal role for excitatory amino acid transporter 2 (EAAT2). Neuroscience 157:80–94.

García-Marín V, García-López P, Freire M (2007) Cajal's contributions to glia research. Trends in Neurosciences 30:479–487.

García-Tardón N, González-González IM, Martínez-Villarreal J, Fernández-Sánchez E, Giménez C, Zafra F (2012) Protein kinase C (PKC)-promoted endocytosis of glutamate transporter GLT-1 requires ubiquitin ligase Nedd4-2-dependent ubiquitination but not phosphorylation. Journal of Biological Chemistry 287:19177–19187.

Genoud C, Quairiaux C, Steiner P, Hirling H, Welker E, Knott G (2006) Plasticity of astrocytic coverage and glutamate transporter expression in adult mouse cortex. PLoS Biology 4:e343.

Girardeau G, Benchenane K, Wiener SI, Buzsáki G, Zugaro MBB (2009) Selective suppression of hippocampal ripples impairs spatial memory. Nature Neuroscience 12:1222–1223.

Goel N, Basner M, Rao H, Dinges DF (2013) Circadian rhythms, sleep deprivation, and human performance. Progress in Molecular Biology and Translational Science 119:155–190.

González J, Iordanidou P, Strom M, Adamantidis A, Burdakov D (2016) Awake dynamics and brain-wide direct inputs of hypothalamic MCH and orexin networks. Nature Communications 7:11395.

González MI, Susarla BT, Robinson MB (2005) Evidence that protein kinase Calpha interacts with and regulates the glial glutamate transporter GLT-1. Journal of Neurochemistry 94:1180–1188.

Gritti I, Manns I, Mainville L, Jones B (2003) Parvalbumin, calbindin, or calretinin in cortically projecting and GABAergic, cholinergic, or glutamatergic basal forebrain neurons of the rat. The Journal of Comparative Neurology 458:11–31.

Grivel J, Cvetkovic V, Bayer L, Machard D, Tobler I, Mühlethaler M, Serafin M (2005) The wake-promoting hypocretin/orexin neurons change their response to noradrenaline after sleep deprivation. The Journal of Neuroscience 25:4127–4130.

Grosche J, Matyash V, Möller T, Verkhratsky A, Reichenbach A, Kettenmann H (1999) Microdomains for neuron-glia interaction: parallel fiber signaling to Bergmann glial cells. Nature Neuroscience 2:139–143.

Grunnet M, Jespersen T, Perrier J-FF (2004) 5-HT1A receptors modulate small-conductance Ca2+-activated K+ channels. Journal Neuroscience Research 78:845–854.

Haber M, Zhou L, Murai KK (2006) Cooperative astrocyte and dendritic spine dynamics at hippocampal excitatory synapses. The Journal of Neuroscience 26:8881–8891.

Hafner M, Stepanek M, Taylor J, Troxel W, Stolk C (2016) Why sleep matters - the economic costs of insufficient sleep: A cross-country comparative analysis. RAND Corporation - Report. http://www.rand.org/content/dam/rand/pubs/research_reports/RR1700/RR1791/RAND_RR1791.pdf

Hagan J et al. (1999) Orexin A activates locus coeruleus cell firing and increases arousal in the rat. Proceedings of the National Academy of Sciences of the United States of America 96:10911–10916.

Hahn J (2010) Comparison of melanin-concentrating hormone and hypocretin/orexin peptide expression patterns in a current parceling scheme of the lateral hypothalamic zone. Neuroscience Letters 468:12–17.

Halassa M, Fellin T, Takano H, Dong J-H, Haydon P (2007) Synaptic Islands Defined by the Territory of a Single Astrocyte. The Journal of Neuroscience 27:6473–6477.

Halassa M, Florian C, Fellin T, Munoz J, Lee S-Y, Abel T, Haydon P, Frank M (2009) Astrocytic Modulation of Sleep Homeostasis and Cognitive Consequences of Sleep Loss. Neuron 61:213–219.

Harada K, Kamiya T, Tsuboi T (2015) Gliotransmitter Release from Astrocytes: Functional, Developmental, and Pathological Implications in the Brain. Frontiers in Neuroscience 9:499.

Harris G, Aston-Jones G (2006) Arousal and reward: a dichotomy in orexin function. Trends in Neuroscience 29:571–577.

Harris GC, Wimmer M, Randall-Thompson JF, Aston-Jones G (2007) Lateral hypothalamic orexin neurons are critically involved in learning to associate an environment with morphine reward. Behavioural Brain Research 183:43–51.

Hassani O, Lee M, Henny P, Jones BE (2009a) Discharge Profiles of Identified GABAergic in Comparison to Cholinergic and Putative Glutamatergic Basal Forebrain Neurons across the Sleep–Wake Cycle. The Journal of Neuroscience 29:11828–11840.

Hassani O, Lee M, Jones B (2009b) Melanin-concentrating hormone neurons discharge in a reciprocal manner to orexin neurons across the sleep–wake cycle. Proceedings of the National Academy of Sciences of the United States of America 106:2418–2422.

Hassani OK, Henny P, Lee MG, Jones BE (2010) GABAergic neurons intermingled with orexin and MCH neurons in the lateral hypothalamus discharge maximally during sleep. The European Journal of Neuroscience 32:448–457.

Henny P, Jones BE (2006a) Innervation of orexin/hypocretin neurons by GABAergic, glutamatergic or cholinergic basal forebrain terminals evidenced by immunostaining for presynaptic vesicular transporter and postsynaptic scaffolding proteins. The Journal of Comparative Neurology 499:645–661.

Henny P, Jones BE (2006b) Vesicular glutamate (VGlut), GABA (VGAT), and acetylcholine (VACht) transporters in basal forebrain axon terminals innervating the lateral hypothalamus. The Journal of Comparative Neurology 496:453–467.

Herman J, Kafoa B, Wainiqolo I, Robinson E, McCaig E, Connor J, Jackson R, Ameratunga S (2014) Driver sleepiness and risk of motor vehicle crash injuries: a population-based case control study in Fiji (TRIP 12). Injury 45:586–591.

Hobson JA, Pace-Schott EF (2002) The cognitive neuroscience of sleep: neuronal systems, consciousness and learning. Nature Reviews Neuroscience 3:679–693.

Horvath, Peyron, Diano, Ivanov, Aston-Jones, Kilduff, van Pol D (1999) Hypocretin (orexin) activation and synaptic innervation of the locus coeruleus noradrenergic system. The Journal of Comparative Neurology 415:145–159.

Horvath T, Gao X-B (2005) Input organization and plasticity of hypocretin neurons Possible clues to obesity's association with insomnia. Cell Metabolism 1:279–286.

Howard ME, Jackson ML, Swann P, Berlowitz DJ, Grunstein RR, Pierce RJ (2014) Deterioration in driving performance during sleep deprivation is similar in professional and nonprofessional drivers. Traffic Injury Prevension 15:132–137.

Huang H, Acuna-Goycolea C, Li Y, Cheng, Obrietan K, van den Pol A (2007) Cannabinoids excite hypothalamic melanin-concentrating hormone but inhibit hypocretin/orexin neurons: implications for cannabinoid actions on food intake and cognitive arousal. The Journal of Neuroscience 27:4870–4881.

Huang H, Bordey A (2004) Glial glutamate transporters limit spillover activation of presynaptic NMDA receptors and influence synaptic inhibition of Purkinje neurons. The Journal of Neuroscience 24:5659–5669.

Huang H, van den Pol A (2007) Rapid direct excitation and long-lasting enhancement of NMDA response by group I metabotropic glutamate receptor activation of hypothalamic melanin-concentrating hormone neurons. The Journal of Neuroscience 27:11560–11572.

Huang Y, Sinha S, Tanaka K, Rothstein J, Bergles D (2004) Astrocyte Glutamate Transporters Regulate Metabotropic Glutamate Receptor-Mediated Excitation of Hippocampal Interneurons. The Journal of Neuroscience 24:4551–4559.

Hur EE, Edwards RH, Rommer, Zaborszky (2009) Vesicular glutamate transporter 1 and vesicular glutamate transporter 2 synapses on cholinergic neurons in the sublenticular gray of the rat basal forebrain: a double-label electron microscopic study. Neuroscience 164:1721–1731.

Ida T, Hara M, Nakamura Y, Kozaki S, Tsunoda S, Ihara H (2008) Cytokine-induced enhancement of calcium-dependent glutamate release from astrocytes mediated by nitric oxide. Neuroscience Letters 432:232–236.

Isaacson J, Nicoll R (1993) The uptake inhibitor L-trans-PDC enhances responses to glutamate but fails to alter the kinetics of excitatory synaptic currents in the hippocampus. Journal of Neurophysiology 70:2187–2191.

Ishibashi M, Gumenchuk I, Miyazaki K, Inoue T, Ross WN, Leonard CS (2016) Hypocretin/Orexin Peptides Alter Spike Encoding by Serotonergic Dorsal Raphe Neurons through Two Distinct Mechanisms That Increase the Late Afterhyperpolarization. The Journal of Neuroscience 36:10097–10115.

Jackson R (2011) Glial cell modulation of circadian rhythms. Glia 59:1341–1350.

Jego S, Glasgow SD, Herrera CG, Ekstrand M, Reed SJ, Boyce R, Friedman J, Burdakov D, Adamantidis AR (2013) Optogenetic identification of a rapid eye movement

sleep modulatory circuit in the hypothalamus. Nature Neuroscience 16:1637–1643.

Jeremic A, Jeftinija K, Stevanovic J, Glavaski A, Jeftinija S (2001) ATP stimulates calcium-dependent glutamate release from cultured astrocytes. Journal of Neurochemistry 77:664–675.

Ji H, Hougaard C, Herrik KF, Strøbaek D, Christophersen P, Shepard PD (2009) Tuning the excitability of midbrain dopamine neurons by modulating the Ca2+ sensitivity of SK channels. The European Journal of Neuroscience 29:1883–1895.

Jiang E, Yan X, Weng H-RR (2012) Glial glutamate transporter and glutamine synthetase regulate GABAergic synaptic strength in the spinal dorsal horn. Journal of Neurochemistry 121:526–536.

Joiner WJ (2016) Unraveling the Evolutionary Determinants of Sleep. Current Biology 26:R1073–R1087.

Jolkkonen E, Miettinen R, Pikkarainen M, Pitkänen A (2002) Projections from the amygdaloid complex to the magnocellular cholinergic basal forebrain in rat. Neuroscience 111:133–149

Juric DM, Loncar D, Carman-Krzan M (2008) Noradrenergic stimulation of BDNF synthesis in astrocytes: mediation via alpha1- and beta1/beta2-adrenergic receptors. Neurochemistry International 52:297–306.

Kalinchuk A, Porkka-Heiskanen T, McCarley R, Basheer R (2015) Cholinergic neurons of the basal forebrain mediate biochemical and electrophysiological mechanisms underlying sleep homeostasis. The European Journal of Neuroscience 41:182–195.

Kalinchuk, Lu, Stenberg, Rosenberg, Porkka-Heiskanen (2006a) Nitric oxide production in the basal forebrain is required for recovery sleep. Journal of Neurochemistry 99:483–498.

Kalinchuk, Stenberg, Rosenberg, Porkka-Heiskanen (2006b) Inducible and neuronal nitric oxide synthases (NOS) have complementary roles in recovery sleep induction. The European Journal of Neuroscience 24:1443–1456.

Kamondi A, Williams JA, Hutcheon B, Reiner PB (1992) Membrane properties of mesopontine cholinergic neurons studied with the whole-cell patch-clamp technique: implications for behavioral state control. Journal of Neurophysiology 68:1359–1372.

Katsuki H, Akaike A (2004) Excitotoxic degeneration of hypothalamic orexin neurons in slice culture. Neurobiology of Disease 15:61–69.

Kaur S, Junek A, Black MA, Semba K (2008) Effects of ibotenate and 192IgG-saporin lesions of the nucleus basalis magnocellularis/substantia innominata on spontaneous sleep and wake states and on recovery sleep after sleep deprivation in rats. The Journal of Neuroscience 28:491–504.

Kim J, Nakajima K, Oomura Y, Wayner MJ, Sasaki K (2009) Electrophysiological effects of orexins/hypocretins on pedunculopontine tegmental neurons in rats: an in vitro study. Peptides 30:191–209.

Kim T, Thankachan S, McKenna J, McNally J, Yang C, Choi J, Chen L, Kocsis B, Deisseroth K, Strecker R, Basheer R, Brown R, McCarley R (2015) Cortically projecting basal forebrain parvalbumin neurons regulate cortical gamma band oscillations. Proceedings of the National Academy of Sciences of the United States of America 112:3535–3540.

Kling RN, McLeod CB, Koehoorn M (2010) Sleep problems and workplace injuries in Canada. Sleep 33:611–618.

Konadhode R, Pelluru D, Blanco-Centurion C, Zayachkivsky A, Liu M, Uhde T, Glen BW, van den Pol AN, Mulholland PJ, Shiromani PJ (2013) Optogenetic Stimulation of MCH Neurons Increases Sleep. The Journal of Neuroscience 33:10257–10263.

Korotkova TM, Sergeeva OA, Ponomarenko AA, Haas HL (2005) Histamine excites noradrenergic neurons in locus coeruleus in rats. Neuropharmacology 49:129–134.

Kostin A, Rai S, Kumar S, Szymusiak R, McGinty D, Alam MN (2011) Nitric oxide production in the perifornical-lateral hypothalamic area and its influences on the modulation of perifornical-lateral hypothalamic area neurons. Neuroscience 179:159–169.

Kostin A, Stenberg D, Kalinchuk AV, Porkka-Heiskanen T (2008) Nitric oxide modulates the discharge rate of basal forebrain neurons. Psychopharmacology 201:147–160.

Kostin A, Stenberg D, Porkka-Heiskanen T (2009) Nitric oxide modulates the discharge rate of basal forebrain neurones: a study in freely moving rats. Journal of Sleep Research 18:447–453.

Koyama Y, Hayaishi O (1994) Firing of neurons in the preoptic/anterior hypothalamic areas in rat: its possible involvement in slow wave sleep and paradoxical sleep. Neuroscience Research 19:31–38.

Kronholm E, Laatikainen T, Peltonen M, Sippola R, Partonen T (2011) Self-reported sleep duration, all-cause mortality, cardiovascular mortality and morbidity in Finland. Sleep Medicine 12:215–221.

Krzisch M, Temprana SG, Mongiat LA, Armida J, Schmutz V, Virtanen MA, Kocher-Braissant J, Kraftsik R, Vutskits L, Conzelmann K-KK, Bergami M, Gage FH, Schinder AF, Toni N (2015) Pre-existing astrocytes form functional perisynaptic processes on neurons generated in the adult hippocampus. Brain Structure and Function 220:2027–2042.

Larsen BR, Assentoft M, Cotrina ML, Hua SZ, Nedergaard M, Kaila K, Voipio J, MacAulay N (2014) Contributions of the Na^+/K^+-ATPase, NKCC1, and Kir4.1 to hippocampal K^+ clearance and volume responses. Glia 62:608–622.

Lee M, Hassani O, Jones B (2005) Discharge of Identified Orexin/Hypocretin Neurons across the Sleep-Waking Cycle. The Journal of Neuroscience 25:6716–6720.

LeGates T, Fernandez D, Hattar S (2014) Light as a central modulator of circadian rhythms, sleep and affect. Nature Reviews Neuroscience 15:443–454.

Lehre, Danbolt (1998) The number of glutamate transporter subtype molecules at glutamatergic synapses: chemical and stereological quantification in young adult rat brain. The Journal of Neuroscience 18:8751–8757.

Levy LM, Warr O, Attwell D (1998) Stoichiometry of the glial glutamate transporter GLT-1 expressed inducibly in a Chinese hamster ovary cell line selected for low endogenous Na+-dependent glutamate uptake. The Journal of Neuroscience 18:9620–9628.

Leybaert L (2005) Neurobarrier coupling in the brain: a partner of neurovascular and neurometabolic coupling? Journal of Cerebral Blood Flow and Metabolism 25:2–16.

Li B, Zhang S, Zhang H, Nu W, Cai L, Hertz L, Peng L (2008) Fluoxetine-mediated 5-HT2B receptor stimulation in astrocytes causes EGF receptor transactivation and ERK phosphorylation. Psychopharmacology 201:443–458.

Li W, Ma L, Yang G, Gan W-BB (2017) REM sleep selectively prunes and maintains new synapses in development and learning. Nature Neuroscience. ePub ahead of print.

Li Y, Gao X, Sakurai T, van den Pol AN (2002) Hypocretin/Orexin excites hypocretin neurons via a local glutamate neuron-A potential mechanism for orchestrating the hypothalamic arousal system. Neuron 36:1169–1181.

Li Y, van den Pol AN (2006) Differential target-dependent actions of coexpressed inhibitory dynorphin and excitatory hypocretin/orexin neuropeptides. The Journal of Neuroscience 26:13037–13047.

Linehan V, Trask R, Briggs C, Rowe T, Hirasawa M (2015) Concentration-dependent activation of dopamine receptors differentially modulates GABA release onto orexin neurons. The European Journal of Neuroscience 42:1976–1983.

Lipnik-Stangelj M, Carman-Krzan M (2004) Activation of histamine H1-receptor enhances neurotrophic factor secretion from cultured astrocytes. Inflammation Research 53:245–252.

Liu QS, Xu Q, Arcuino G, Kang J, Nedergaard M (2004) Astrocyte-mediated activation of neuronal kainate receptors. Proceedings of the National Academy of Sciences of the United States of America 101:3172–3177.

Liu R-J, van den Pol A, Aghajanian G (2002) Hypocretins (orexins) regulate serotonin neurons in the dorsal raphe nucleus by excitatory direct and inhibitory indirect actions. The Journal of Neuroscience 22:9453–9464.

Liu Z-WW, Gan G, Suyama S, Gao X-BB (2011) Intracellular energy status regulates activity in hypocretin/orexin neurones: a link between energy and behavioural states. Journal of Physiology 589:4157–4166.

Livingstone MS, Hubel DH (1981) Effects of sleep and arousal on the processing of visual information in the cat. Nature 291:554–561.

Longair M, Baker D, Armstrong D (2011) Simple Neurite Tracer: open source software for reconstruction, visualization and analysis of neuronal processes. Bioinformatics 27:2453–2454.

Luisier, Blu T, Unser (2011) Image Denoising in Mixed Poisson–Gaussian Noise. IEEE Transactions on Image Processing 20:696–708.

Luisier F, Blu T, Unser M (2007) A new SURE approach to image denoising: interscale orthonormal wavelet thresholding. IEEE transactions on Image Processing 16:593–606.

Lyytikäinen P, Lallukka T, Lahelma E, Rahkonen O (2011) Sleep problems and major weight gain: a follow-up study. International Journal of Obesity 35:109–114.

Maingret F, Coste B, Hao J, Giamarchi A, Allen D, Crest M, Litchfield DW, Adelman JP, Delmas P (2008) Neurotransmitter modulation of small-conductance Ca2+-activated K+ channels by regulation of Ca2+ gating. Neuron 59:439–449.

Manns ID, Alonso A, Jones BE (2000) Discharge properties of juxtacellularly labeled and immunohistochemically identified cholinergic basal forebrain neurons recorded in association with the electroencephalogram in anesthetized rats. The Journal of Neuroscience 20:1505–1518.

Marcaggi P, Billups D, Attwell D (2003) The role of glial glutamate transporters in maintaining the independent operation of juvenile mouse cerebellar parallel fibre synapses. The Journal of Physiology 552:89–107.

Martiniuk AL, Senserrick T, Lo S, Williamson A, Du W, Grunstein RR, Woodward M, Glozier N, Stevenson M, Norton R, Ivers RQ (2013) Sleep-deprived young drivers and the risk for crash: the DRIVE prospective cohort study. JAMA Pediatrics 167:647–655.

Martín R, Bajo-Grañeras R, Moratalla R, Perea G, Araque A (2015) Circuit-specific signaling in astrocyte-neuron networks in basal ganglia pathways. Science 349:730–734.

Matos-Ocasio F, Hernández-López A, Thompson KJ (2014) Ceftriaxone, a GLT-1 transporter activator, disrupts hippocampal learning 2 in rats. Pharmacology Biochemistry and Behavior 122:118-121

McAdoo DJ, Xu G, Robak G, Hughes MG, Price EM (2000) Evidence that reversed glutamate uptake contributes significantly to glutamate release following experimental injury to the rat spinal cord. Brain Research 865:283–285.

McDermott CM, Schrader LA (2011) Activation of κ opioid receptors increases intrinsic excitability of dentate gyrus granule cells. Journal of Physiology 589:3517–3532.

Mignot E (2008) Why we sleep: the temporal organization of recovery. PLoS Biology 6:e106.

Mistlberger RE (2005) Circadian regulation of sleep in mammals: role of the suprachiasmatic nucleus. Brain Research Reviews 49:429–454.

Mochizuki T, Yamatodani A, Okakura K, Horii A, Inagaki N, Wada H (1992) Circadian rhythm of histamine release from the hypothalamus of freely moving rats. Physiology and Behavior 51:391–394.

Modirrousta M, Mainville L, Jones B (2005) Orexin and MCH neurons express c-Fos differently after sleep deprivation vs. recovery and bear different adrenergic receptors. The European Journal of Neuroscience 21:2807–2816.

Molotkov D, Zobova S, Arcas JM, Khiroug L (2013) Calcium-induced outgrowth of astrocytic peripheral processes requires actin binding by Profilin-1. Cell Calcium 53:338–348.

Monti J, Torterolo P, Lagos P (2013) Melanin-concentrating hormone control of sleep-wake behavior. Sleep Medicine Reviews 17:293–298.

Muraki Y, Yamanaka A, Tsujino N, Kilduff TS, Goto K, Sakurai T (2004) Serotonergic regulation of the orexin/hypocretin neurons through the 5-HT1A receptor. The Journal of Neuroscience 24:7159–7166.

Murphy-Royal C, Dupuis J, Varela J, Panatier A, Pinson B, Baufreton J, Groc L, Oliet S (2015) Surface diffusion of astrocytic glutamate transporters shapes synaptic transmission. Nature Neuroscience 18:219–226.

Muschamp JW, Hollander JA, Thompson JL, Voren G, Hassinger LC, Onvani S, Kamenecka TM, Borgland SL, Kenny PJ, Carlezon WA (2014) Hypocretin (orexin) facilitates reward by attenuating the antireward effects of its cotransmitter dynorphin in ventral tegmental area. Proceedings of the National Academy of Sciences of the United States of America 111:E1648–55.

Møllerud S, Kastrup JS, Pickering DS (2016) A pharmacological profile of the high-affinity GluK5 kainate receptor. European Journal of Pharmacology 788:315–320.

Nadin BM, Pfaffinger PJ (2010) Dipeptidyl peptidase-like protein 6 is required for normal electrophysiological properties of cerebellar granule cells. The Journal of Neuroscience 30:8551–8565.

Nakagawa T, Otsubo Y, Yatani Y, Shirakawa H, Kaneko S (2008) Mechanisms of substrate transport-induced clustering of a glial glutamate transporter GLT-1 in astroglial–neuronal cultures. European Journal of Neuroscience 28:1719–1730.

National Sleep Foundation (2013) International bedroom poll. National Sleep Foundation. https://sleepfoundation.org/sites/default/files/RPT495a.pdf

Navarrete M, Araque A (2008) Endocannabinoids mediate neuron-astrocyte communication. Neuron 57:883–893.

Neher E (1992) Correction for liquid junction potentials in patch clamp experiments. Methods in Enzymology 207:123-131

Nofzinger, Buysse, Miewald, Meltzer (2002) Human regional cerebral glucose metabolism during non-rapid eye movement sleep in relation to waking. Brain 125;1105-1115

Oberheim NA, Goldman SA, Nedergaard M (2012) Heterogeneity of astrocytic form and function. Methods in Molecular Biology 814:23–45.

Oliet SH, Piet R, Poulain DA (2001) Control of Glutamate Clearance and Synaptic Efficacy by Glial Coverage of Neurons. Science 292:923–926.

Omrani A, Melone M, Bellesi M, Safiulina V, Aida T, Tanaka K, Cherubini E, Conti F (2009) Up-regulation of GLT-1 severely impairs LTD at mossy fibre-CA3 synapses. The Journal of Physiology 587:4575–4588.

Pan H-CC, Chou Y-CC, Sun SH (2015) P2X7 R-mediated Ca(2+) -independent d-serine release via pannexin-1 of the P2X7 R-pannexin-1 complex in astrocytes. Glia 63:877–893.

Pan WJ, Osmanović SS, Shefner SA (1994) Adenosine decreases action potential duration by modulation of A-current in rat locus coeruleus neurons. The Journal of Neuroscience 14:1114–1122.

Panatier A, Vallée J, Haber M, Murai KK, Lacaille J-CC, Robitaille R (2011) Astrocytes are endogenous regulators of basal transmission at central synapses. Cell 146:785–798.

Pannasch U, Freche D, Dallérac G, Ghézali G, Escartin C, Ezan P, Cohen-Salmon M, Benchenane K, Abudara V, Dufour A, Lübke J, Déglon N, Knott G, Holcman D, Rouach N (2014) Connexin 30 sets synaptic strength by controlling astroglial synapse invasion. Nature Neuroscience 17:549–558.

Panula P, Pirvola U, Auvinen S, Airaksinen MS (1989) Histamine-immunoreactive nerve fibers in the rat brain. Neuroscience 28:585–610.

Parks GS, Olivas ND, Ikrar T, Sanathara NM, Wang L, Wang Z, Civelli O, Xu X (2014a) Histamine inhibits the melanin-concentrating hormone system: implications for sleep and arousal. Journal of Physiology 592:2183–2196.

Parks GS, Wang L, Wang Z, Civelli O (2014b) Identification of neuropeptide receptors expressed by melanin-concentrating hormone neurons. The Journal of Comparative Neurology 522:3817–3833.

Parmentier R, Ohtsu H, Djebbara-Hannas Z, Valatx J-LL, Watanabe T, Lin J-SS (2002) Anatomical, physiological, and pharmacological characteristics of histidine decarboxylase knock-out mice: evidence for the role of brain histamine in behavioral and sleep-wake control. Journal of Neuroscience 22:7695–7711.

Parsons MP, Belanger-Willoughby N, Linehan V, Hirasawa M (2012a) ATP-sensitive potassium channels mediate the thermosensory response of orexin neurons. Journal of Physiology 590:4707–4715.

Parsons MP, Burt J, Cranford A, Alberto C, Zipperlen K, Hirasawa M (2012b) Nociceptin induces hypophagia in the perifornical and lateral hypothalamic area. PLoS one 7:e45350.

Parsons MP, Hirasawa M (2010) ATP-sensitive potassium channel-mediated lactate effect on orexin neurons: implications for brain energetics during arousal. The Journal of Neuroscience 30:8061–8070.

Pascual O, Casper KB, Kubera C, Zhang J, Revilla-Sanchez R, Sul J-YY, Takano H, Moss SJ, McCarthy K, Haydon PG (2005) Astrocytic purinergic signaling coordinates synaptic networks. Science 310:113–116.

Paukert M, Agarwal A, Cha J, Doze VA, Kang JU, Bergles DE (2014) Norepinephrine controls astroglial responsiveness to local circuit activity. Neuron 82:1263–1270.

Pelluru D, Konadhode R, Bhat N, Shiromani P (2016) Optogenetic stimulation of astrocytes in the posterior hypothalamus increases sleep at night in C57BL/6J mice. European Journal of Neuroscience 43:1298–1306.

Perea G, Sur M, Araque A (2014) Neuron-glia networks: integral gear of brain function. Frontiers in Cellular Neuroscience 8:378.

Perez-Alvarez A, Navarrete M, Covelo A, Martin E, Araque A (2014) Structural and Functional Plasticity of Astrocyte Processes and Dendritic Spine Interactions. The Journal of Neuroscience 34:12738–12744.

Petit J-M, Magistretti PJ (2016) Regulation of neuron–astrocyte metabolic coupling across the sleep–wake cycle. Neuroscience 323:135–156.

Petr GT, Sun Y, Frederick NM, Zhou Y, Dhamne SC, Hameed MQ, Miranda C, Bedoya EA, Fischer KD, Armsen W, Wang J, Danbolt NC, Rotenberg A, Aoki CJ, Rosenberg PA (2015) Conditional Deletion of the Glutamate Transporter GLT-1 Reveals That Astrocytic GLT-1 Protects against Fatal Epilepsy While Neuronal GLT-1 Contributes Significantly to Glutamate Uptake into Synaptosomes. The Journal of Neuroscience 35:5187–5201.

Peyron, Tighe, van den Pol, de Lecea, Heller, Sutcliffe, Kilduff (1998) Neurons containing hypocretin (orexin) project to multiple neuronal systems. The Journal of Neuroscience 18:9996–10015.

Picciotto M, Higley M, Mineur Y (2012) Acetylcholine as a neuromodulator: cholinergic signaling shapes nervous system function and behavior. Neuron 76:116–129.

Piet R, Bonhomme R, Theodosis DT, Poulain DA, Oliet SHH (2003) Modulation of GABAergic transmission by endogenous glutamate in the rat supraoptic nucleus. European Journal of Neuroscience 17:1777–1785.

Piet R, Vargová L, Syková E, Poulain D, Oliet S (2004) Physiological contribution of the astrocytic environment of neurons to intersynaptic crosstalk. Proceedings of the National Academy of Sciences of the United States of America 101:2151–2155.

Pompeiano M, Cirelli C, Tononi G (1994) Immediate-early genes in spontaneous wakefulness and sleep: expression of c-fos and NGFI-A mRNA and protein. Journal of Sleep Research 3:80–96.

Porkka-Heiskanen, Strecker, McCarley (2000) Brain site-specificity of extracellular adenosine concentration changes during sleep deprivation and spontaneous sleep: an in vivo microdialysis study. Neuroscience 99:507–517.

Porkka-Heiskanen T, Strecker RE, Thakkar M, Bjorkum AA, Greene RW, McCarley RW (1997) Adenosine: a mediator of the sleep-inducing effects of prolonged wakefulness. Science 276:1265–1268.

Portas CM, Krakow K, Allen P, Josephs O, Armony JL, Frith CD (2000) Auditory processing across the sleep-wake cycle: simultaneous EEG and fMRI monitoring in humans. Neuron 28:991–999.

Poskanzer K, Yuste R (2016) Astrocytes regulate cortical state switching in vivo. Proceedings of the National Academy of Sciences of the United States of America 113:E2675–E2684.

Potter GD, Skene DJ, Arendt J, Cade JE, Grant PJ, Hardie LJ (2016) Circadian Rhythm and Sleep Disruption: Causes, Metabolic Consequences, and Countermeasures. Endocrine Reviews 37:584–608.

Rangaraj VR, Knutson KL (2016) Association between sleep deficiency and cardiometabolic disease: implications for health disparities. Sleep Medicine 18:19–35.

Rao Y, Liu Z, Borok E, Rabenstein R, Shanabrough M, Lu M, Picciotto M, Horvath T, Gao X (2007) Prolonged wakefulness induces experience- dependent synaptic plasticity in mouse hypocretin / orexin neurons. The Journal of Neuroscience 117:11405–11415.

Rao Y, Lu M, Ge F, Marsh DJ, Qian S, Wang AH, Picciotto MR, Gao X-BB (2008) Regulation of synaptic efficacy in hypocretin/orexin-containing neurons by melanin concentrating hormone in the lateral hypothalamus. The Journal of Neuroscience 28:9101–9110.

Richardson KA, Aston-Jones G (2012) Lateral hypothalamic orexin/hypocretin neurons that project to ventral tegmental area are differentially activated with morphine preference. The Journal of Neuroscience 32:3809–3817.

Richter C, Woods I, Schier A (2014) Neuropeptidergic Control of Sleep and Wakefulness. Annual Review of Neuroscience 37:503–531.

Rossi DJ, Oshima T, Attwell D (2000) Glutamate release in severe brain ischaemia is mainly by reversed uptake. Nature 403:316–321.

Rothschild G, Eban E, Frank LM (2016) A cortical-hippocampal-cortical loop of information processing during memory consolidation. Nat Neurosci. 20:251-259

Rusakov D, Kullmann D (1998) Extrasynaptic glutamate diffusion in the hippocampus: ultrastructural constraints, uptake, and receptor activation. The Journal of Neuroscience 18:3158–3170.

Safavi-Abbasi S, Wolff JR, Missler M (2001) Rapid morphological changes in astrocytes are accompanied by redistribution but not by quantitative changes of cytoskeletal proteins. Glia 36:102–115.

Sah P, Faber ES (2002) Channels underlying neuronal calcium-activated potassium currents. Progress in Neurobiology 66:345–353.

Saito YC, Tsujino N, Hasegawa E, Akashi K, Abe M, Mieda M, Sakimura K, Sakurai T (2013) GABAergic neurons in the preoptic area send direct inhibitory projections to orexin neurons. Frontiers in Neural Circuits 7:192.

Sakai K (2011) Sleep-waking discharge profiles of dorsal raphe nucleus neurons in mice. Neuroscience 197:200–224.

Sakurai T, Nagata R, Yamanaka A, Kawamura H, Tsujino N, Muraki Y, Kageyama H, Kunita S, Takahashi S, Goto K, Koyama Y, Shioda S, Yanagisawa M (2005) Input of Orexin/Hypocretin Neurons Revealed by a Genetically Encoded Tracer in Mice. Neuron 46:297–308.

Samuels ER, Szabadi E (2008) Functional neuroanatomy of the noradrenergic locus coeruleus: its roles in the regulation of arousal and autonomic function part I: principles of functional organisation. Current Neuropharmacology 6:235–253.

Saper CB, Fuller PM, Pedersen NP, Lu J, Scammell TE (2010) Sleep state switching. Neuron 68:1023–1042.

Sartor GC, Aston-Jones GS (2012) A septal-hypothalamic pathway drives orexin neurons, which is necessary for conditioned cocaine preference. The Journal of Neuroscience 32:4623–4631.

Schipke CG, Heuser I, Peters O (2011) Antidepressants act on glial cells: SSRIs and serotonin elicit astrocyte calcium signaling in the mouse prefrontal cortex. Journal of Psychiatric Research 45:242–248.

Schöne C, Apergis-Schoute J, Sakurai T, Adamantidis A, Burdakov D (2014) Coreleased Orexin and Glutamate Evoke Nonredundant Spike Outputs and Computations in Histamine Neurons. Cell Reports 7:1–8.

Schöne C, Cao Z, Apergis-Schoute J, Adamantidis A, Sakurai T, Burdakov D (2012) Optogenetic probing of fast glutamatergic transmission from hypocretin/orexin to histamine neurons in situ. The Journal of Neuroscience 32:12437–12443.

Schöne C, Venner A, Knowles D, Karnani M, Burdakov D (2011) Dichotomous cellular properties of mouse orexin/hypocretin neurons. The Journal of Physiology 589:2767–2779.

Sehgal M, Song C, Ehlers VL, Moyer JR (2013) Learning to learn - intrinsic plasticity as a metaplasticity mechanism for memory formation. Neurobiology of Learning and Memory 105:186–199.

Semyanov A, Kullmann DM (2000) Modulation of GABAergic signaling among interneurons by metabotropic glutamate receptors. Neuron 25:663–672.

Sethi J, Sanchez-Alavez M, Tabarean IV (2011) Kv4.2 mediates histamine modulation of preoptic neuron activity and body temperature. PLoS ONE 6:e29134.

Sharma V (2009) Period Responses to Zeitgeber Signals Stabilize Circadian Clocks During Entrainment. Chronobiology International 20:389–404.

Sheldon A, González M, Krizman-Genda E, Susarla B, Robinson M (2008) Ubiquitination-mediated internalization and degradation of the astroglial glutamate transporter, GLT-1. Neurochemistry International 53:296–308.

Shelton MK, McCarthy KD (2000) Hippocampal astrocytes exhibit Ca2+-elevating muscarinic cholinergic and histaminergic receptors in situ. Journal of Neurochemistry 74:555–563.

Shen X, Wu Y, Zhang D (2016) Nighttime sleep duration, 24-hour sleep duration and risk of all-cause mortality among adults: a meta-analysis of prospective cohort studies. Science Reports 6:21480.

Sheng M, Hoogenraad CC (2007) The postsynaptic architecture of excitatory synapses: a more quantitative view. Annual Review of Biochemistry 76:823–847.

Shigetomi E, Bushong EA, Haustein MD, Tong X, Jackson-Weaver O, Kracun S, Xu J, Sofroniew MV, Ellisman MH, Khakh BS (2013) Imaging calcium microdomains within entire astrocyte territories and endfeet with GCaMPs expressed using adeno-associated viruses. Journal of General Physiology 141:633–647.

Shiromani PJ, Lu J, Wagner D, Thakkar J, Greco MA, Basheer R, Thakkar M (2000) Compensatory sleep response to 12 h wakefulness in young and old rats. American Journal of Physiology. Regulatory, Integrative and Comparative Physiology 278:R125–33.

Shram N, Netchiporouk L, Cespuglio R (2002) Lactate in the brain of the freely moving rat: voltammetric monitoring of the changes related to the sleep-wake states. The European Journal of Neuroscience 16:461–466.

Shu Q, Hu Z-L, Huang C, Yu X-W, Fan H, Yang J-W, Fang P, Ni L, Chen J-G, Wang F (2014) Orexin-A Promotes Cell Migration in Cultured Rat Astrocytes via Ca2+-Dependent PKC± and ERK1/2 Signals. PloS ONE 9:e95259.

Shu Q, Zhang J, Ma W, Lei Y, Zhou D (2016) Orexin-A promotes Glu uptake by OX1R/PKCα/ERK1/2/GLT-1 pathway in astrocytes and protects co-cultured astrocytes and neurons against apoptosis in anoxia/hypoglycemic injury in vitro. Molecular and Cellular Biochemistry 425:103-112

Siegel J (2005) Clues to the functions of mammalian sleep. Nature 437:1264–1271.

Sourdet V, Russier M, Daoudal G, Ankri N, Debanne D (2003) Long-term enhancement of neuronal excitability and temporal fidelity mediated by metabotropic glutamate receptor subtype 5. The Journal of Neuroscience 23:10238–10248.

Stocker M (2004) Ca(2+)-activated K+ channels: molecular determinants and function of the SK family. Nature Reviews Neuroscience 5:758–770.

Sun W, McConnell E, Pare J-F, Xu Q, Chen M, Peng W, Lovatt D, Han X, Smith Y, Nedergaard M (2013) Glutamate-Dependent Neuroglial Calcium Signaling Differs Between Young and Adult Brain. Science 339:197–200.

Suntsova N, Szymusiak R, Alam MN, Guzman-Marin R, McGinty D (2002) Sleep-waking discharge patterns of median preoptic nucleus neurons in rats. Journal of Physiology 543:665–677.

Tahara Y, Aoyama S, Shibata S (2017) The mammalian circadian clock and its entrainment by stress and exercise. Journal of Physiological Sciences 67:1–10.

Takahashi K, Kayama Y, Lin JS, Sakai K (2010) Locus coeruleus neuronal activity during the sleep-waking cycle in mice. Neuroscience 169:1115–1126.

Takahashi K, Lin J-SS, Sakai K (2006) Neuronal activity of histaminergic tuberomammillary neurons during wake-sleep states in the mouse. The Journal of Neuroscience 26:10292–10298.

Takata N, Mishima T, Hisatsune C, Nagai T, Ebisui E, Mikoshiba K, Hirase H (2011) Astrocyte calcium signaling transforms cholinergic modulation to cortical plasticity in vivo. The Journal of Neuroscience 31:18155–18165.

Tanaka K, Watase K, Manabe T, Yamada K, Watanabe M, Takahashi K, Iwama H, Nishikawa T, Ichihara N, Kikuchi T, Okuyama S, Kawashima N, Hori S, Takimoto M, Wada K (1997) Epilepsy and exacerbation of brain injury in mice lacking the glutamate transporter GLT-1. Science 276:1699–1702.

Tang F, Lane S, Korsak A, Paton JF, Gourine AV, Kasparov S, Teschemacher AG (2014) Lactate-mediated glia-neuronal signalling in the mammalian brain. Nature Communications 5:3284.

Tang SL, Tran V, Wagner EJ (2005) Sex differences in the cannabinoid modulation of an A-type K+ current in neurons of the mammalian hypothalamus. Journal of Neurophysiology 94:2983–2986.

Tartar JL, McKenna JT, Ward CP, McCarley RW, Strecker RE, Brown RE (2010) Sleep fragmentation reduces hippocampal CA1 pyramidal cell excitability and response to adenosine. Neuroscience Letters 469:1–5.

Theodosis D, Poulain D (1993) Activity-dependent neuronal-glial and synaptic plasticity in the adult mammalian hypothalamus. Neuroscience 57:501–535.

Thorpy MJ (2012) Classification of sleep disorders. Neurotherapeutics 9:687–701.

Uehli K, Mehta AJ, Miedinger D, Hug K, Schindler C, Holsboer-Trachsler E, Leuppi JDD, Künzli N (2014) Sleep problems and work injuries: a systematic review and meta-analysis. Sleep Medicine Reviews 18:61–73.

Uschakov A, Grivel J, Cvetkovic-Lopes V, Bayer L, Bernheim L, Jones BE, Mühlethaler M, Serafin M (2011) Sleep-deprivation regulates α-2 adrenergic responses of rat hypocretin/orexin neurons. PLoS ONE 6:e16672.

Van den Pol A, Acuna-Goycolea C, Clark K, Ghosh P (2004) Physiological properties of hypothalamic MCH neurons identified with selective expression of reporter gene after recombinant virus infection. Neuron 42:635–652.

Van Dongen HP, Maislin G, Mullington JM, Dinges DF (2003) The cumulative cost of additional wakefulness: dose-response effects on neurobehavioral functions and sleep physiology from chronic sleep restriction and total sleep deprivation. Sleep 26:117–126.

Vazey EM, Aston-Jones G (2014) Designer receptor manipulations reveal a role of the locus coeruleus noradrenergic system in isoflurane general anesthesia. Proceedings of the National Academy of Sciences of the United States of America 111:3859–3864.

Venance L, Glowinski J (2003) Heterogeneity of spike frequency adaptation among medium spiny neurones from the rat striatum. Neuroscience 122:77–92.

Ventura R, Harris K (1999) Three-dimensional relationships between hippocampal synapses and astrocytes. The Journal of Neuroscience 19:6897–6906.

Vetrivelan R, Kong D, Ferrari LL, Arrigoni E, Madara JC, Bandaru SS, Lowell BB, Lu J, Saper CB (2016) Melanin-concentrating hormone neurons specifically promote rapid eye movement sleep in mice. Neuroscience 336:102–113.

Vyazovskiy VV, Cirelli C, Pfister-Genskow M, Faraguna U, Tononi G (2008) Molecular and electrophysiological evidence for net synaptic potentiation in wake and depression in sleep. Nature Neuroscience 11:200–208.

Wagner E, Rønnekleiv O, Kelly M (2001) The noradrenergic inhibition of an apamin-sensitive, small-conductance Ca2+-activated K+ channel in hypothalamic -aminobutyric acid neurons: pharmacology, estrogen sensitivity, and relevance to the control of the reproductive axis. Journal of Pharmacology and Experimental Therapeutics 299:21–30.

Wallraff A, Köhling R, Heinemann U, Theis M, Willecke K, Steinhäuser C (2006) The impact of astrocytic gap junctional coupling on potassium buffering in the hippocampus. The Journal of Neuroscience 26:5438–5447.

Wang X-FF, Hu W-WW, Yan H-JJ, Tan L, Gao J-QQ, Tian Y-YY, Shi X-JJ, Hou W-WW, Li J, Shen Y, Chen Z (2013) Modulation of astrocytic glutamine synthetase expression and cell viability by histamine in cultured cortical astrocytes exposed to OGD insults. Neuroscience Letters 549:69–73.

Watson NF, Badr MS, Belenky G, Bliwise DL, Buxton OM, Buysse D, Dinges DF, Gangwisch J, Grandner MA, Kushida C, Malhotra RK, Martin JL, Patel SR, Quan SF, Tasali E (2015) Joint Consensus Statement of the American Academy of Sleep Medicine and Sleep Research Society on the Recommended Amount of Sleep for a Healthy Adult: Methodology and Discussion. Journal of Clinical Sleep Medicine 11:931–952.

Weber F, Dan Y (2016) Circuit-based interrogation of sleep control. Nature 538:51–59.

Welsh DK, Takahashi JS, Kay SA (2010) Suprachiasmatic nucleus: cell autonomy and network properties. Annuual Review of Physiology 72:551–577.

Weng H-R, Chen JH, Pan ZZ, Nie (2007) Glial glutamate transporter 1 regulates the spatial and temporal coding of glutamatergic synaptic transmission in spinal lamina II neurons. Neuroscience 149:898–907.

Wigren H-K, Rytkönen K-M, Porkka-Heiskanen T (2009) Basal forebrain lactate release and promotion of cortical arousal during prolonged waking is attenuated in aging. The Journal of Neuroscience 29:11698–11707.

Williams RH, Alexopoulos H, Jensen LT, Fugger L, Burdakov D (2008) Adaptive sugar sensors in hypothalamic feeding circuits. Proceedings of the National Academy of Sciences of the United States of America 105:11975–11980.

Williamson AM, Feyer AM (2000) Moderate sleep deprivation produces impairments in cognitive and motor performance equivalent to legally prescribed levels of alcohol intoxication. Occupational and Environmental Medicine 57:649–655.

Winters B, Huang Y, Dong Y, Krueger J (2011) Sleep loss alters synaptic and intrinsic neuronal properties in mouse prefrontal cortex. Brain Research 1420:1–7.

Wisor JP, Rempe MJ, Schmidt MA, Moore ME, Clegern WC (2012) Sleep slow-wave activity regulates cerebral glycolytic metabolism. Cerebral Cortex 23:1978-1987.

Wu M, Zaborszky L, Hajszan T, van den Pol A, Alreja M (2004) Hypocretin/Orexin Innervation and Excitation of Identified Septohippocampal Cholinergic Neurons. The Journal of Neuroscience 24:3527–3536.

Xia J, Chen F, Ye J, Yan J, Wang H, Duan S, Hu Z (2009) Activity-dependent release of adenosine inhibits the glutamatergic synaptic transmission and plasticity in the hypothalamic hypocretin/orexin neurons. Neuroscience 162:980–988.

Xia J, Xiong J, Wang H, Duan S, Ye J, Hu Z (2012) Presynaptic inhibition of GABAergic synaptic transmission by adenosine in mouse hypothalamic hypocretin neurons. Neuroscience 201:46–56.

Xiao Q, Gu F, Caporaso N, Matthews CE (2016) Relationship between sleep characteristics and measures of body size and composition in a nationally-representative sample. BMC Obesity 3:48.

Xie L, Kang H, Xu Q, Chen M, Liao Y, Thiyagarajan M, O'Donnell J, Christensen D, Nicholson C, Iliff J, Takano T, Deane R, Nedergaard M (2013) Sleep drives metabolite clearance from the adult brain. Science 342:373–377.

Xu M, Chung S, Zhang S, Zhong P, Ma C, Chang W-CC, Weissbourd B, Sakai N, Luo L, Nishino S, Dan Y (2015) Basal forebrain circuit for sleep-wake control. Nature Neuroscience 18:1641–1647.

Yamanaka A, Muraki Y, Ichiki K, Tsujino N, Kilduff TS, Goto K, Sakurai T (2006) Orexin neurons are directly and indirectly regulated by catecholamines in a complex manner. Journal of Neurophysiology 96:284–298.

Yamanaka A, Muraki Y, Tsujino N, Goto K, Sakurai T (2003) Regulation of orexin neurons by the monoaminergic and cholinergic systems. Biochemical and Biophysical Research Communications 303:120–129.

Yamanaka A, Tabuchi S, Tsunematsu T, Fukazawa Y, Tominaga M (2010) Orexin Directly Excites Orexin Neurons through Orexin 2 Receptor. The Journal of Neuroscience 30:12642–12652.

Yamanaka A, Tsujino N, Funahashi H, Honda K, Guan JL, Wang Q-PP, Tominaga M, Goto K, Shioda S, Sakurai T (2002) Orexins activate histaminergic neurons via the orexin 2 receptor. Biochemical and Biophysical Research Communications 290:1237–1245.

Yang C, Franciosi S, Brown R (2013a) Adenosine inhibits the excitatory synaptic inputs to Basal forebrain cholinergic, GABAergic, and parvalbumin neurons in mice. Frontiers in Neurology 4:77.

Yang C, McKenna J, Zant J, Winston S, Basheer R, Brown R (2014) Cholinergic neurons excite cortically projecting basal forebrain GABAergic neurons. The Journal of Neuroscience 34:2832–2844.

Yang EJ, Harris AZ, Pettit DL (2006) Variable kainate receptor distributions of oriens interneurons. Journal of Neurophysiology 96:1683–1689.

Yang J, Li M-XX, Luo Y, Chen T, Liu J, Fang P, Jiang B, Hu Z-LL, Jin Y, Chen J-GG, Wang F (2013b) Chronic ceftriaxone treatment rescues hippocampal memory deficit in AQP4 knockout mice via activation of GLT-1. Neuropharmacology 75:213–222.

Yeo Y, Ma SH, Park SK, Chang S-HH, Shin H-RR, Kang D, Yoo K-YY (2013) A prospective cohort study on the relationship of sleep duration with all-cause and disease-specific mortality in the Korean Multi-center Cancer Cohort study. Journal of Preventive Medicine and Public Health 46:271–281.

Yoo S-SS, Hu PT, Gujar N, Jolesz FA, Walker MP (2007) A deficit in the ability to form new human memories without sleep. Nature Neuroscience 10:385–392.

Yoshida K, McCormack S, España RA, Crocker A, Scammell TE (2006) Afferents to the orexin neurons of the rat brain. The Journal of Comparative Neurology 494:845–861.

Zheng K, Scimemi A, Rusakov D (2008) Receptor Actions of Synaptically Released Glutamate: The Role of Transporters on the Scale from Nanometers to Microns. Biophysical Journal 95:4584–4596.

Zhou W-LL, Gao X-BB, Picciotto MR (2015) Acetylcholine Acts through Nicotinic Receptors to Enhance the Firing Rate of a Subset of Hypocretin Neurons in the Mouse Hypothalamus through Distinct Presynaptic and Postsynaptic Mechanisms. eNeuro 2:e0052.

Zhou Y, Danbolt NC (2013) GABA and Glutamate Transporters in Brain. Frontiers in Endocrinology 4:165.

Zou Z, Lu Y, Zha Y, Yang H (2016) Endocannabinoid 2-Arachidonoylglycerol Suppresses LPS-Induced Inhibition of A-Type Potassium Channel Currents in Caudate Nucleus Neurons Through CB1 Receptor. Journal of Molecular Neuroscience 59:493–503.

APPENDIX A: ACTIVITY PROFILES OF SELECT SLEEP/WAKE REGULATORY NEURONAL POPULATIONS

Table A.1. Activity profiles of key sleep/wake neuronal populations by behavioural state.

Brain region		Neurotransmitter	Neuronal Activity			References
			Wake	NREM	REM	
Brainstem						
	LC	Noradrenaline	+++	-	-	(Takahashi et al., 2010)
	DR	Serotonin	+++	+	+	(Sakai et al., 2011)
Hypothalamus						
	TMN	Histamine	+++	-	-	(Takahashi et al., 2006)
	LH	Orexin	+++	-	-	(Takahashi et al., 2008) (Lee et al., 2005)
		Melanin Concentrating Hormone	-/+*	+	+++	(Hassani et al., 2009b)
Basal Forebrain						
		Acetycholine	++	-	+++	(Hassani et al., 2009a)
		GABA (Parvabumin-positive)	++	-	+++	(Hassani et al., 2009a)

+, ++, +++ Arbitrary relative amounts of firing activity; - Inactivity; -/+ Ambiguity
Abbreviations: DR - Dorsal Raphe, LC - Locus Coeruleus, LH - Lateral Hypothalamus, TMN - Tuberomammillary Nucleus
* (González et al., 2016)

APPENDIX B: CORRELATIONAL ANALYSES BETWEEN ELECTROPHYSIOLOGICAL MEASURES AND TIME-SINCE-DISSECTION

Because circadian rhythms can persist in vitro (Beaulé et al., 2011), all electrophysiological experiments were performed prior to the onset of the dark phase to limit potential circadian influences. Yet, as the recordings were conducted over a 5-hour window, there were at least two potential confounds that could interfere with my interpretations of the data. The first was clearly circadian influence. The second applied to the data obtained from the SD condition; accrued sleep pressure could possibly dissipate in vitro. I therefore performed linear regression analyses on Time Since Dissection versus a variety of electrophysiological measures to ensure that neither confound could account for the effects I measured. Measures that were unaffected by sleep-state condition were grouped for regression analyses, and measures that differed by sleep-state condition were analysed separately.

Figure B.1. There is no correlation between Time Since Dissection and baseline differences in synaptic transmission to LH neurons following SD compared to Rest. (A) Linear regressions demonstrating no correlation between PPR and Time Since Dissection in ORX neurons. There is an effect of sleep-state history, demonstrated by the significantly different y-intercept of the regression slope for SD compared to Rest (consistent with Figure 2.6A). (B) Linear regressions demonstrating no correlation between slow EPSC amplitude and Time Since Dissection in MCH neurons. There is an effect of sleep-state history, demonstrated by the significantly different y-intercept of the regression slope for SD compared to Rest (consistent with Figure 2.8H).

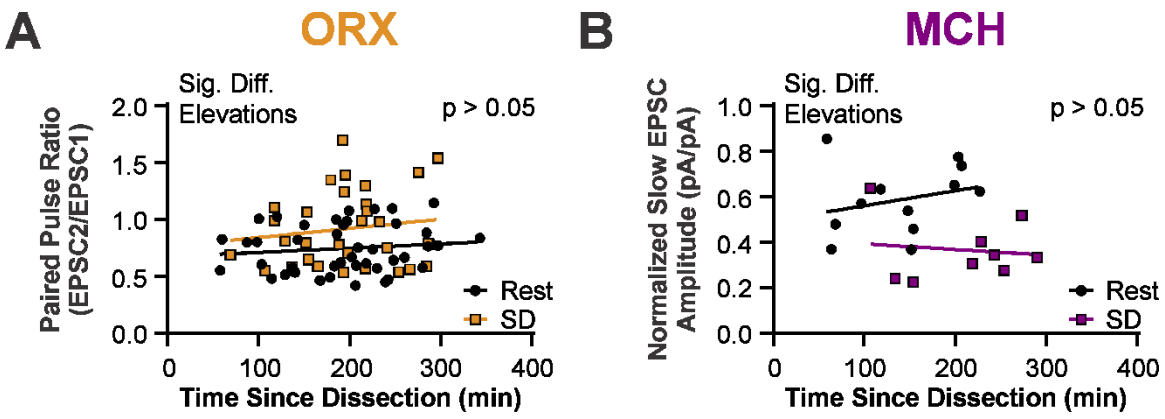
A
ORX
B
MCH
Sig. Diff.
Elevations
p > 0.05
Paired Pulse Ratio
(EPSC2/EPSC1)
2.0
1.5
1.0
0.5
0.0
0
100
200
300
400
Time Since Dissection (min)
Rest
SD
Sig. Diff.
Elevations
p > 0.05
Normalized Slow EPSC
Amplitude (pA/pA)
1.0
0.8
0.6
0.4
0.2
0.0
0
100
200
300
400
Time Since Dissection (min)
Rest
SD

Figure B.2. Correlation analyses of Time Since Dissection versus intrinsic membrane properties. (A,B) Linear regressions of Time Since Dissection compared to RMP in ORX neurons (A) and MCH neurons (B). There is no correlation between these measures in ORX neurons, and a mild negative correlation between these measures in MCH neurons ($P = 0.0299$). (C,D) Linear regressions of Time Since Dissection compared to membrane capacitance in ORX neurons (C) and MCH neurons (D). There is no correlation between these measures in either cell-type. (E,F) Linear regressions of Time Since Dissection compared to membrane resistance in ORX neurons (E) and MCH neurons (F). There is a mild positive correlation between these measures in ORX neurons ($P = 0.0165$), and no correlation between these measures in MCH neurons. (G) Linear regressions of Time Since Dissection and number of spikes induced by a current step (200 pA) in D-type ORX neurons. There is a mild positive correlation between these measures following Rest ($P = 0.0405$), but not SD. There is an effect of sleep-state history, demonstrated by the significantly different y-intercept of the regression slope for SD compared to Rest (consistent with Figure 4.5A). (H) Linear regressions of Time Since Dissection and number of spikes induced by a current step (200 pA) in MCH neurons. There is no correlation between these measures in either sleep-state condition. There is an effect of sleep-state history, demonstrated by the significantly different y-intercept of the regression slope for SD compared to Rest (consistent with Figure 4.1C).

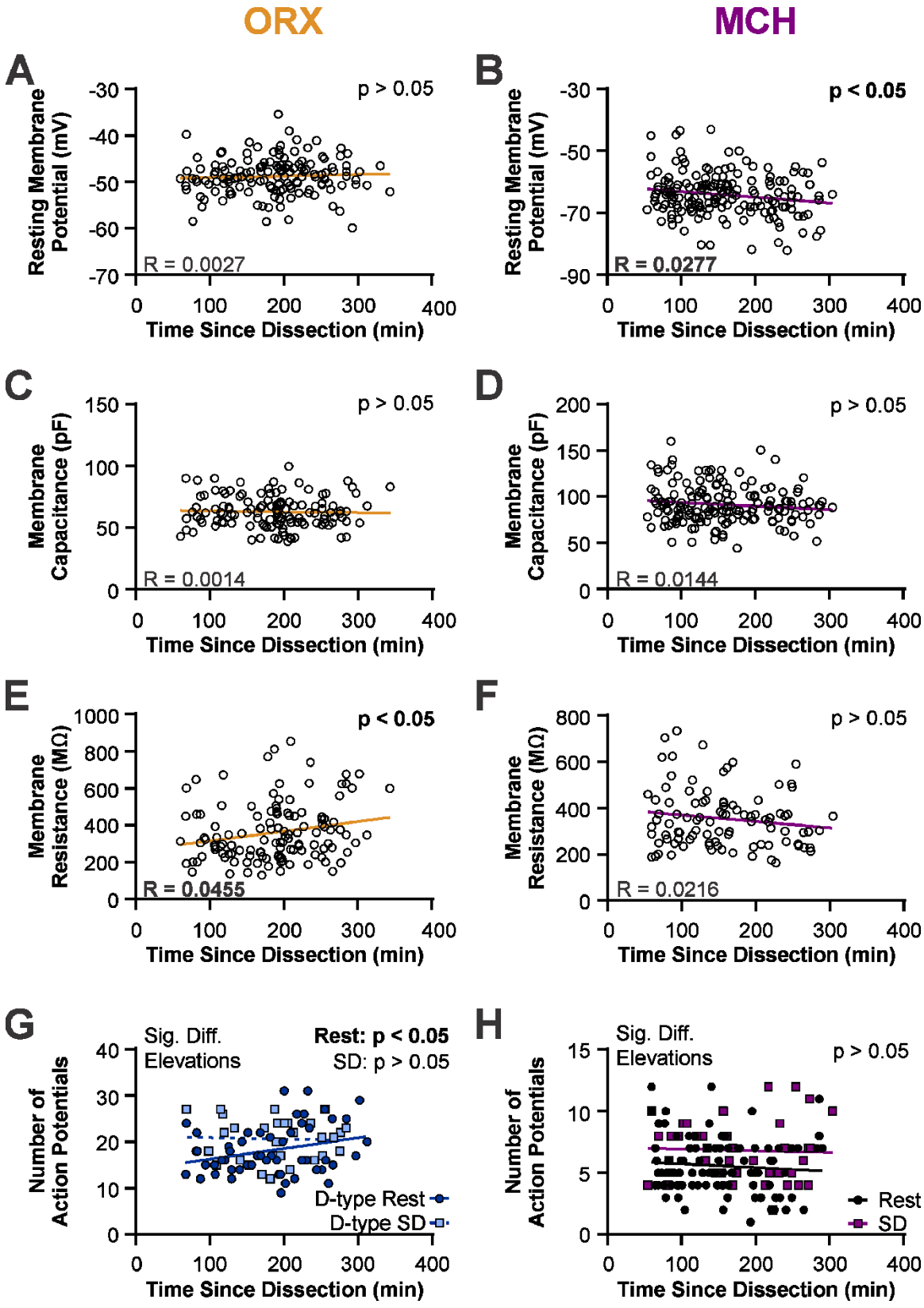
ORX
MCH
A
Resting Membrane Potential (mV)
p > 0.05
R = 0.0027
Time Since Dissection (min)
B
Resting Membrane Potential (mV)
p < 0.05
R = 0.0277
Time Since Dissection (min)
C
Membrane Capacitance (pF)
p > 0.05
R = 0.0014
Time Since Dissection (min)
D
Membrane Capacitance (pF)
p > 0.05
R = 0.0144
Time Since Dissection (min)
E
Membrane Resistance (MΩ)
p < 0.05
R = 0.0455
Time Since Dissection (min)
F
Membrane Resistance (MΩ)
p > 0.05
R = 0.0216
Time Since Dissection (min)
G
Number of Action Potentials
Sig. Diff. Elevations
Rest: p < 0.05
SD: p > 0.05
D-type Rest
D-type SD
Time Since Dissection (min)
H
Number of Action Potentials
Sig. Diff. Elevations
p > 0.05
Rest
SD
Time Since Dissection (min)

APPENDIX C: CORRELATIONAL ANALYSES BETWEEN ELECTROPHYSIOLOGICAL MEASURES AND AGE OF RAT

The experiments in this document were conducted from postnatal day 29 to 58. To ensure that developmental effects could not account for the changes I measured, I performed linear regression analyses on age of rat versus a variety of electrophysiological measures. Measures that were unaffected by sleep-state condition were grouped for regression analyses, and measures that differed by sleep-state condition were analysed separately.

Figure C.1. There is no correlation between age of rat and baseline differences in synaptic transmission to LH neurons following SD compared to Rest. (A) Linear regressions demonstrating no correlation between PPR and age of rat in ORX neurons. There is an effect of sleep-state history, demonstrated by the significantly different y-intercept of the regression slope for SD compared to Rest (consistent with Figure 2.6A). (B) Linear regressions demonstrating no correlation between slow EPSC amplitude and age of rat in MCH neurons. There is an effect of sleep-state history, demonstrated by the significantly different y-intercept of the regression slope for SD compared to Rest (consistent with Figure 2.8H).

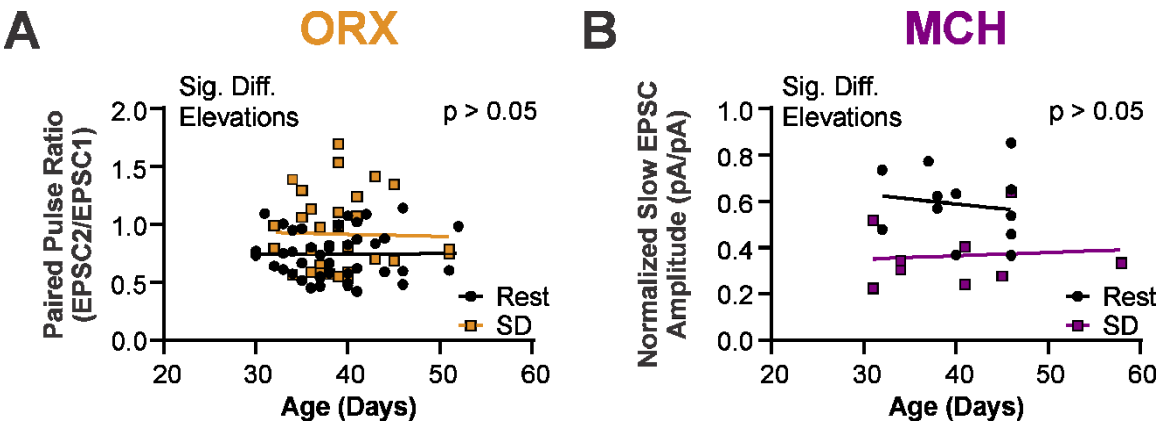
A
ORX
Sig. Diff.
Elevations
p > 0.05
Paired Pulse Ratio
(EPSC2/EPSC1)
2.0
1.5
1.0
0.5
0.0
20
30
40
50
60
Age (Days)
Rest
SD
B
MCH
Sig. Diff.
Elevations
p > 0.05
Normalized Slow EPSC
Amplitude (pA/pA)
1.0
0.8
0.6
0.4
0.2
0.0
20
30
40
50
60
Age (Days)
Rest
SD

Figure C.2. Correlation analyses of age of rat versus intrinsic membrane properties. (A,B) Linear regressions of age of rat compared to RMP in ORX neurons (A) and MCH neurons (B). There is no correlation between these measures in ORX neurons, and a mild positive correlation between these measures in MCH neurons ($P = 0.0214$). (C,D) Linear regressions of age of rat compared to membrane capacitance in ORX neurons (C) and MCH neurons (D). There is no correlation between these measures in either cell-type. (E,F) Linear regressions of age of rat compared to membrane resistance in ORX neurons (E) and MCH neurons (F). There is no correlation between these measures in either cell-type. (G) Linear regressions of age of rat and number of spikes induced by a current step (200 pA) in D-type ORX neurons. There is a mild positive correlation between these measures following Rest ($P = 0.0233$), but not SD. There is an effect of sleep-state history, demonstrated by the significantly different regression slope for SD compared to Rest (consistent with Figure 4.5A). (H) Linear regressions of age of rat and number of spikes induced by a current step (200 pA) in MCH neurons. There is a mild positive correlation between these measures following Rest ($P = 0.0189$), but not SD. There is an effect of sleep-state history, demonstrated by the significantly different y-intercept of the regression slope for SD compared to Rest (consistent with Figure 4.1C).

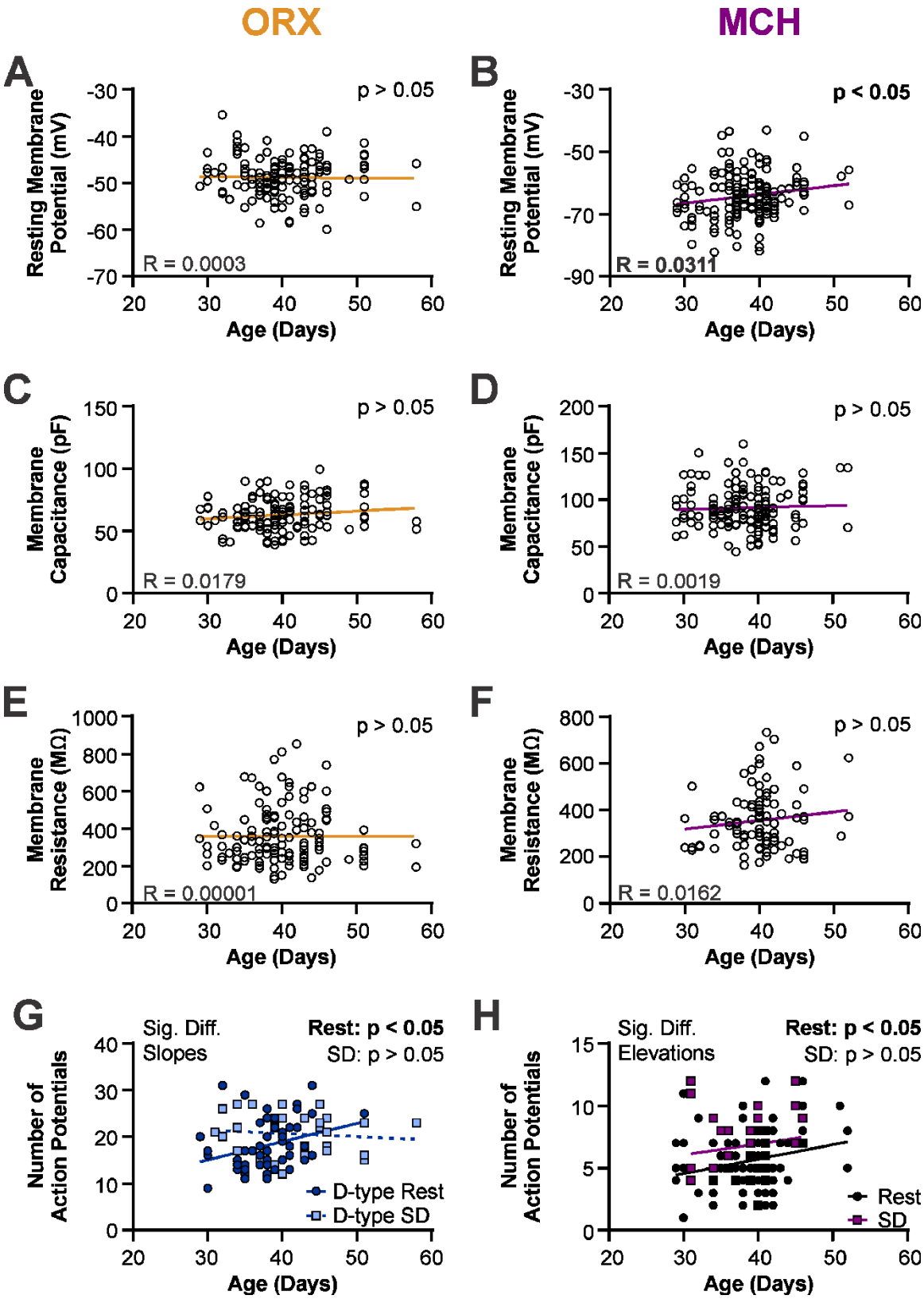
ORX
MCH
A
B
C
D
E
F
G
H
Resting Membrane Potential (mV)
Membrane Capacitance (pF)
Membrane Resistance (MΩ)
Number of Action Potentials
Age (Days)
p > 0.05
p < 0.05
R = 0.0003
R = 0.0311
R = 0.0179
R = 0.0019
R = 0.00001
R = 0.0162
Sig. Diff. Slopes
Rest: p < 0.05
SD: p > 0.05
D-type Rest
D-type SD
Sig. Diff. Elevations
Rest
SD

APPENDIX D: THE EFFECTS OF SD ON SYNAPTIC PLASTICITY ARE SIMILAR FOR D-TYPE AND H-TYPE ORX NEURONS

As only D-type ORX neurons responded to SD with intrinsic plasticity (Chapter 4), I re-examined the data from Chapter 2 demonstrating synaptic plasticity in ORX neurons following SD compared to Rest. Specifically, I broke down the PPR data (Figure 2.6A) by ORX neuron subtype.

All PPR experiments up to this point in the document have been at 25 Hz (inter-pulse interval = 40 ms). In this figure-alone, I have included PPR data at 50 Hz (inter-pulse Interval = 20 ms).

Figure D.1. SD increases PPR in both D-type and H-type ORX neurons compared to Rest. (A) PPR at 25 Hz by ORX neuron subtype and sleep-state condition. There was a main-effect for sleep-state condition ($P = 0.0123$, 2-way ANOVA). (B) PPR at 50 Hz by ORX neuron subtype and sleep-state condition. There was a main-effect for sleep-state condition ($P = 0.0001$, 2-way ANOVA). *P < 0.05, **P < 0.01.

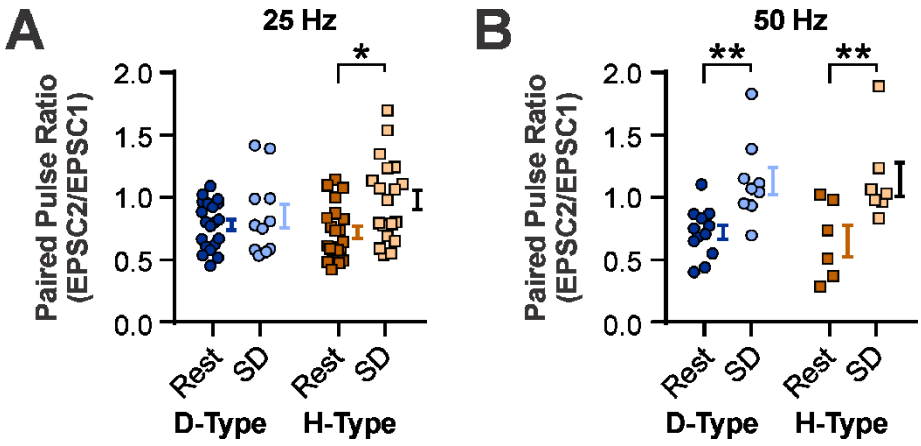
A
25 Hz
*
Paired Pulse Ratio
(EPSC2/EPSC1)
2.0
1.5
1.0
0.5
0.0
Rest
SD
Rest
SD
D-Type
H-Type
B
50 Hz
**
**
Paired Pulse Ratio
(EPSC2/EPSC1)
2.0
1.5
1.0
0.5
0.0
Rest
SD
Rest
SD
D-Type
H-Type

APPENDIX E: ELECTROPHYSIOLOGY IN WISTAR RATS

Through immunoconfocal experiments performed using *Wistar* rats, I demonstrated that GLT1 apposition with sleep/wake LH neurons following SD is different than following Rest. With whole-cell patch-clamp electrophysiology using *Sprague Dawley* rats, I discovered SD-dependent changes in excitatory synaptic transmission to LH neurons that were consistent with the anatomical GLT1 immunoconfocal data. Due to the possibility of inconsistencies between these two different rat strains, I replicated some ORX neuron electrophysiology experiments in slices obtained from Wistar rats following Rest or SD. The methods for these experiments are identical to those in Section 2.3 and Section 4.2, as appropriate.

There were no strain differences in ORX neuron RMP (n = 83 for Rest, and n = 61 for SD in Sprague Dawley; n = 9 for Rest, and n = 11 for SD in Wistar; $P = 0.7175$ for rat strain, 2-way ANOVA; Figure E.1A). There was also no strain effect on number of APs induced by positive current steps (600 ms; $P = 0.8571$ for rat strain in Rest, mixed-model ANOVA; Figure E.1B). Finally, there were no strain differences on PPR in ORX neurons (n = 43 for Rest, and n = 31 for SD in Sprague Dawley; n = 7 for Rest, and n = 8 for SD in Wistar; $P = 0.7763$ for rat strain, 2-way ANOVA; Figure E.1C). Importantly, like in Sprague Dawley rats, SD results in an increase in PPR in ORX neurons from Wistar rats ($P = 0.0112$ for Wistar post-hoc comparison, 2-way ANOVA; Figure E.1C).

These data demonstrate that release probability of excitatory synapses to ORX neurons in Wistar rats decreases following SD. These data are consistent with the immunoconfocal GLT1 data from Wistar rats and the electrophysiological data from Sprague Dawley rats.

Figure E.1. There are no strain differences in ORX neurons from Sprague Dawley and Wistar Rats. (A) RMP in ORX neurons from Sprague Dawley and Wistar rats by sleep-state condition. The Sprague Dawley data was replicated from Figure 4.2B. (B) The number of action potentials in ORX neurons from Sprague Dawley and Wistar rats in response to positive current steps by sleep-state condition. The Sprague Dawley data was replicated from Figure 4.2C. (C) PPR in ORX neurons from Sprague Dawley and Wistar rats by sleep-state condition. The Sprague Dawley data was replicated from Figure 2.6A. *$P < 0.05$.

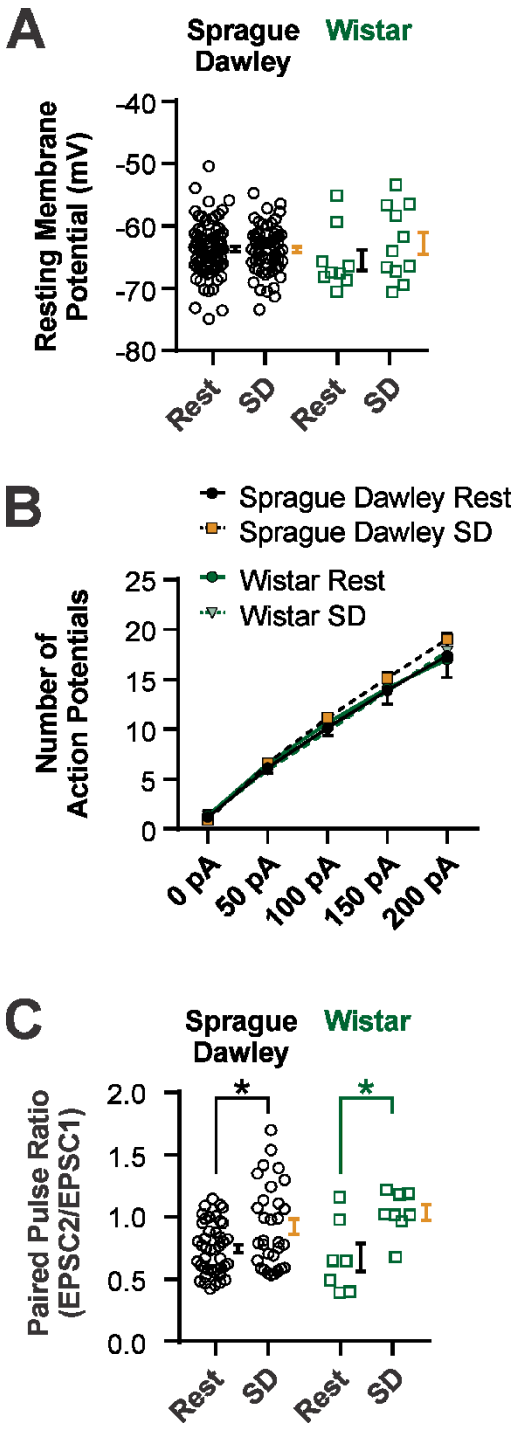
A
Sprague Dawley
Wistar
Resting Membrane Potential (mV)
-40
-50
-60
-70
-80
Rest
SD
Rest
SD
B
Sprague Dawley Rest
Sprague Dawley SD
Wistar Rest
Wistar SD
Number of Action Potentials
25
20
15
10
5
0
0 pA
50 pA
100 pA
150 pA
200 pA
C
Sprague Dawley
Wistar
Paired Pulse Ratio (EPSC2/EPSC1)
2.0
1.5
1.0
0.5
0.0
*
*
Rest
SD
Rest
SD

APPENDIX F: MINIATURE EPSCS IN LH NEURONS BY SLEEP-STATE CONDITION

I demonstrated that SD decreases release probability compared to Rest in ORX neurons but not MCH neurons. However, a previous report demonstrated that miniature EPSC (mEPSC) frequency and amplitude increased in ORX neurons following 4 h of acute SD in mice (Rao et al., 2007). Due to the discrepancy between my data and the data from Rao et al., I examined the frequency and amplitude of mEPSCs in LH neurons following Rest and SD in the rat. The methods for these experiments are identical to those in Section 2.3. Tetrodotoxin (TTX; 1 μM; see Section 3.2) was added to the ACSF to block sodium currents and isolate mEPSCs for 10 minutes prior to mEPSC quantification. mEPSC frequency and amplitude were calculated over 3 x 30 seconds for each neuron (MiniAnalysis 6.0 software; Synaptosoft, Decatur, GA). Average mEPSC frequency and amplitude were calculated and plotted in Figure F.1.

Figure F.1. SD increases mEPSC frequency compared to Rest specifically in MCH neurons. (A) Sample traces of ORX neuron mEPSCs in the Rest condition (top) and the SD condition (bottom). (B) Sample traces of MCH neuron mEPSCs in the Rest condition (top) and the SD condition (bottom). (C) mEPSC frequency following Rest and SD in ORX neurons ($P = 0.6278$). (D). mEPSC amplitude following Rest and SD in ORX neurons ($P = 8499$). (E) mEPSC frequency following Rest and SD in MCH neurons ($P = 0.0165$). (F) mEPSC amplitude following Rest and SD in MCH neurons ($P = 0.0686$). *P < 0.05.

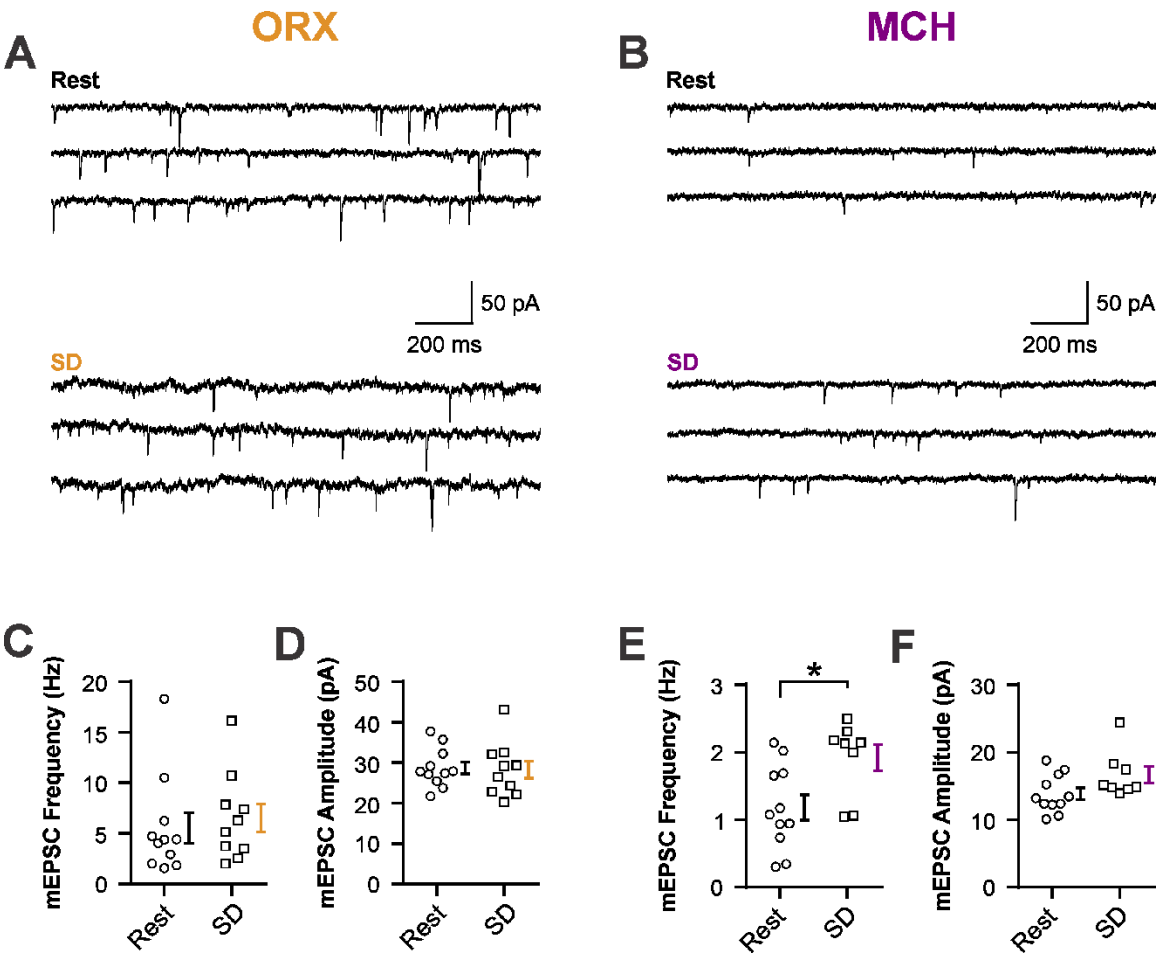
A
ORX
Rest
50 pA
200 ms
SD
B
MCH
Rest
50 pA
200 ms
SD
C
mEPSC Frequency (Hz)
20
15
10
5
0
Rest
SD
D
mEPSC Amplitude (pA)
50
40
30
20
10
0
Rest
SD
E
mEPSC Frequency (Hz)
*
3
2
1
0
Rest
SD
F
mEPSC Amplitude (pA)
30
20
10
0
Rest
SD

APPENDIX G: SUMMARY OF SD-DEPENDENT CHANGES IN THE LH

Table G.1. Summary of Synaptic and Intrinsic Changes Following Acute SD in LH Neurons.

	Orexin Neurons (Wake-Promoting)		MCH Neurons (Sleep-Promoting)	
Synaptic Measures	**Rest** (Inactive)	**SD** (Active)	**Rest** (Active)	**SD** (Inactive)
GLT1 Apposition	High	Low	Low	High
PPR		↑	—	—
Group III mGluR	Inactive	Active		
Synaptic Depression		↓	—	—
Slow EPSC	—	—		↓
mEPSC Frequency	—	—		↑

	D-type		H-type			
Intrinsic Measures	**Rest** (Inactive)	**SD** (Active)	**Rest** (Inactive)	**SD** (Active)	**Rest** (Active)	**SD** (Inactive)
No. of Spikes (200 pA)		↑	—	—		↑
AHP Amplitude		↓	—	—		
Spike Adaptation		↓	—	—	—	—
Latency to First Spike	—	—	—	—		↓